Turbine Building Model Properties, SSI Analyses, and Structural Integrity Evaluation

January 2011

©2011 Mitsubishi Heavy Industries, Ltd.
All Rights Reserved

Prepared:

T. Shimizu

Tomofumi Shimizu, Manager
Turbine Plant Engineering Section
Nuclear Turbine Plant Engineering Department

1. 27. 2011
Date

Reviewed:

J. Kojima.

Toshiki Kojima, Manager
Turbine Plant Engineering Section
Nuclear Turbine Plant Engineering Department

1.27.2011
Date

Approved:

H. Tateishi

Hideo Tateishi, Section Manager
Turbine Plant Engineering Section
Nuclear Turbine Plant Engineering Department

1. 27. 2011
Date

Revision History

Revision	Page	Description
0	All	Original Issue

© 2011
MITSUBISHI HEAVY INDUSTRIES, LTD.
All Rights Reserved

This document has been prepared by Mitsubishi Heavy Industries, Ltd. ("MHI") in connection with the U.S. Nuclear Regulatory Commission's ("NRC") licensing review of MHI's US-APWR nuclear power plant design. No right to disclose, use or copy any of the information in this document, other that by the NRC and its contractors in support of the licensing review of the US-APWR, is authorized without the express written permission of MHI.

This document contains technology information and intellectual property relating to the US-APWR and it is delivered to the NRC on the express condition that it not be disclosed, copied or reproduced in whole or in part, or used for the benefit of anyone other than MHI without the express written permission of MHI, except as set forth in the previous paragraph.

This document is protected by the laws of Japan, U.S. copyright law, international treaties and conventions, and the applicable laws of any country where it is being used.

Mitsubishi Heavy Industries, Ltd.
16-5, Konan 2-chome, Minato-ku
Tokyo 108-8215 Japan

Abstract

The purpose of this technical report is to present the structural models, soil-structure interaction (SSI) analyses, and structural integrity evaluation of the US-APWR Standard Plant Turbine Building (T/B) and Electrical Room as referenced by US-APWR Design Control Document (DCD), Chapter 3 (Reference 11).

Table of Contents

Acronym/Symbol List 6
1.0 Introduction 7
2.0 Purpose 9
3.0 Objectives 10
3.1 Maximum Relative Displacement 10
3.2 Modeling Soil-Structure Interaction using ACS SASSI for the Turbine Island 10
3.3 Turbine Building and Electrical Room Steel Member Stress Ratios 10
3.4 Turbine Building and Electrical Room Sliding and Overturning Analysis 10
4.0 US-APWR Standard Plant Structures 11
4.1 Turbine Building (T/B) 11
4.2 Electrical Room 12
4.3 Essential Service Water Pipe Tunnel (ESWPT) 12
4.4 Turbine Pedestal 13
5.0 Soil-Structure Interaction Model Development 14
5.1 Soil-Structure Interaction Analysis Methodology 14
5.2 Development of Site Input Parameters 15
5.2.1 Subsurface Profile/Properties 15
5.2.2 CSDRS Compatible Ground Motion Time Histories 16
5.3 Development of GT STRUDL Structural TI Models 16
5.4 Development of ACS SASSI Model of TI 17
6.0 Finite Element Model Validation 19
6.1 Model Validation Methodology 19
6.2 1g Static Analysis 20
6.3 Modal Analysis 20
6.4 Mode-Superposition Transient Dynamic Analysis 21
7.0 Analysis Results 23
7.1 Soil-Structure Interaction Analysis Results 23
7.1.1 Approaches for Developing Maximum Relative Displacement 23
7.1.2 Results of Maximum Relative Displacements 24
7.1.3 Evaluation of 4 inch Space 24
7.2 SSE Steel Member Stress Ratios 25
7.3 Turbine Building and Electrical Room Sliding and Overturning Analysis 26
8.0 Conclusions 27
9.0 References 28

Table of Contents (Continued)

Tables

Table 5-1. Strain Compatible Dynamic Properties for Generic Subsurface Profile 270-200 for the Turbine Island SSI Analyses 29
Table 5-2. Strain Compatible Dynamic Properties for Generic Subsurface Profile 2032-100 for the Turbine Island SSI Analyses 31
Table 6-1. Seismic Weight of the Turbine Building, Electrical Room and Essential Service Water Pipe Tunnel Finite Element Models 32
Table 6-2. Mass Properties of the Combined Turbine Building and Electrical Room Finite Element Models 32
Table 6-3. Mass Properties of the Essential Service Water Pipe Tunnel Finite Element Models 32
Table 6-4. Modal Properties of Dominant Modes X Direction (East-West) of Fine Mesh GT STRUDL Model 33
Table 6-5. Modal Properties of Dominant Modes Y Direction (North-South) of Fine Mesh GT STRUDL Model 33
Table 6-6. Modal Properties of Dominant Modes Z Direction (Vertical) of Fine Mesh GT STRUDL Model 33
Table 6-7. Maximum Displacements in X Direction (East-West) Due to X Direction Ground Motion 34
Table 6-8. Maximum Displacements in Y Direction (North-South) Due to Y Direction Ground Motion 34
Table 6-9. Maximum Displacements in Z Direction (Vertical) Due to Z Direction Ground Motion 35
Table 7-1. Maximum Relative Displacement for Y Direction (North-South) Relative to Free-Field Input Motion 36
Table 7-2. Sliding Factor of Safety 37
Table 7-3. Overturning Factor of Safety 37

Figures

Figure 4-1. Plan Arrangement of Turbine Island and Adjacent Reactor Building and Power Source Buildings 38
Figure 4-2. Turbine Island Configuration – Elevation View Looking Southeast 39
Figure 4-3. Turbine Island Configuration – Elevation View Looking North 40
Figure 4-4. Cross Section Through Turbine Building and Essential Services Water Pipe Tunnel 41
Figure 4-5. Cross Section Through North Walls of Turbine Building and Electrical Room 42
Figure 4-6. Cross Section Through Electrical Room and Essential Services Water Pipe Tunnel 43
Figure 5-1. US-APWR Certified Seismic Design Response Spectra 44
Figure 5-2. US-APWR Certified Site Design Response Spectra Compatible Acceleration Time Histories 45
Figure 5-3. Combined Turbine Island ACS SASSI Finite Element Model - North Side, Looking South 46

Figure 5-4. Combined Turbine Island ACS SASSI Finite Element Model - East Side, Looking West 47
Figure 5-5. Combined Turbine Island ACS SASSI Finite Element Model - South Side, Looking North 48
Figure 5-6. Combined Turbine Island ACS SASSI Finite Element Model - West Side, Looking East 49
Figure 5-7. Combined Turbine Island ACS SASSI Finite Element Model - Substructures, Engineered Backfill and Essential Service Water Pipe Tunnel 50
Figure 5-8. Combined Turbine Island ACS SASSI Finite Element Model – Interior of Turbine Building Substructure with First Floor Slab Removed, Engineered Backfill and Essential Service Water Pipe Tunnel 51
Figure 6-1. X (East-West) and Y (North-South) Directions Displacement Comparison of Fine and Coarse Mesh Models Under 1g Load Applied in X and Y Directions, Respectively Turbine Building Column BT-8T 52
Figure 6-2. Z (Vertical) Direction Displacement Comparison of Fine and Coarse Mesh Models Under 1g Load Applied in Z Direction Turbine Building Column BT-8T 53
Figure 6-3. X (East-West) and Y (North-South) Directions Displacement Comparison of Fine and Coarse Mesh Models Under 1g Load Applied in X and Y Directions, Respectively Turbine Building Column AT-3T 54
Figure 6-4. Z (Vertical) Direction Displacement Comparison of Fine and Coarse Mesh Models Under 1g Load Applied in Z Direction Turbine Building Column AT-3T 55
Figure 6-5. X (East-West) and Y (North-South) Directions Displacement Comparison of Fine and Coarse Mesh Models Under 1g Load Applied in X and Y Directions, Respectively Electrical Room Column AT-1T 56
Figure 6-6. Z (Vertical) Direction Displacement Comparison of Fine and Coarse Mesh Models Under 1g Load Applied in Z Direction Electrical Room Column AT-1T 57
Figure 6-7. X (East-West) and Y (North-South) Directions Displacement Comparison of Fine and Coarse Mesh Models Under 1g Load Applied in X and Y Directions, Respectively Essential Service Water Pipe Tunnel ACS SASSI Node 11401 58
Figure 6-8. Z (Vertical) Direction Displacement Comparison of Fine and Coarse Mesh Models Under 1g Load Applied in Z Direction Essential Service Water Pipe Tunnel ACS SASSI Node 11401 59
Figure 6-9. Comparison of Turbine Building and Electrical Room Mesh Dynamic Mass Participation in X (East-West), Y (North-South) and Z (Vertical) Directions 60
Figure 6-10. Comparison of Essential Service Water Pipe Tunnel Mesh Dynamic Mass Participation in X (East-West), Y (North-South) and Z (Vertical) Directions 61
Figure 6-11. Node Locations for Fixed Base Relative Displacement Time History and Response Spectra Comparisons 62
Figure 6-12. Fixed Base Relative Displacement Time History Comparison Between Fine Mesh GT STRUDL Model and ACS SASSI Model, Node 560 in X, Y, and Z Directions 63
Figure 6-13. Fixed Base Relative Displacement Time History Comparison Between Fine Mesh GT STRUDL Model and ACS SASSI Model, Node 972 in X, Y, and Z Directions 64

Figure 6-14. Fixed Base Relative Displacement Time History Comparison Between Fine Mesh GT STRUDL Model and ACS SASSI Model, Node 1473 in X, Y, and Z Directions 65
Figure 6-15. Fixed Base Relative Displacement Time History Comparison Between Fine Mesh GT STRUDL Model and ACS SASSI Model, Node 5041 in X, Y, and Z Directions 66
Figure 6-16. Fixed Base Relative Displacement Time History Comparison Between Fine Mesh GT STRUDL Model and ACS SASSI Model, Node 11401 in X, Y, and Z Directions 67
Figure 6-17. Fixed Base Response Spectra Comparison Between Fine Mesh GT STRUDL Model and ACS SASSI Model, Node 560 in X, Y, and Z Directions (5 Percent Damping) 68
Figure 6-18. Fixed Base Response Spectra Comparison Between Fine Mesh GT STRUDL Model and ACS SASSI Model, Node 1440 in X, Y, and Z Directions (5 Percent Damping) 69
Figure 6-19. Fixed Base Response Spectra Comparison Between Fine Mesh GT STRUDL Model and ACS SASSI Model, Node 2600 in X, Y, and Z Directions (5 Percent Damping) 70
Figure 6-20. Fixed Base Response Spectra Comparison Between Fine Mesh GT STRUDL Model and ACS SASSI Model, Node 11401 in X, Y, and Z Directions (5 Percent Damping) 71
Figure 7-1. Selected Node Locations in Turbine Island for Computing Relative Displacements 72
Figure 7-2. Acceleration Transfer Function and Relative Displacement with Respect to Free-Field Input Motion at Node 290 - Y Direction (North-South) for Profile 270-200 73
Figure 7-3. Acceleration Transfer Function and Relative Displacement with Respect to Free-Field Input Motion at Node 290 - Y Direction (North-South) for Profile 2032-100 74
Figure 7-4. Acceleration Transfer Function and Relative Displacement with Respect to Free-Field Input Motion at Node 386 - Y Direction (North-South) for Profile 270-200 75
Figure 7-5. Acceleration Transfer Function and Relative Displacement with Respect to Free-Field Input Motion at Node 386 - Y Direction (North-South) for Profile 2032-100 76
Figure 7-6. Acceleration Transfer Function and Relative Displacement with Respect to Free-Field Input Motion at Node 560 - Y Direction (North-South) for Profile 270-200 77
Figure 7-7. Acceleration Transfer Function and Relative Displacement with Respect to Free-Field Input Motion at Node 560 - Y Direction (North-South) for Profile 2032-100 78
Figure 7-8. Acceleration Transfer Function and Relative Displacement with Respect to Free-Field Input Motion at Node 879 - Y Direction (North-South) for Profile 270-200 79
Figure 7-9. Acceleration Transfer Function and Relative Displacement with Respect to Free-Field Input Motion at Node 879 - Y Direction (North-South) for Profile 2032-100 80
Figure 7-10. Acceleration Transfer Function and Relative Displacement with Respect to Free-Field Input Motion at Node 908 - Y Direction (North-South) for Profile 270-200 81

Figure 7-11. Acceleration Transfer Function and Relative Displacement with Respect to Free-Field Input Motion at Node 908 - Y Direction (North-South) for Profile 2032-100 82
Figure 7-12. Acceleration Transfer Function and Relative Displacement with Respect to Free-Field Input Motion at Node 972 - Y Direction (North-South) for Profile 270-200 83
Figure 7-13. Acceleration Transfer Function and Relative Displacement with Respect to Free-Field Input Motion at Node 972 - Y Direction (North-South) for Profile 2032-100 84
Figure 7-14. Acceleration Transfer Function and Relative Displacement with Respect to Free-Field Input Motion at Node 1473 - Y Direction (North-South) for Profile 270-200 85
Figure 7-15. Acceleration Transfer Function and Relative Displacement with Respect to Free-Field Input Motion at Node 1473 - Y Direction (North-South) for Profile 2032-100 86
Figure 7-16. Acceleration Transfer Function and Relative Displacement with Respect to Free-Field Input Motion at Node 1581 - Y Direction (North-South) for Profile 270-200 87
Figure 7-17. Acceleration Transfer Function and Relative Displacement with Respect to Free-Field Input Motion at Node 1581 - Y Direction (North-South) for Profile 2032-100 88
Figure 7-18. Acceleration Transfer Function and Relative Displacement with Respect to Free-Field Input Motion at Node 3261 - Y Direction (North-South) for Profile 270-200 89
Figure 7-19. Acceleration Transfer Function and Relative Displacement with Respect to Free-Field Input Motion at Node 3261 - Y Direction (North-South) for Profile 2032-100 90
Figure 7-20. Acceleration Transfer Function and Relative Displacement with Respect to Free-Field Input Motion at Node 5041 - Y Direction (North-South) for Profile 270-200 91
Figure 7-21. Acceleration Transfer Function and Relative Displacement with Respect to Free-Field Input Motion at Node 5041 - Y Direction (North-South) for Profile 2032-100Reference 13 92

ACRONYM/SYMBOL LIST

AISC	American Institute of Steel Construction
ASCE	American Society of Civil Engineers
ASTM	American Society for Testing and Materials
CSDRS	Certified Seismic Design Response Spectra
DCD	Design Control Document
d_{max}	The maximum recommended thickness of a subsurface profile layer with a given shear wave velocity
ESWPT	Essential Service Water Pipe Tunnel
FE	Finite Element
f_n	Highest (or cut-off) frequency of analysis
g	gravity
H1	North-South, Y Direction
H2	East-West, X Direction
Hz	Hertz
MHI	Mitsubishi Heavy Industries, Ltd
NRC	Nuclear Regulatory Commission
NUREG	US Nuclear Regulatory Commission Regulation
PS/B	Power Source Building
R/B	Reactor Building
SSE	Safe Shutdown Earthquake
SSI	Soil-Structure Interaction
T/B	Turbine Building
TFI	Transfer function interpolated
TFU	Transfer function un-interpolated
TI	Turbine Island
US-APWR	United States - Advanced Pressurized Water Reactor
V	Vertical, Z direction
V_s	Shear Wave Velocity
3-D	Three dimensional

1.0 INTRODUCTION

This report documents the soil-structure interaction (SSI) analyses of the Turbine Island (TI), which includes the Turbine Building (T/B), Electrical Room, Turbine Pedestal, and a section of the Essential Service Water Pipe Tunnel (ESWPT) located under the north end of the T/B and Electrical Room of the United States - Advanced Pressurized Water Reactor (US-APWR) standard plant. The SSI analyses were performed to estimate the lateral displacement of the T/B and Electrical Room relative to the Reactor Building (R/B) and one of the Power Source Buildings (PS/B) of the Nuclear Island.

Also presented in this report are stress ratios for select T/B and Electrical Room steel members estimated using GT STRUDL and ACS SASSI based on the fixed-base condition, and results of a sliding and overturning analysis of the T/B and Electrical Room.

As stated in US-APWR Design Control Document (DCD), Revision 2, Subsection 3.7.2.4 (Reference 11), SSI effects are considered in the seismic response analysis of all major Seismic Category I and Seismic Category II buildings and structures that are part of the US-APWR standard and non-standard plants. The ACS SASSI computer program was used for the SSI analyses described in this report. The SSI analyses were conducted using methods and approaches consistent with ASCE 4-98 (Reference 8). The ESWPT is classified as a Seismic Category I structure, and the T/B and Electrical Room are classified as Seismic Category II structures. The Turbine Pedestal is classified as a non-seismic structure.

The design input ground motion and generic subsurface profiles used in the SSI analyses were developed in Reference 3. The design input ground motion consists of three time history components compatible to the US-APWR certified seismic design response spectra (CSDRS) for a safe shutdown earthquake (SSE) event with a peak ground acceleration of 0.3g. The time histories were developed in full compliance with the criteria of Standard Review Plan 3.7.1 (Reference 1), Subsection 3.7.1.II.1B. The generic subsurface profiles were modified for compatibility with the configuration of the structures analyzed.

Finite element (FE) structural models were created using the software package GT STRUDL, Version 30.0. The GT STRUDL FE models included detailed models of the T/B, Electrical Room, and a section of the ESWPT, and a simplified representation of the Turbine Pedestal. Although not part of the standard plant, a section of the ESWPT was included in the model only to determine the localized effect the tunnel may have on the TI analysis. The GT STRUDL FE structural model was then converted into ACS SASSI format for performing the SSI dynamic analysis. Validation analyses results are presented in Section 6, demonstrating the GT STRUDL structural model is accurately represented by the ACS SASSI model for dynamic vibration.

The results of the SSI analyses are presented as the maximum displacements relative to the free-field ground motion (herein referred to as relative displacement) at multiple locations of the T/B, and the Electrical Room adjacent to the R/B and PS/B of the Nuclear Island. The approach used to estimate the maximum relative displacements are discussed. The maximum relative displacements of the TI were combined with the maximum relative displacements of R/B and PS/B from Reference 10 to evaluate if the space between the buildings is sufficient to prevent contact of the buildings during a 0.3g SSE event. The 0.3g SSE is for a 0.3g peak ground acceleration for the two horizontal directions and the vertical direction.

The T/B height (193’-1”) in analysis is higher than DCD next revision (rev.3) to apply for

increase of crane hook height, because analysis of this higher and heavier building will generates bigger seismic response. (Comparison T/B height in the analysis with DCD, Reference 13)

2.0 PURPOSE

The purpose of the SSI analysis of the TI is to evaluate the sufficiency of the 4 inch space between the T/B and Electrical Room relative to the R/B, and the PS/B based on SSI analysis results of the TI FE model. This report discusses the technical approach used for the SSI analysis for the TI, and provides the estimated displacements of the T/B and Electrical Room relative to the R/B and PS/B.

This report provides allowable stress ratios for select T/B and Electrical Room steel members calculated using GT STRUDL and ACS SASSI based on the fixed base condition. Also provided are the results of a sliding and overturning analysis of the T/B and Electrical Room based on GT STRUDL results.

Included in this report are discussions of the following:

- Two generic layered subsurface profiles and strain compatible properties for the TI FE model. The two generic subsurface profiles were selected from eight profiles presented in Reference 3. Any required modifications to the profiles are addressed.
- Development of the FE structural model for the TI in both GT STRUDL and ACS SASSI.
- Validation of the TI ACS SASSI structural model against the GT STRUDL structural model.
- TI SSI analyses results.
- Allowable stress ratios calculated using GT STRUDL and ACS SASSI for select T/B and Electrical Room steel members.
- T/B and Electrical Room sliding and overturning analysis results.

3.0 OBJECTIVES

3.1 Maximum Relative Displacement

The primary objective of the SSI analysis of the TI was to evaluate if the space between the T/B and Electrical Room relative to the R/B and PS/B is sufficient to prevent contact of the structures during a 0.3 g peak ground acceleration SSE event. Based on the DCD Revision 2 (Reference 11), the space between the structures is set at 4 inches. The maximum displacements at select locations of the T/B and Electrical Room adjacent to the R/B and PS/B were estimated using the SSI analyses. The estimated maximum T/B and Electrical Room relative displacement immediately adjacent to the R/B and PS/B was combined with the estimated maximum R/B and PS/B relative displacement at the same elevation (Reference 10), which was used to evaluate the sufficiency of the space between the buildings.

3.2 Modeling Soil-Structure Interaction using ACS SASSI for the Turbine Island

To perform the SSI analysis, the TI structural FE model was combined with the subsurface conditions of interest; therefore, the secondary objective was to develop a representative model to perform the SSI. To perform the SSI analysis, the software ACS SASSI, Version 2.3.0 was selected. ACS SASSI is a FE computer software that combines the structural model with the subsurface conditions for performing three-dimensional nonlinear SSI analyses. ACS SASSI uses complex damping formulation to account for dissipation of energy. ACS SASSI addresses the effects of the frequency dependence of the foundation impedance and scattering of input ground motion.

The three-dimensional FE model of the TI for structural analysis was developed using the GT STRUDL software package. The concrete substructure portion of the T/B and Electrical Room model used in the GT STRUDL model for structural analysis had too fine (small) a FE mesh size for use in ACS SASSI; therefore, in GT STRUDL the element sizes were increased, resulting in a coarser FE mesh. For both the original fine mesh substructure model and the reduced size coarse mesh substructure model, the portions for the steel superstructure remain the same. Once completed, the coarse mesh model was translated to ACS SASSI. The performance of the coarse mesh ACS SASSI FE model was validated to confirm it appropriately represents the fine mesh GT STRUDL model by performing fixed-base analyses for both models and comparing the results.

3.3 Turbine Building and Electrical Room Steel Member Stress Ratios

The objective of reviewing member allowable stress ratios was to verify that the GT STRUDL and ACS SASSI fixed-base condition stresses are less than or equal to the allowable member stresses .

3.4 Turbine Building and Electrical Room Sliding and Overturning Analysis

The objective of the sliding and overturning analysis of the T/B and Electrical Room was to determine if the factors of safety against sliding and overturning were adequate based on the loading determined from the GT STRUDL fixed-base analysis. These factors of safety were then compared to NRC Standard Review Plan 3.8.5 (Reference 12).

4.0 US-APWR STANDARD PLANT STRUCTURES

The TI model includes the T/B, Electrical Room, Turbine Pedestal, and for this analysis, a section of the ESWPT. Although the ESWPT is not part of the standard plant, a section of the ESWPT was included in the model only to determine the localized effect the tunnel may have on the TI analysis. Figure 4-1 shows the plan arrangement of the TI and also shows the locations of the adjacent ESWPT, R/B and PS/B. The overall configuration of the TI is depicted in Figures 4-2 and 4-3, which provide two general views of the TI. Subsections 5.3 and 5.4 discuss the development of the model and provide figures showing the configuration of the TI. The following subsections provide a brief description of the components of the TI.

4.1 Turbine Building (T/B)

The T/B has column row plan dimensions of 367 by 180 feet. The T/B is classified as a Seismic Category II structure that houses the non-safety related equipment of the turbine generator and its auxiliary systems, (main condenser, feedwater heaters, moisture separator reheaters, etc.). The T/B is designed to withstand the full SSE loads, i.e., 0.3g, including the load of the overhead traveling crane.

As a Seismic Category II building, the T/B is designed to prevent it from impacting the function or integrity of adjacent Seismic Category I structures. The T/B is oriented in such a way that any plane perpendicular to the turbine generator axis does not intersect with the R/B. This arrangement minimizes the probability of a missile from the turbine generator striking the R/B, which is consistent with the guidance of Regulatory Guide 1.115 (Reference 5).

The T/B steel superstructure is a braced steel frame, panel clad structure designed in accordance with American Institute of Steel Construction (AISC) N690-1994 (R2004) (Reference 6). The T/B superstructure is supported on the top slab of the reinforced concrete substructure, with the superstructure loads transferred to the supporting basemat through the substructure.

The substructure is a reinforced concrete basement that accommodates the Circulating Water Inlet/Outlet pipes and Condenser Vault/Pumps. The substructure is designed in accordance with ACI 349-01 (Reference 7). The geometry of the T/B substructure is based on the DCD, Revision 2 (Reference 11). The bottom of the substructure base slab is 27 feet 2 inches below plant grade, at elevation -24 feet 7 inches. The T/B substructure consists of a first floor slab at the ground level, a reinforced concrete basemat, and reinforced concrete exterior/interior walls. The basemat is 6 feet 7 inches thick, the walls are 3 feet 4 inches thick, and the first floor slab thickness varies from 1 foot 8 inches to 6 feet 7 inches.

The T/B first floor slab extends over the ESWPT (discussed in Subsection 4.3) and is supported at the north end by a foundation wall located between the R/B foundation and the ESWPT. Figure 4-4 provides a cross section showing where the ESWPT passes under the T/B. The location of the cross section is shown on Figure 4-1. The foundation north wall of the T/B has the same bottom elevation as the bottom of the ESWPT foundation mat, -28 feet 4 inches. The R/B foundation, the north foundation wall of the T/B, and the ESWPT are physically separated with 4 inch spaces. The north foundation wall of the T/B has a number of penetrations that are aligned with penetrations through the north side of ESWPT. The cross section on Figure 4-5 shows the penetrations through the north wall of the T/B.

4.2 Electrical Room

The Electrical Room has column row plan dimensions of 201 feet 3 inches by 78 feet 10 inches. The Electrical Room is a Seismic Category II structure that houses the non-safety related equipment associated with operation of the turbine generator and its auxiliary systems. As a Seismic Category II building, the Electrical Room is designed to prevent it from impacting the function or integrity of adjacent Seismic Category I structures. The Electrical Room is also structurally separated from the T/B.

The Electrical Room superstructure is a braced steel frame, panel clad structure, designed in accordance with AISC N690-1994 (R2004) (Reference 6). The frame is mounted on a reinforced concrete substructure, which consists of a slab-on-grade. The Electrical Room is designed to withstand the full SSE loads, i.e., 0.3g peak ground acceleration for the two horizontal directions and the vertical direction.

Fill from the bottom of the Electrical Room concrete slab-on-grade to the elevation of the bottom of the T/B substructure consists of engineered backfill. The engineered backfill thickness is approximately 25 feet. This fill material was used to provide the minimum shear wave velocity of 1,000 feet per second as required by the DCD, Revision 2, Section 3.7.1.1 (Reference 11).

The Electrical Room slab-on-grade extends over the ESWPT (discussed in Subsection 4.3) and is supported at the north end by a foundation wall located between the R/B foundation and the ESWPT. The slab is not supported by and is not in direct contact with the ESWPT. Figure 4-6 provides a cross section where the ESWPT passes under the Electrical Room. The location of the cross section is shown on Figure 4-1. The north foundation wall of the Electrical Room has the same bottom elevation as the bottom of the ESWPT foundation mat, -28 feet 4 inches. The R/B foundation, the north wall of the Electrical Room slab, and the ESWPT are physically separated with 4 inch spaces. The north foundation wall of the Electrical Room has a penetration that is aligned with a corresponding penetration through the north side of ESWPT. The cross section on Figure 4-5 shows the penetration through the north wall of the Electrical Room.

4.3 Essential Service Water Pipe Tunnel (ESWPT)

Although the ESWPT is not part of the standard plant, a section of the ESWPT was included in the model only to determine the localized effect the tunnel may have on the TI analysis. The ESWPT passes below the north end of the T/B and Electrical Room immediately adjacent to the R/B and PS/Bs. The ESWPT is a reinforced concrete structure, which is classified as a Seismic Category I structure based on the DCD, Revision 2, Table 3.2-4 (Reference 11). As a Seismic Category I structure, the ESWPT is designed to withstand the full SSE loads.

The ESWPT is separated into two rectangular passages separated by a common middle wall, as shown in Figures 4-4 and 4-6. The passages contain pipelines that convey water from the Ultimate Heat Sink to the R/B. Openings are provided in the north side of the ESWPT and on the R/B south side to allow the pipes to enter the R/B. These openings also align with the penetrations through the T/B and Electrical Room north foundation walls.

In cross section, the ESWPT is 25 feet wide and 18 feet 8 inches tall. The bottom of the base slab of the ESWPT is located 30 feet 11 inches below grade, at an elevation of -28 feet 4 inches. The roof, floor, and two side walls are 2 feet thick and the middle wall is 1 foot thick.

The ESWPT is structurally independent of the T/B and Electrical Room, as it is separated by a 4 inch space.

4.4 Turbine Pedestal

The turbine pedestal is a non-safety, non-seismic, reinforced concrete structure and is located in the center of the T/B. The turbine pedestal is structurally independent of the T/B superstructure and foundation. For the purpose of evaluating the space between the T/B and Electrical Room relative to the R/B and the PS/B, the weight of the turbine pedestal was included in the ACS SASSI model. The pedestal weight was uniformly distributed over the full soil contact area of the pedestal foundation. This will permit the impact of the pedestal weight to be included in the dynamic SSI analyses. Structural features of the turbine pedestal are not included. The bottom of the turbine pedestal was set at the same elevation in the SSI analysis as the bottom of the T/B basemat, elevation -24 feet 7 inches.

5.0 SOIL-STRUCTURE INTERACTION MODEL DEVELOPMENT

5.1 Soil-Structure Interaction Analysis Methodology

The SSI analysis methodology implemented for the TI is summarized in this subsection. Detailed discussions regarding the SSI analysis methodology are provided in the remainder of Section 5. The SSI analyses of US-APWR TI were performed using the ACS SASSI computer software, which employs the complex response method and FE technique to solve for the seismic response of a SSI system in the frequency domain.

In summary, the SSI analysis methodology implemented for the TI consisted of the following basic elements:

- Selecting subsurface profiles and establishing site input parameters including strain compatible dynamic subsurface material properties and input ground motions.

- Developing FE models independently for the T/B steel superstructure, Electrical Room steel superstructure, T/B concrete substructure, Electrical Room concrete substructure, and a section of the ESWPT in GT STRUDL for structural design. The T/B and Electrical Room concrete substructure models were developed using a fine FE mesh to facilitate structural design.

- Modifying the original fine mesh T/B and Electrical Room concrete substructure models in GT STRUDL to generate a coarse mesh FE structural model. The mesh sizes for the T/B and Electrical Room concrete substructures in GT STRUDL were modified to reduce the model size in ACS SASSI without loosing the accuracy of the model. The mesh sizes for the T/B and Electrical Room steel superstructures were unchanged.

- The superstructure and coarse mesh substructure models for the T/B and Electrical Room were combined in GT STRUDL and then was translated to ACS SASSI for the SSI analyses. The separately developed ESWPT GT STRUDL model was translated to ACS SASSI and combined with the T/B and Electrical Room model for the SSI analysis.

- Importing strain compatible dynamic subsurface material properties, and CSDRS compatible time histories (two horizontal directions and one vertical direction) into ACS SASSI input files.

- Validating that the coarse and fine mesh GT STRUDL models responded similarly. This was achieved by performing a 1g fixed-base condition analysis, modal analysis, and mode superposition time history analysis in GT STRUDL in accordance with Standard Review Plan 3.7.2 (Reference 9).

- Validating that the T/B and Electrical Room, and ESWPT models were properly translated from GT STRUDL to ACS SASSI. This was achieved by performing an ACS SASSI SSI analysis using the translated model under a fixed base condition and then comparing the relative displacements and response spectra with the results obtained from the mode superposition dynamic analysis performed in GT STRUDL.

- Performing SSI analyses in ACS SASSI for two generic layered subsurface profiles. For each SSI analysis, acceleration transfer functions were computed using discrete frequencies. Confirmation was then made that sufficient frequencies were included by inspecting the relationship between the interpolated and un-interpolated acceleration transfer functions.

- Processing the SSI analysis results to obtain relative displacement time histories for each input ground motion component at selected points of interests.

- The final relative displacement time histories of selected TI nodes were computed by combining algebraically, at each time-step, the three independent displacement time history components. The maximum relative displacements were extracted from the final relative displacement time histories as the absolute maximum value of the displacement series.

- Evaluating if the planned 4 inch space between the TI, and the R/B and PS/B is sufficient.

5.2 Development of Site Input Parameters

To be consistent for the SSI analysis of the R/B and PS/B, the same subsurface material profiles and CSDRS compatible ground motion histories were used for the SSI analysis of the TI (References 3 and 4).

5.2.1 Subsurface Profile/Properties

For the TI SSI analysis, two generic subsurface profiles with strain compatible properties from the ground surface to hard rock were selected from the eight subsurface profiles developed by MHI for the SSI analyses of the R/B and PS/B (References 3 and 4). The eight subsurface profiles are considered to represent the range of possible subsurface conditions for typical sites within the continental United States. Subsurface profiles 270-200 and 2032-100 were selected for this SSI analysis because they are the softest and stiffest subsurface profiles of the eight, respectively. Therefore, generic layered subsurface profiles 270-200 and 2032-100 represent the extremes in properties of subsurface materials for typical sites within the continental United States. For the TI SSI analysis, these profiles were truncated at the bottom of the T/B basemat (see Subsection 4.1 for additional discussion on the bottom elevation of the T/B basemat).

In accordance with the ACS SASSI manual (Reference 2), the thickness of each subsurface layer of the profiles was limited to less than 20 percent of the wave length of the material the wave is passing through at the highest (or cut-off) frequency, f_n, of analysis. The maximum recommended thickness, d_{max}, of a subsurface profile layer, with a given shear wave velocity, V_s, was evaluated by solving the following equation:

$$d_{\max} = \frac{V_s}{5 \cdot f_n} \qquad \text{(Equation 5-1)}$$

The strain compatible subsurface material properties for the two generic layered subsurface profiles used for SSI analyses of the TI are provided in Tables 5-1 and 5-2. The top of Layer 1 in Tables 5-1 and 5-2 is located at the bottom of the T/B basemat. The layer thicknesses for all the subsurface profiles shown in Tables 5-1 and 5-2 satisfy the requirement of Equation 5-1.

5.2.2 CSDRS Compatible Ground Motion Time Histories

The CSDRS compatible ground motion time histories used in this analysis were developed by MHI in Reference 3. The ground motion used consists of three statistically independent acceleration time histories, X, Y, and Z, which represent the TI input ground motions in east-west, north-south, and vertical directions, respectively. The acceleration time histories were developed through a spectra matching approach using the Mt Baldy, California recording of the January 14, 1994, Northridge earthquake (magnitude **M**6.7) as the seed ground motion. The development of the acceleration time histories is in compliance with the requirements of NUREG-0800 Standard Review Plan 3.7.1 (Reference 1), Subsection 3.7.1.II.1B, Option 1, Approach 2.

For the TI SSI analyses, the CSDRS compatible time history ground motions were applied as free-field ground motion at the bottom of the T/B basemat, at elevation -24 feet 7 inches.

Figure 5-1 presents the 5 percent damped horizontal and vertical CSDRS. Figure 5-2 presents the three acceleration time histories used as input ground motion for site independent SSI analyses. The time step and duration of the acceleration time histories are 0.005 second and 22.085 seconds, respectively.

5.3 Development of GT STRUDL Structural TI Models

To facilitate completion of the SSI analysis in ACS SASSI, structural models were first developed using GT STRUDL, Version 30.0. The following GT STRUDL models were developed:

- T/B and Electrical Room steel superstructure,
- T/B and Electrical Room concrete substructure.
- ESWPT concrete structure.

The T/B and Electrical Room concrete substructure models were developed for structural design using a fine mesh FE model. In order to reduce the size of the model for subsequent ACS SASSI use, an additional coarse mesh substructure model was developed.

The structural models for the T/B and Electrical Room steel superstructures, T/B and Electrical Room concrete substructures, and ESWPT were developed independently. The superstructure and substructure models for the T/B and Electrical Room were combined in GT STRUDL. As the ESWPT is structurally separate, it was left as a separate model in GT STRUDL.

The following paragraphs discuss development of the GT STRUDL models. Subsection 5.4 discusses conversion to a coarse mesh GT STRUDL substructure model and translation to an ACS SASSI compatible model.

The steel superstructure portion of the T/B and Electrical Room models were developed by establishing nodes at steel connections, and then connecting the nodes with steel members.

The fine mesh elements for the reinforced concrete T/B and Electrical Room substructures were evenly spaced between column rows and aligned in the east-west, north-south, and vertical directions. The reinforced concrete T/B substructure and Electrical Room slab-on-grade were modeled with plate elements that account for both bending and shear deformations, and provide both plate stress and plate bending results. The plate elements of the fine mesh model were located at the center of the concrete floors and walls.

The condensate pump foundation is a mass concrete structure with pipe and pump-can openings, which was modeled with solid elements.

Along a portion of the west side and all of the south edge of the T/B, the first floor slab is cantilevered out from the basement walls. As the TI SSI was performed as a surface structure in accordance with American Society of Civil Engineers (ASCE) 4-98 (Reference 8), the space below the cantilevered portions of the first floor slab to the bottom elevation of the T/B substructure was modeled as engineered backfill material which satisfies the DCD, Revision 2, Section 3.7.1.1 (Reference 11) requirements for competent material. The engineered backfill material was modeled using solid elements.

For the Electrical Room substructure model, engineered backfill material was placed from the bottom of the reinforced concrete slab-on-grade to the bottom of the substructure of the T/B. The engineered backfill material was modeled using solid elements and satisfies the DCD, Revision 2, Section 3.7.1.1 (Reference 11) requirements for competent material. The solid elements for the engineered backfill material below the T/B cantilever on the west side of the T/B and for the engineered backfill material below the Electrical Room were connected using joint ties. Additionally, the engineered backfill below the Electrical Room that is adjacent to the T/B substructure concrete, is connected to the substructure concrete using joint ties.

The ESWPT FE mesh spacing was established to align the model joints longitudinally with the pipeline locations in the ESWPT, and the mesh is evenly spaced between openings in the ESWPT adjacent to the R/B. The ESWPT foundation was modeled with plate elements that account for both bending and shear deformations, and yield both plate stress and plate bending results. Since tunnel walls, roof, and floor are relatively thin, the plate elements were modeled at the center of the walls, roof, and floor.

5.4 Development of ACS SASSI Model of TI

Once the GT STRUDL models for structural design were completed, the T/B and Electrical Room substructure model was modified to reduce the model size to facilitate running in ACS SASSI. Primarily, the mesh size for the T/B and Electrical Room substructure concrete elements was increased to reduce the number of nodes and elements, resulting in a coarser FE mesh. This coarse mesh structural model was then translated from GT STRUDL to ACS SASSI.

The reinforced concrete T/B and Electrical Room substructure coarse element dimensions were increased. A horizontal coarse mesh size of approximately 13 by 13 feet was adopted depending on column row spacings. For the engineered backfill material, the mesh size was also increased, with the horizontal mesh size set to match that of the overlying concrete.

In the fine mesh T/B substructure model, the plate elements used to represent the bottom of the substructure basemat were located at the center of the basemat's vertical dimension; therefore, the model did not extend to the full depth of the T/B substructure. For the coarse mesh T/B substructure model, to appropriately simulate the soil-structure interaction, the basemat plate elements were shifted to the physical bottom of the substructure basemat. To connect the lowered substructure basemat elements, a single row of T/B substructure wall plate elements were modeled extending from the top to the bottom of the basemat. The wall plate elements properties were set to represent those of the basemat.

The Electrical Room substructure plate elements were located at the center of the slab-on-grade vertical dimension. The ESWPT plate elements for the bottom of the tunnel were modeled at the center of the vertical dimension of the tunnel bottom slab, but the elements were located at the same elevation as the bottom of the T/B substructure basemat, elevation -24 feet 7 inches.

The engineered backfill material below the Electrical Room and below the T/B first floor cantilevers was simulated using solid elements. The solid elements were extended to the level of the bottom of the T/B substructure basemat. The properties of the engineered backfill material were a unit weight of 150 pounds per cubic foot, and an elastic modulus developed based on an unconfined compressive strength of 2,500 pound per square inch. The calculated shear wave velocity for this material exceeds the DCD, Revision 2 (Reference 11) minimum requirement of 1,000 feet per second. For the Electrical Room, the solid elements were connected to the concrete slab-on-grade plate elements using springs to allow for movement between the engineered backfill material and the foundation concrete.

After the coarse mesh T/B and Electrical Room substructure model was fully developed in GT STRUDL, the model elements were combined in GT STRUDL to create a single model of the steel superstructure, concrete substructures, and engineered backfill. This combined model was then converted to an ACS SASSI compatible model. To facilitate the SSI analysis of the TI, the ESWPT model was added to the combined T/B and Electrical Room model for analysis in ACS SASSI as shown on Figures 5-3 to 5-8.

The bottom of the ESWPT foundation and the north wall of the T/B and Electrical Room immediately adjacent to the R/B and PS/B are approximately 3 feet 9 inches (elevation -28 feet 4 inches) below the bottom of the remainder of the T/B basemat. This vertical difference was considered insignificant for the SSI analysis; therefore, in the ACS SASSI FE model, the bottom of all portions of the T/B, Electrical Room north wall, and ESWPT were set at the same depth below ground surface as the main portion of the T/B.

The TI model was established in ACS SASSI as a surface structure, ignoring the embedment. In ACS SASSI, interaction nodes were established where all the structural model nodes contacted the subsurface profile. The subsurface profiles described in Section 5.2 were included in the ACS SASSI model for different runs. The SSI analyses were performed using 4 percent material damping for all structure elements.

A parametric study was performed to establish the Radius of Central Zone for the ACS SASSI model. The softest subsurface profile 270-200 was used for the parametric study. Based on the average mesh sizes, the Radius of Central Zone for ESWPT was 3.3 feet and was 11 feet for the T/B and Electrical Room. When the relative displacements of the model were compared using the two Radius of Central Zone values, the ESWPT radius of 3.3 feet generally resulted in larger relative displacements. For cases where the 11 foot radius generated larger displacements, the relative displacements were only slightly larger than the relative displacement for the 3.3 foot radius. For the location where the maximum relative displacements were identified (Node 1440 discussed in Section 7), the estimated relative displacements for the 3.3 foot Radius of Central Zone were larger than those for the 11 foot radius. Based on the parametric study, the 3.3 foot Radius of Central Zone was used for the SSI analysis of both of the subsurface profiles.

Figures 5-3 through 5-8 provide views of the ACS SASSI model used to perform the SSI analyses.

6.0 FINITE ELEMENT MODEL VALIDATION

6.1 Model Validation Methodology

Validation of the FE models was performed to confirm the following:

- The fine mesh and coarse mesh 3-D structural models developed in GT STRUDL respond similarly.
- The fine mesh GT STRUDL models used for structural design responds similarly to the coarse mesh GT STRUDL models translated into ACS SASSI.

A comparison of the response of the fine and coarse mesh T/B and Electrical Room GT STRUDL models was performed to confirm that an increase of element size did not impact the model structural response, i.e., to confirm that the FE mesh of the fine and coarse models both capture the local structural responses and the structural responses of significant modes of vibration. An ESWPT GT STRUDL model with a mesh finer than used for the ACS SASSI analyses was also prepared to confirm that the element size of the ESWPT did not impact the model structural response.

The adequacy of the FE GT STRUDL models was investigated through validation analyses in compliance with the requirements of NUREG-0800 Standard Review Plan 3.7.2 (Reference 9), Subsection 3.7.2.II, which consists of the following:

- A 1g static analysis to compare the structural weight, the mass properties, and the stiffness of the structures between the fine and coarse mesh models.
- Modal analysis to compare the dominant natural frequencies and mass participation factors of the structures between the fine and coarse mesh models.
- Mode superposition transient dynamic analysis to investigate the displacement response for various nodes of the structures between the fine and coarse mesh models.

All of the validation analyses in GT STRUDL were performed with a fixed base condition.

Comparison of the response of the GT STRUDL model having the fine mesh T/B and Electrical Room substructures with the coarse mesh GT STRUDL model was performed to confirm that the local structural responses and the structural responses of significant modes of vibration of the two models were similar. To validate that the structural models were properly translated from GT STRUDL to ACS SASSI, a SSI analysis was performed with the translated structural model resting on a half-space with very high shear wave velocity to simulate a fixed base condition. Relative displacements and response spectra were obtained from the SSI validation analysis in ACS SASSI at selected nodes and were compared to the results obtained from the mode superposition dynamic analysis performed in GT STRUDL.

The following subsections discuss the validation runs performed and provide conclusions regarding the quality of the model.

6.2 1g Static Analysis

The 1g static analysis was performed for both the fine and coarse mesh combined T/B and Electrical Room models, and ESWPT models in GT STRUDL with the fixed base condition. The analysis results for the structural weight of the models, the mass properties, and the stiffness of the structure for each model were then compared.

Table 6-1 presents the seismic weight (combined structure and equipment weight) of the coarse mesh models compared to the fine mesh models. To facilitate the comparison, the structural models are broken-down into components consisting of the T/B and Electrical Room superstructure, T/B and Electrical Room substructures, the T/B and Electrical Room engineered backfill material, and the ESWPT. The ratio of the component weights between the models were close to 1, with ratios between 0.930 and 1.095 indicating good agreement between the models.

For the combined T/B and Electrical Room substructure model, Table 6-2 presents the mass properties of the fine mesh model compared to the coarse mesh model. These properties include the center of mass and mass moment of inertia.

For the ESWPT, Table 6-3 presents the mass properties of the fine mesh model compared to the coarse mesh model. These properties include the center of mass and mass moment of inertia.

For the combined T/B and Electrical Room substructures, and the ESWPT, the comparisons of the mass properties show that the center of mass and mass moment of inertias of the fine and coarse mesh models are comparable.

The stiffness of the fine and coarse mesh structural models was compared in the X, Y, and Z directions under the 1g load condition. For the T/B and Electrical Room, the displacements of three locations were compared. Figures 6-1 through 6-6 show the displacement distribution comparisons for the X, Y, and Z directions of the three locations. The displacement for the fine and coarse mesh models compare well, showing the models respond similarly.

For the ESWPT, the stiffness of the fine and coarse mesh structural models was compared in the X, Y, and Z directions under the 1g load condition at the center of the tunnel length. Figures 6-7 and 6-8 show the displacement distribution comparisons for all three directions of the ESWPT at node 11401 shown on Figure 6-11. The displacement for the fine and coarse mesh models compare well, showing the models respond similarly.

6.3 Modal Analysis

Modal analyses were performed for the fine and coarse mesh T/B and Electrical Room models, and the fine and coarse mesh ESWPT models in GT STRUDL with the fixed base condition. Software and hardware constraints limited the maximum frequencies that could be analyzed using GT STRUDL. For the combined T/B and Electrical Room fine mesh model, the modal analyses could be performed up to a frequency of 21 Hz. For the combined T/B and Electrical Room coarse mesh model, the modal analyses could be performed up to a frequency of 50 Hz. The limitation for the fine mesh model was associated with the current GT STRUDL version and the large model size. For the ESWPT, a separate modal analysis was performed, because the EWSPT is completely separate from the T/B and Electrical Room. The ESWPT modal analysis

could be performed to a frequency of 186 Hz for the fine mesh model, and for the coarse mesh model to a frequency of 165 Hz.

For the T/B and Electrical Room, Figure 6-9 shows the results of modal analyses for the fine and coarse mesh models in the X, Y, and Z directions. For the ESWPT, Figure 6-10 shows the results of modal analyses for the fine and coarse mesh models in the X, Y, and Z directions. The agreement between the dynamic mass participation of the fine and coarse mesh models verifies that the coarse mesh model is adequate to capture the dynamic properties of the structure. The first two to four dominant modal properties for the X, Y and Z direction vibrations for the combined T/B and Electrical Room, and EWSPT are shown on Tables 6-4 through 6-6, respectively.

6.4 Mode-Superposition Transient Dynamic Analysis

Mode-superposition method was used to perform the time-history analysis in GT STRUDL for the fine and coarse mesh models, with a constant 4 percent modal damping applied to all modes. The ACS SASSI analysis only allows one component input motion for each run; therefore, to allow comparison, the mode-superposition analyses in the GT STRUDL were performed in the same manner. Both the GT STRUDL analysis and the ACS SASSI analysis were performed for the fixed base condition. The ACS SASSI analysis was performed for a cut-off frequency of 50 Hz for comparison to the coarse mesh GT STRUDL model of the combined T/B and Electrical Room, and both the fine and coarse mesh GT STRUDL models of the ESWPT. For the fine mesh GT STRUDL model of the combined T/B and Electrical Room, 21 Hz was the maximum frequency that could be achieved during modal analysis because of the large model size and the limitation of the current GT STRUDL version. The ACS SASSI analysis results were extracted for the 21 Hz cut-off frequency for comparison with the fine mesh GT STRUDL model of the combined T/B and Electrical Room.

Relative displacement time histories were compared between the ACS SASSI results and the GT STRUDL results of the fine mesh combined T/B and Electrical Room, and ESWPT models. The nodes where the comparisons are presented are shown on Figure 6-11. The relative displacement time histories of the selected nodes for GT STRUDL and ACS SASSI are compared in Figures 6-12 through 6-16 and the maximum relative displacements are compared for the selected nodes in Table 6-7 through 6-9. Both the relative displacement time histories and the maximum relative displacements agree well between GT STRUDL and ACS SASSI, indicating the ASC SASSI model represents the fine mesh GT STRUDL model well.

For comparison of response spectra from the GT STRUDL mode-superposition analyses, the ACS SASSI results were extracted for the 21 and 50 Hz cut-off frequencies. The response spectra for the GT STRUDL and ACS SASSI analyses were compared between the following:

- The fine mesh GT STRUDL model and the ACS SASSI model.
- The coarse mesh GT STRUDL model and the ACS SASSI model.
- The fine mesh GT STRUDL model and the coarse mesh GT STRUDL model.

The nodes where the comparisons are presented are shown on Figure 6-11. The response spectra for the T/B and Electrical Room fine mesh GT STRUDL model, the T/B and Electrical Room coarse mesh GT STRUDL model, and ACS SASSI model for select nodes are compared in Figures 6-17 through 6-19. Overall for the combined T/B and Electrical Room, at frequencies

less than 21 Hz, good agreement was observed between the response spectra for all models, indicating that the mesh size was not impacting the results, and the ACS SASSI model accurately represented the dynamic properties of the fine mesh model used for structural design. At higher frequencies, the results for the fine mesh GT STRUDL model with a cut-off frequency of 21 Hz matches well with the results of the ACS SASSI results with a cut-off frequency of 21 Hz, and the coarse mesh GT STRUDL and ACS SASSI models that reached a 50 Hz cut-off frequency also matched well. The results for the models with a cut-off frequency of 21 Hz do not match with the models with a cut-off frequency of 50 Hz at higher frequencies, because contributions greater than 21 Hz are not represented in the models with a cut-off frequency of 21 Hz.

The response spectra for the ESWPT fine mesh GT STRUDL model, the ESWPT coarse mesh GT STRUDL model, and ACS SASSI model for Node 11401 are compared in Figure 6-20. Overall for the ESWPT, good agreement was observed between the response spectra for all models, indicating that the mesh size was not impacting the results, and the ACS SASSI model accurately represented the dynamic properties of the fine mesh model used for structural design.

7.0 ANALYSIS RESULTS

The results of the analyses performed are discussed in this section.

7.1 Soil-Structure Interaction Analysis Results

The SSI analysis results are provided as the maximum relative displacements at the selected nodes of the TI that are obtained from the analysis of the two generic layered subsurface profiles. The maximum relative displacements were computed with respect to the input ground surface motion in the free-field.

7.1.1 Approaches for Developing Maximum Relative Displacement

The relative displacements of select TI nodes with respect to the ground surface motion in the free-field were calculated using the ACS SASSI RELDISP module. The RELDISP module computes nodal relative displacements based on a direct analytical approach in complex frequency domain. A reference node in the free-field was defined for computing the displacements relative to the free-field ground motion. Before computing the displacements relative to the free-field ground motion, the absolute acceleration transfer functions at the reference node and the select TI nodes were computed using ACS SASSI MOTION module.

The relative displacements using the RELDISP module are computed using the following steps:

- Define the reference node and the select TI nodes where the displacements relative to the free-field ground motion are to be determined.
- Compute acceleration transfer functions relative to the reference node using the absolute acceleration transfer functions computed for the select nodes with the ACS SASSI MOTION module.
- Compute the relative displacement transfer functions directly from the relative acceleration transfer functions.
- Compute the relative displacement response in frequency domain by convolution between the relative displacement transfer functions and the Fourier transform of the input acceleration time history (control motion).
- Compute the relative displacement time histories from the relative displacements in frequency domain using the inverse Fourier transformation.
- Compute the combined relative displacement time histories in a particular direction, X, Y or Z using time domain superposition of the co-directional effects computed for each seismic motion directional input in the X, Y or Z directions.
- Obtain the maximum relative displacement for each subsurface profile from the combined displacement time histories. The final maximum relative displacement is the maximum relative displacements of the two generic subsurface profiles.

7.1.2 Results of Maximum Relative Displacements

To investigate the TI dynamic behavior in terms of the maximum relative displacements, 24 node locations were selected. These 24 nodes were selected at key locations of interest within the TI as show in Figure 7-1. With the exception of Nodes 1581, 2570, 3261, and 3311 located at the top of the T/B superstructure, the nodes shown in Figure 7-1 are located immediately adjacent to the R/B and PS/B.

Prior to computing the displacements, acceleration transfer functions were plotted for the selected nodes and reviewed to check if the number of frequencies included in the SSI analyses were sufficient to obtain accurate results for the relative displacements. Figures 7-2 through 7-21 show the acceleration transfer function amplitudes for 10 of the 24 selected nodes for subsurface profiles 270-200 and 2032-100. The acceleration transfer function un-interpolated (TFU) values plotted in Figures 7-2 through 7-21 are the calculated amplitudes at frequencies where SSI analyses were performed; while the acceleration transfer function interpolated (TFI) line was developed by interpolation between the TFU values. The good agreement between the trend of the TFI and the TFU values at each SSI frequency indicates that sufficient frequencies were included in the SSI analysis to appropriately represent the acceleration transfer function, which will result in accurate results for the relative displacements. The TFI and the TFU for the remaining 14 nodes show similar levels of agreement.

Figures 7-2 through 7-21 also show the relative displacement time histories for 10 of the 24 selected nodes for subsurface profiles 270-200 and 2032-100. The plots show the relative displacement time histories vibrating along the zero displacement value without any drift, which indicates that the relative displacement time histories were computed correctly.

Table 7-1 shows the SSI computed maximum relative displacements in the Y (north-south) direction at the 24 selected TI locations with respect to the free-field input ground surface motion for subsurface profiles 270-200 and 2032-100. The relative displacements for the two subsurface profiles in the Y direction (north-south) range from 0.004 inch at the bottom of the Electrical Room north wall at nodes 933, 940, and 957 to 4.46 inches at node 3261 located at the top of the south end of the T/B superstructure. The maximum TI displacements, immediately adjacent to the R/B and PS/B, occurred at the T/B second floor at Elevation 60.5 feet and at the roof top of the Electrical Room at Elevation 63.5 feet. The node numbers at these elevations are shown in Figure 7-1, and are 972, 1440, and 1473 for the T/B, and 5041 and 5111 for the Electrical Room. The maximum relative displacement of all these nodes in the Y direction (north-south) in Table 7-1 is 2.32 inches near the middle of the T/B at node 1440.

7.1.3 Evaluation of 4 inch Space

To evaluate the sufficiency of the 4 inch space between the TI, and the R/B and PS/B, the absolute value of the maximum TI, and R/B and PS/B displacements were considered. The excess space available was calculated with the following:

- Using the maximum absolute values of the relative displacements of the T/B, Electrical Room, R/B, and PS/B.
- Assuming the maximum relative displacements of the TI, and the R/B and PS/B are simultaneous.
- Assuming the maximum relative displacements of the TI, and the R/B and PS/B are in opposite phase.

Immediately adjacent to the R/B and PS/B, the maximum relative displacement with respect to free-field input ground surface motion of the TI in the north-south direction is 2.32 inch, which occurs at the T/B second floor node 1440 at Elevation 60.5 feet (see Figure 7-1). For the R/B and the PS/B, greater north-south displacement occurs at the R/B (Reference 4); therefore, R/B displacements are used to evaluate the 4 inch space. Using Reference 10, the maximum relative displacement with respect to free-field input ground surface motion of the R/B at Elevation 60.5 feet is approximately 0.92 inches.

The excess space available if the maximum T/B and R/B displacements occur toward each other is as follows:

Excess Space Available = 4 inch (space between T/B, and R/B and PS/B) - 2.32 inch (absolute value of T/B maximum displacement) - 0.92 inch (absolute value of R/B maximum displacement)

Excess Space Available = 0.76 inch

As the excess space available is positive, the TI will not contact the R/B or PS/B during a SSE.

The possibility of having a calculated excess space available less than 0.76 inch is considered unlikely for the following reasons:

- The CSDRS compatible motions were applied at the base of the T/B. The CSDRS compatible motions are free-field motions at the ground surface, which are larger than the motions that would occur at the base of the T/B that is located 27 feet 2 inches below the ground surface.

- The SSI was performed for the T/B as a surface structure; however, the T/B is embedded 27 feet 2 inches into the ground. The soil surrounding the structure will act to restrain the movement of the T/B, thereby reducing the displacements.

- The maximum relative displacements of the TI, and the R/B and PS/B are assumed to be simultaneous and in the opposite phase. The possibility for the maximum displacements between the two structures occurring at the same time in opposite directions is considered to be extremely unlikely.

7.2 SSE Steel Member Stress Ratios

The T/B and Electrical Room were modeled and analyzed in GT STRUDL, Version 30.0 using the CSDRS compatible time history input motions developed for the 0.3g SSE, which is in accordance with DCD, Revision 2 (Reference 11). The design was performed in accordance with the requirements of AISC N690-1994 (R2004) (Reference 6) and DCD, Revision 2 (Reference 11). Both plate and rolled steel members for the superstructure have an allowable yield stress of 50 kips per square inch (American Society for Testing and Materials [ASTM] A992/ASTM A572, GR 50).

The stress ratio was calculated as the member stress from GT STRUDL or ACS SASSI divided by the allowable member stress. For all the members, the stress ratio is less than or equal to 1.0, indicating that the calculated member stresses are less than or equal to the allowable member stresses.

7.3 Turbine Building and Electrical Room Sliding and Overturning Analysis

Overturning and sliding of the T/B and Electrical Room in the Y (north-south) direction were evaluated for lateral loads applied to the foundation through external environmental loads such as wind, tornado, and seismic. Overturning and sliding in the X (east-west) direction is not discussed, because movement in the X (east-west) direction does not impact the 4 inch space between the TI, and the R/B and PS/B.

The resistance to sliding is provided by friction at the base and sides of the substructures. The factors of safety against sliding for the T/B and Electrical Room are provided in Table 7-2. For three load combinations listed in the table, the factors of safety against sliding all meet or exceed the requirements of Standard Review Plan 3.8.5 (Reference 12).

Lateral loads acting on the T/B and Electrical Room can result in overturning moments on the foundation when they act above the bottom of the substructure. Overturning moments are resisted by the weight of the steel, concrete, and other vertical loads in the structure which produce a counteracting moment about the axis of rotation (edge about which the foundation rotates).

The overturning moment about the northwest and southeast corners of the T/B basemat was estimated using the LIST REACTIONS command in GT STRUDL. Moments about the northwest corner give rotations about the north and west edges of the T/B basemat, while moments about the southeast corner give rotations about the south and east edges of the T/B basemat. Once the controlling load combination was identified, the moments of each of the load components about the respective corner was determined and identified as an overturning or resisting moment. A similar approach was used for the Electrical Room.

The factors of safety against overturning for the T/B and Electrical Room are provided in Table 7-3. For the three load combinations, the factors of safety against sliding all meet or exceed the requirements of Standard Review Plan 3.8.5 (Reference 12).

8.0 CONCLUSIONS

Where the TI is immediately adjacent to the R/B and PS/B, the maximum relative displacement with respect to free-field input ground surface motion of the TI toward the R/B and PS/B is 2.32 inch at elevation 60.5 feet. At the same elevation, the maximum displacement of the R/B and PS/B toward the TI is 0.92 inches. With the 4 inch space between the TI, and the R/B and PS/B, this leaves 0.76 inch of excess space between the TI, and the R/B and PS/B during a SSE. Therefore, it is concluded that the 4 inch space between the TI, and R/B and PS/B is sufficient to prevent contact between the buildings during a SSE.

The member stress ratios calculated with GT STRUDL and ACS SASSI are all less than or equal to 1, showing that the structural members are not overstressed.

For the load combinations considered, the factors of safety against sliding and overturning in the Y (north-south) direction all meet or exceed the requirements of Standard Review Plan 3.8.5 (Reference 12).

9.0 REFERENCES

1. Seismic Design Parameters, NUREG-0800 Section 3.7.1, Revision 3, U.S. Nuclear Regulatory Commission, Washington DC, March 2007.

2. ACS SASSI NQA Version 2.3.0, Users Manuals, Revision 2, Ghiocel Predictive Technologies, Inc., November 10, 2009.

3. Seismic Design Bases of the US-APWR Standard Plant, MUAP-10001, Revision 1, Mitsubishi Heavy Industries, Ltd., May 2010.

4. Soil Structure Interaction Analysis and Results for the US-APWR Standard Plant, MUAP-10006, Revision 0, Mitsubishi Heavy Industries, Ltd, April 2010.

5. Protection Against Low-Trajectory Turbine Missiles, Regulatory Guide 1.115, Revision 1, U.S. Nuclear Regulatory Commission, Washington DC, July 1977.

6. Specification for the Design, Fabrication and Erection of Steel Safety-Related for Nuclear Facilities, ANSI/AISC N690-1994 (R2004), American Institute of Steel Construction, October 2004.

7. Code Requirements for Nuclear Safety-Related Concrete Structures and Commentary, ACI 349-01/349R-01, American Concrete Institute, January 2001.

8. Seismic Analysis of Safety-Related Nuclear Structures and Commentary, ASCE 4-98, American Society of Civil Engineers, 2000.

9. Seismic System Analysis, NUREG-0800 Section 3.7.2, Revision 3, U.S. Nuclear Regulatory Commission, Washington, DC, March 2007.

10. Black & Veatch, Request for Information, Request No.: MHI-RFI-2010-0094, Revision 0, Subject: Deflection of Nuclear Island Structures, File No.: 164475.18.9270, Date Requested: 9/15/2010.

11. Design Control Document for the US-APWR, Revision 2, Mitsubishi Heavy Industries, LTD, October 2009.

12. Foundations, NUREG-0800 Section 3.8.5, Revision 2, U.S. Nuclear Regulatory Commission, Washington, DC, March 2007.

13. Comparison T/B Height in the Analysis with DCD

Table 5-1. Strain Compatible Dynamic Properties for Generic Subsurface Profile 270-200 for the Turbine Island SSI Analyses

Turbine Island Layering	Thickness (feet)	Total Unit Weight (kcf)	Shear Wave Velocity (feet/second)	Compression Wave Velocity (feet/second)	Damping for Shear Wave	Damping for Compression Wave
1	4.50	0.125	1323.6	5624.7	0.0256	0.0256
2	4.29	0.125	1280.1	5506.6	0.0288	0.0288
3	4.29	0.125	1280.1	5506.6	0.0288	0.0288
4	4.29	0.125	1302.1	5644.4	0.0303	0.0303
5	4.29	0.125	1302.1	5644.4	0.0303	0.0303
6	4.29	0.125	1334.0	5800.0	0.0313	0.0313
7	4.29	0.125	1334.0	5800.0	0.0313	0.0313
8	4.29	0.125	1334.0	5800.0	0.0313	0.0313
9	4.29	0.125	1303.4	5709.7	0.0334	0.0334
10	4.29	0.125	1303.4	5709.7	0.0334	0.0334
11	4.29	0.125	1334.7	5870.9	0.0339	0.0339
12	4.29	0.125	1334.7	5870.9	0.0339	0.0339
13	4.29	0.125	1372.1	6038.2	0.0341	0.0341
14	4.69	0.125	1361.6	6029.7	0.0262	0.0262
15	4.69	0.125	1361.6	6029.7	0.0262	0.0262
16	4.69	0.125	1416.5	6264.9	0.0258	0.0258
17	4.69	0.125	1416.5	6264.9	0.0258	0.0258
18	4.69	0.125	1450.0	6404.8	0.0260	0.0260
19	4.69	0.125	1450.0	6404.8	0.0260	0.0260
20	4.69	0.125	1456.1	6451.5	0.0265	0.0265
21	4.69	0.125	1456.1	6451.5	0.0265	0.0265
22	4.69	0.125	1434.5	6390.9	0.0277	0.0277
23	4.69	0.125	1434.5	6390.9	0.0277	0.0277
24	4.69	0.125	1415.8	6325.4	0.0287	0.0287
25	4.69	0.125	1415.8	6325.4	0.0287	0.0287
26	5.00	0.131	1482.5	6570.7	0.0273	0.0273
27	5.00	0.131	1482.5	6570.7	0.0273	0.0273
28	5.00	0.131	1493.9	6636.0	0.0276	0.0276
29	5.00	0.131	1493.9	6636.0	0.0276	0.0276
30	5.00	0.131	1534.4	6803.8	0.0274	0.0274
31	5.00	0.131	1534.4	6803.8	0.0274	0.0274
32	5.00	0.131	1541.7	6855.2	0.0278	0.0278
33	5.00	0.131	1541.7	6855.2	0.0278	0.0278
34	5.00	0.131	1598.6	7089.6	0.0272	0.0272
35	5.00	0.131	1598.6	7089.6	0.0272	0.0272
36	5.00	0.131	1543.7	6888.2	0.0286	0.0286
37	5.00	0.131	1543.7	6888.2	0.0286	0.0286
38	12.50	0.134	3317.2	7812.2	0.0050	0.0050
39	12.50	0.134	3317.2	7812.2	0.0050	0.0050
40	12.50	0.134	3317.2	7812.2	0.0050	0.0050
41	12.50	0.134	3317.2	7812.2	0.0050	0.0050
42	12.50	0.134	3317.2	7812.2	0.0050	0.0050
43	12.50	0.134	3317.2	7812.2	0.0050	0.0050

Table 5-1. Strain Compatible Dynamic Properties for Generic Subsurface Profile 270-200 for the Turbine Island SSI Analyses

Turbine Island Layering	Thickness (feet)	Total Unit Weight (kcf)	Shear Wave Velocity (feet/second)	Compression Wave Velocity (feet/second)	Damping for Shear Wave	Damping for Compression Wave
44	12.50	0.134	3317.2	7812.2	0.0050	0.0050
45	12.50	0.134	3317.2	7812.2	0.0050	0.0050
46	12.50	0.134	3317.2	7812.2	0.0050	0.0050
47	12.50	0.134	3317.2	7812.2	0.0050	0.0050
48	12.50	0.134	3317.2	7812.2	0.0050	0.0050
49	12.50	0.134	3317.2	7812.2	0.0050	0.0050
50	12.50	0.134	3317.2	7812.2	0.0050	0.0050
51	12.50	0.134	3317.2	7812.2	0.0050	0.0050
52	12.50	0.134	3317.2	7812.2	0.0050	0.0050
53	12.50	0.134	3317.2	7812.2	0.0050	0.0050
54	12.50	0.134	3317.2	7812.2	0.0050	0.0050
55	12.50	0.134	3317.2	7812.2	0.0050	0.0050
56	12.50	0.134	3317.2	7812.2	0.0050	0.0050
57	12.50	0.134	3317.2	7812.2	0.0050	0.0050
58	12.50	0.134	3317.2	7812.2	0.0050	0.0050
59	12.50	0.134	3317.2	7812.2	0.0050	0.0050
60	12.50	0.134	3317.2	7812.2	0.0050	0.0050
61	12.50	0.134	3317.2	7812.2	0.0050	0.0050
62	12.50	0.134	3317.2	7812.2	0.0050	0.0050
63	12.50	0.134	3317.2	7812.2	0.0050	0.0050
64	12.50	0.134	3317.2	7812.2	0.0050	0.0050
65	12.50	0.134	3317.2	7812.2	0.0050	0.0050
66	12.50	0.134	3317.2	7812.2	0.0050	0.0050
67	12.50	0.134	3317.2	7812.2	0.0050	0.0050
68	12.50	0.134	3317.2	7812.2	0.0050	0.0050
69	12.50	0.134	3317.2	7812.2	0.0050	0.0050
70	12.50	0.134	3317.2	7812.2	0.0050	0.0050
71	12.50	0.134	3317.2	7812.2	0.0050	0.0050
72	12.50	0.134	3317.2	7812.2	0.0050	0.0050
73	12.50	0.134	3317.2	7812.2	0.0050	0.0050
74	12.50	0.134	3317.2	7812.2	0.0050	0.0050
Half-Space		0.134	3317.2	7812.2	0.0050	0.0050

kcf: kips per cubic foot

Table 5-2. Strain Compatible Dynamic Properties for Generic Subsurface Profile 2032-100 for the Turbine Island SSI Analyses

Turbine Island Layering	Thickness (feet)	Total Unit Weight (kcf)	Shear Wave Velocity (feet/second)	Compression Wave Velocity (feet/second)	Damping for Shear Wave	Damping for Compression Wave
1	6.17	0.140	6315.1	11044.0	0.0323	0.0323
2	6.66	0.140	6548.4	11343.0	0.0323	0.0323
3	10.00	0.140	7126.0	12343.0	0.0316	0.0316
4	16.67	0.140	7332.7	12701.0	0.0316	0.0316
5	16.67	0.140	7746.3	13417.0	0.0316	0.0316
6	16.66	0.140	8127.5	14077.0	0.0316	0.0316
7	30.00	0.157	8599.3	16794.0	0.0050	0.0050
8	30.00	0.157	8599.3	16794.0	0.0050	0.0050
9	30.00	0.157	8599.3	16794.0	0.0050	0.0050
10	30.00	0.157	8599.3	16794.0	0.0050	0.0050
11	30.00	0.157	8599.3	16794.0	0.0050	0.0050
12	30.00	0.157	8599.3	16794.0	0.0050	0.0050
13	30.00	0.157	8599.3	16794.0	0.0050	0.0050
14	30.00	0.157	8599.3	16794.0	0.0050	0.0050
15	30.00	0.157	8599.3	16794.0	0.0050	0.0050
16	30.00	0.157	8599.3	16794.0	0.0050	0.0050
17	30.00	0.157	8599.3	16794.0	0.0050	0.0050
18	30.00	0.157	8599.3	16794.0	0.0050	0.0050
19	30.00	0.157	8599.3	16794.0	0.0050	0.0050
20	30.00	0.157	8599.3	16794.0	0.0050	0.0050
21	30.00	0.157	8599.3	16794.0	0.0050	0.0050
22	30.00	0.157	8599.3	16794.0	0.0050	0.0050
23	30.00	0.157	8599.3	16794.0	0.0050	0.0050
24	30.00	0.157	8599.3	16794.0	0.0050	0.0050
25	30.00	0.157	8599.3	16794.0	0.0050	0.0050
26	30.00	0.157	8599.3	16794.0	0.0050	0.0050
Half-Space		0.157	8599.3	16794.0	0.0050	0.0050

kcf: kips per cubic foot

Table 6-1. Seismic Weight of the Turbine Building, Electrical Room and Essential Service Water Pipe Tunnel Finite Element Models

Structural Component	Seismic Weight (kips)		Ratio (1)/(2)
	Fine Mesh(1)	Coarse Mesh(2)	
Superstructure – T/B and Electrical Room	97,960	97,960	1.0000
T/B Substructure	114,313	104,357	1.0954
Electrical Room Substructure	14,967	15,116	0.9901
T/B Engineered Backfill	25,089	25,067	1.0009
Electrical Room Engineered Backfill	39,037	41,997	0.9295
Total T/B and Electrical Room	291,366	284,497	1.0241
ESWPT	11,310	11,310	1.0000

Table 6-2. Mass Properties of the Combined Turbine Building and Electrical Room Finite Element Models

Model Direction	Mass Center Coordinates (feet)		Mass Moment of Inertia about the Center of Mass (kip-feet-second^2)		
	Fine Mesh	Coarse Mesh	Fine Mesh(1)	Coarse Mesh(2)	Ratio (1)/(2)
X	126.9	125.2	113,555,000	113,415,000	1.0012
Y	-187.7	-186.9	60,083,000	61,573,000	0.9758
Z	32.63	32.00	130,896,000	131,449,000	0.9958

Table 6-3. Mass Properties of the Essential Service Water Pipe Tunnel Finite Element Models

Model Direction	Mass Center Coordinates (feet)		Mass Moment of Inertia about Center of Mass (kip-feet-second^2)		
	Fine Mesh	Coarse Mesh	Fine Mesh(1)	Coarse Mesh(2)	Ratio (1)/(2)
X	130.6	130.7	23,640	21,780	1.0854
Y	-13.7	-13.7	2,111,390	2,030,060	1.0401
Z	-15.1	-14.6	2,122,230	2,041,270	1.0397

Table 6-4. Modal Properties of Dominant Modes X Direction (East-West) of Fine Mesh GT STRUDL Model

Mode	Frequency (Hz)	Period (second)	Participation Factor (percent)	Effective Mass (kips-second^2/foot)
Combined T/B and Electrical Room				
6	1.24	0.804	28.5	2,041
70	2.42	0.413	2.49	178
121	2.92	0.343	1.39	99
180	3.46	0.289	0.83	60
ESWPT				
40	47.5	0.210	30.5	73.3
45	50.6	0.0198	24.5	58.9

Table 6-5. Modal Properties of Dominant Modes Y Direction (North-South) of Fine Mesh GT STRUDL Model

Mode	Frequency (Hz)	Period (second)	Participation Factor (percent)	Effective Mass (kips-second^2/foot)
Combined T/B and Electrical Room				
39	1.70	0.590	19.0	1,360
96	2.62	0.382	2.27	163
42	1.76	0.567	2.15	154
155	3.26	0.307	2.01	144
ESWPT				
1	7.67	0.130	79.8	192
56	53.8	0.0186	3.05	7.30

Table 6-6. Modal Properties of Dominant Modes Z Direction (Vertical) of Fine Mesh GT STRUDL Model

Mode	Frequency (Hz)	Period (second)	Participation Factor (percent)	Effective Mass (kips-second^2/foot)
Combined T/B and Electrical Room				
108	2.75	0.364	1.89	135
240	3.87	0.258	1.70	122
312	4.22	0.237	1.19	85
223	3.76	0.266	1.01	72
ESWPT				
90	66.0	0.0152	7.85	18.9
96	68.3	0.0146	7.50	18.0

Table 6-7. Maximum Displacements in X Direction (East-West) Due to X Direction Ground Motion

Selected Nodes	Maximum Displacement[1] (inches)		Ratio[2] (1)/(2)
	GT STRUDL (1)	ACS SASSI (2)	
560	0.0134	0.0136	0.98
972	1.1212	1.0969	1.02
1473	1.1598	1.1533	1.01
5041	0.6562	0.6608	0.99
11401	0.0018	0.0017	1.04

Notes:
[1] Maximum displacements are rounded.
[2] The ratio is based on unrounded values in columns 1 and 2.

Table 6-8. Maximum Displacements in Y Direction (North-South) Due to Y Direction Ground Motion

Selected Nodes	Maximum Displacement[1] (inches)		Ratio[2] (1)/(2)
	GT STRUDL (1)	ACS SASSI (2)	
560	0.0110	0.0152	0.73
972	0.9165	0.9427	0.97
1473	0.7980	0.7925	1.01
5041	1.0018	0.8468	1.18
11401	0.1722	0.1897	0.91

Notes:
[1] Maximum displacements are rounded.
[2] The ratio is based on unrounded values in columns 1 and 2.

Table 6-9. Maximum Displacements in Z Direction (Vertical) Due to Z Direction Ground Motion

Selected Nodes	Maximum Displacement[1] (inches)		Ratio[2] (1)/(2)
	GT STRUDL (1)	ACS SASSI (2)	
560	0.0050	0.0046	1.08
972	0.0227	0.0208	1.09
1473	0.0207	0.0177	1.17
5041	0.0240	0.0209	1.15
11401	0.0005	0.0005	0.92

Notes:
[1] Maximum displacements are rounded.
[2]The ratio is based on unrounded values in columns 1 and 2.

Table 7-1. Maximum Relative Displacement for Y Direction (North-South) Relative to Free-Field Input Motion

Node	Displacements from ACS SASSI Profile 270-200 (inches)	Displacements from ACS SASSI Profile 2032-100 (inches)
290	0.22	0.02
386	0.27	0.06
560	0.23	0.03
879	0.29	0.07
908	0.22	0.02
933	0.10	0.004
939	0.15	0.005
940	0.15	0.004
946	0.16	0.005
957	0.12	0.004
972	1.07	1.13
1385	0.50	0.40
1440	2.32	2.12
1441	1.27	0.97
1473	1.17	0.81
1474	0.60	0.32
1581	4.29	3.65
2570	3.85	3.12
3261	4.46	3.84
3311	3.50	2.81
5041	1.42	1.05
5042	0.66	0.40
5111	1.39	0.97
5112	1.14	0.78

Table 7-2. Sliding Factor of Safety

DCD Load Combinations	Calculated Sliding Factor of Safety	Required Factor of Safety per Standard Review Plan 3.8.5
Turbine Building		
D + H + W	2.5	1.5
D + H + W_t	2.1	1.1
D + H + E'	1.1	1.1
Electrical Room		
D + H + W	14.4	1.5
D + H + W_t	8.6	1.1
D + H + E'	1.9	1.1

Abbreviations:
D – Dead Load
H – Load due to lateral earth and groundwater pressure
W – Wind Load
W_t - Tornado Load
E' – SSE Load

Table 7-3. Overturning Factor of Safety

DCD Load Combinations	Calculated Overturning Factor of Safety	Required Factor of Safety per Standard Review Plan 3.8.5
Turbine Building		
D + H + W	14.1	1.5
D + H + W_t	10.6	1.1
D + H + E'	2.4	1.1
Electrical Room		
D + H + W	28.5	1.5
D + H + W_t	20.0	1.1
D + H + E'	4.1	1.1

Abbreviations:
D – Dead Load
H – Load due to lateral earth and groundwater pressure
W – Wind Load
W_t - Tornado Load
E' – SSE Load

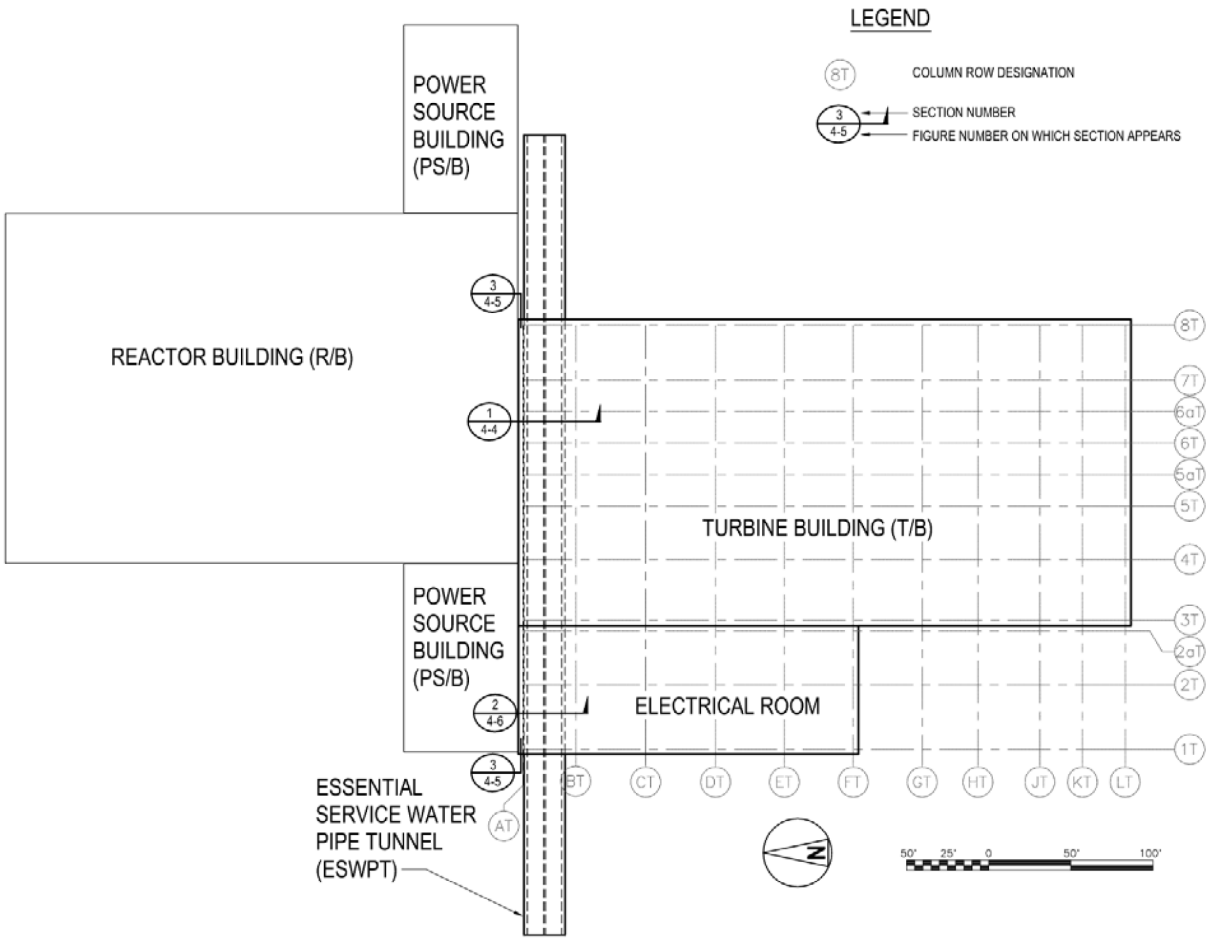

Figure 4-1. Plan Arrangement of Turbine Island and Adjacent Reactor Building and Power Source Buildings

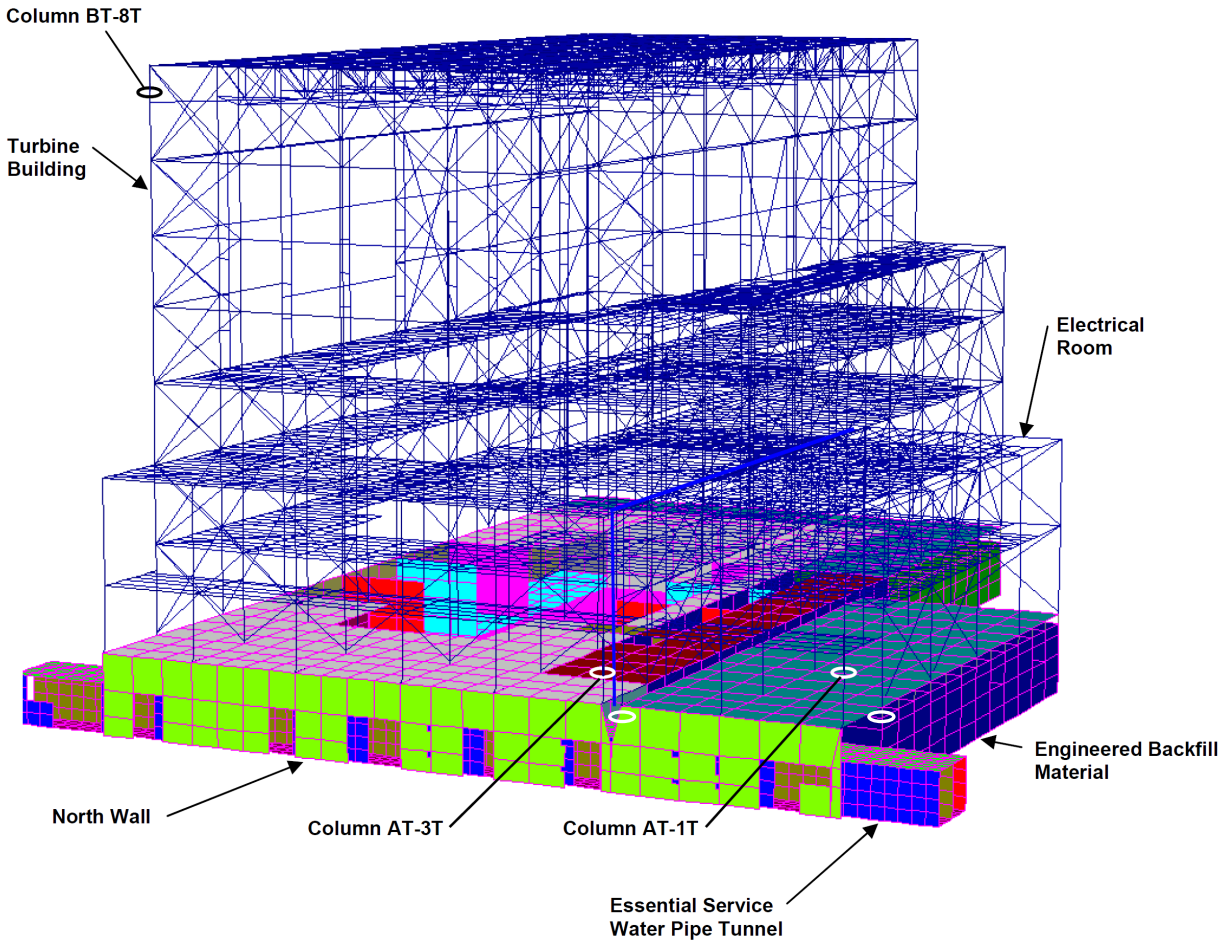

Figure 4-2. Turbine Island Configuration – Elevation View Looking Southeast

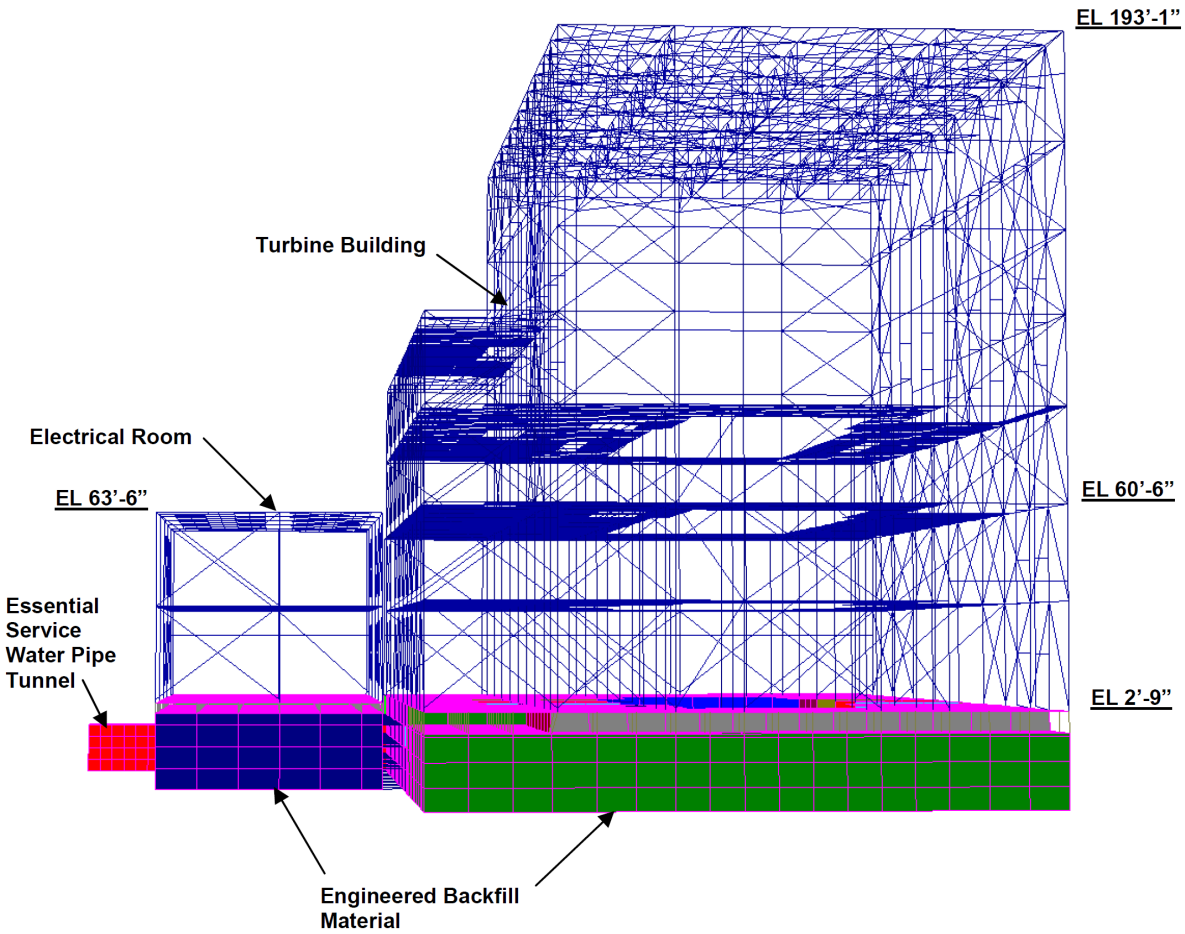

Figure 4-3. Turbine Island Configuration – Elevation View Looking North

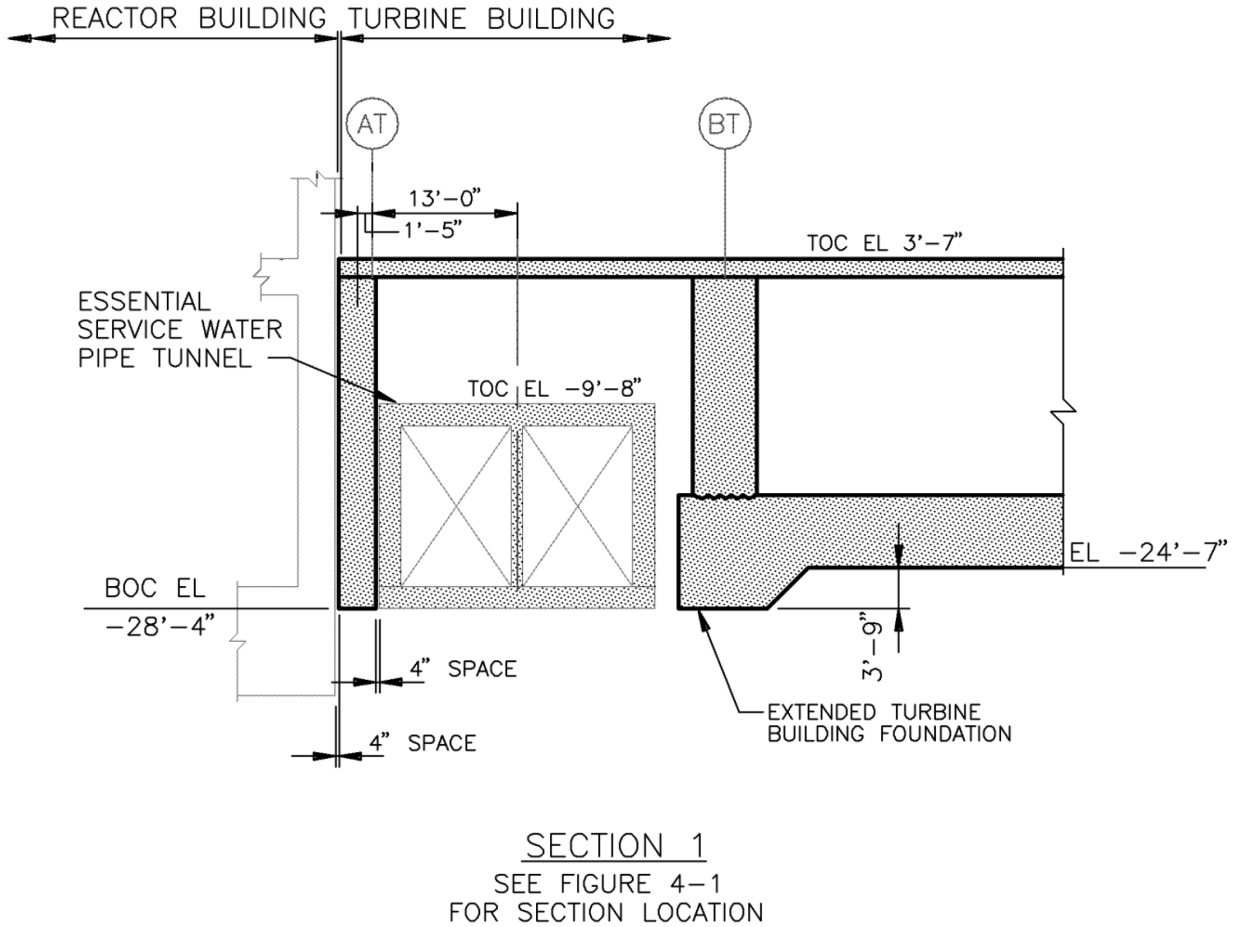

Figure 4-4. Cross Section Through Turbine Building and Essential Services Water Pipe Tunnel

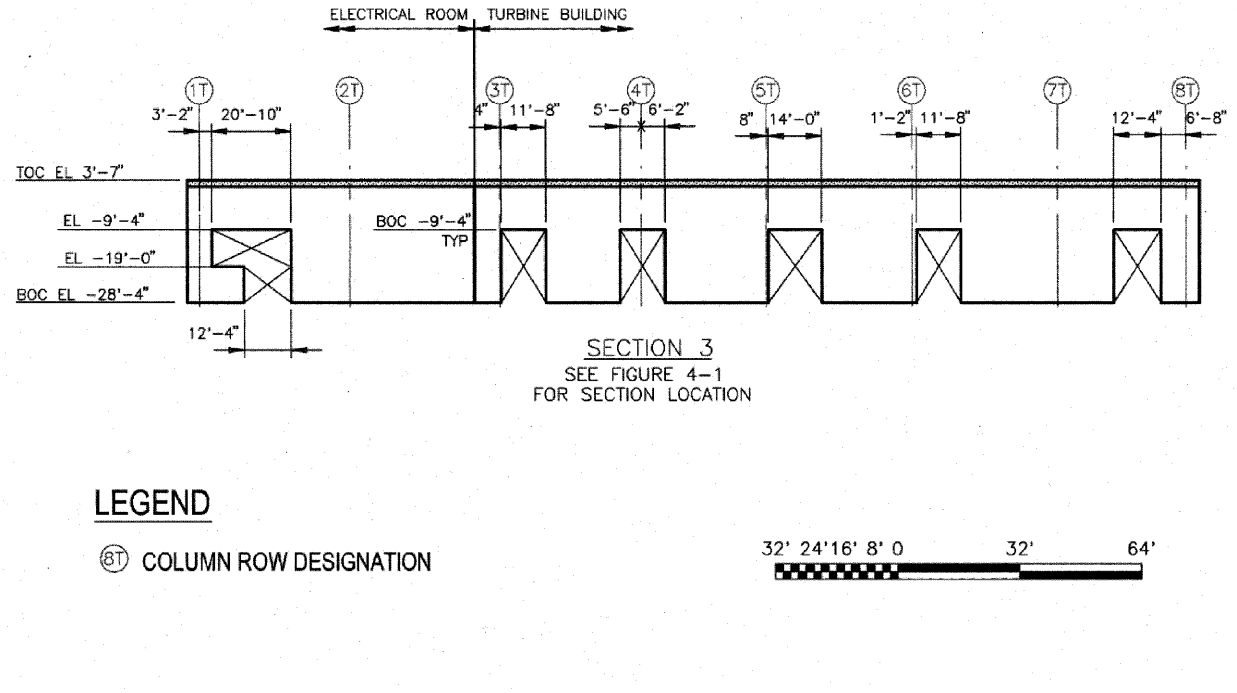

Figure 4-5. Cross Section Through North Walls of Turbine Building and Electrical Room

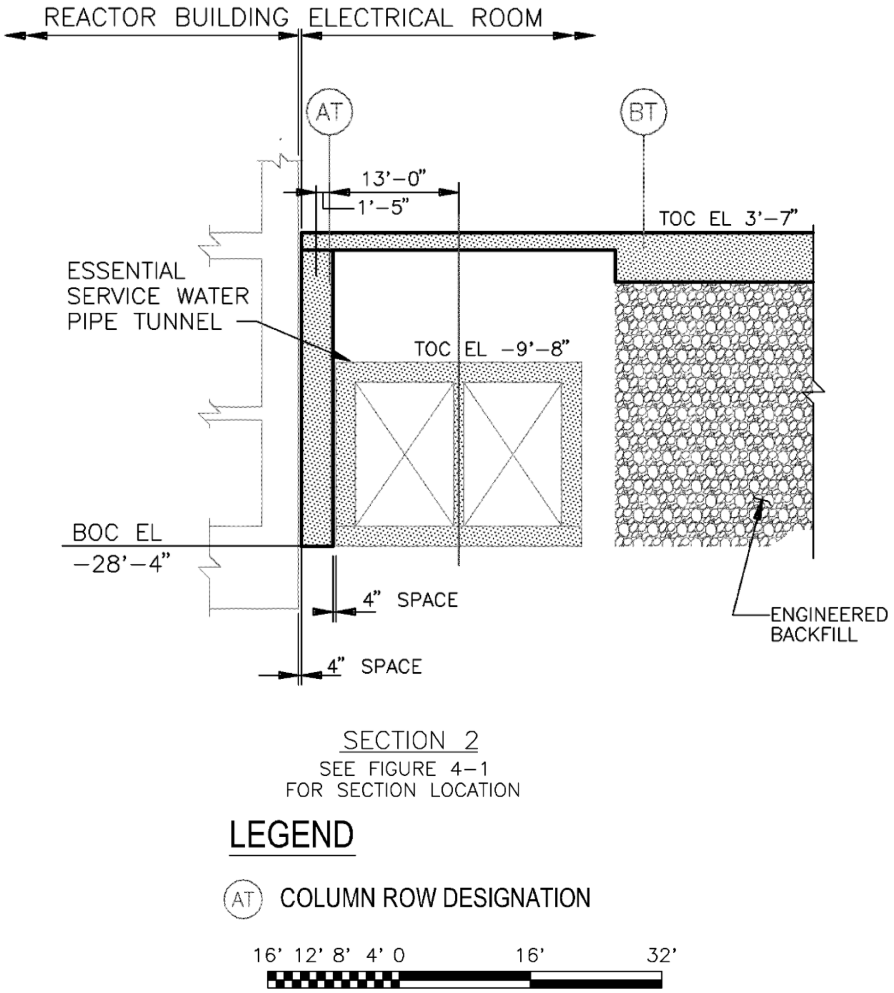

Figure 4-6. Cross Section Through Electrical Room and Essential Services Water Pipe Tunnel

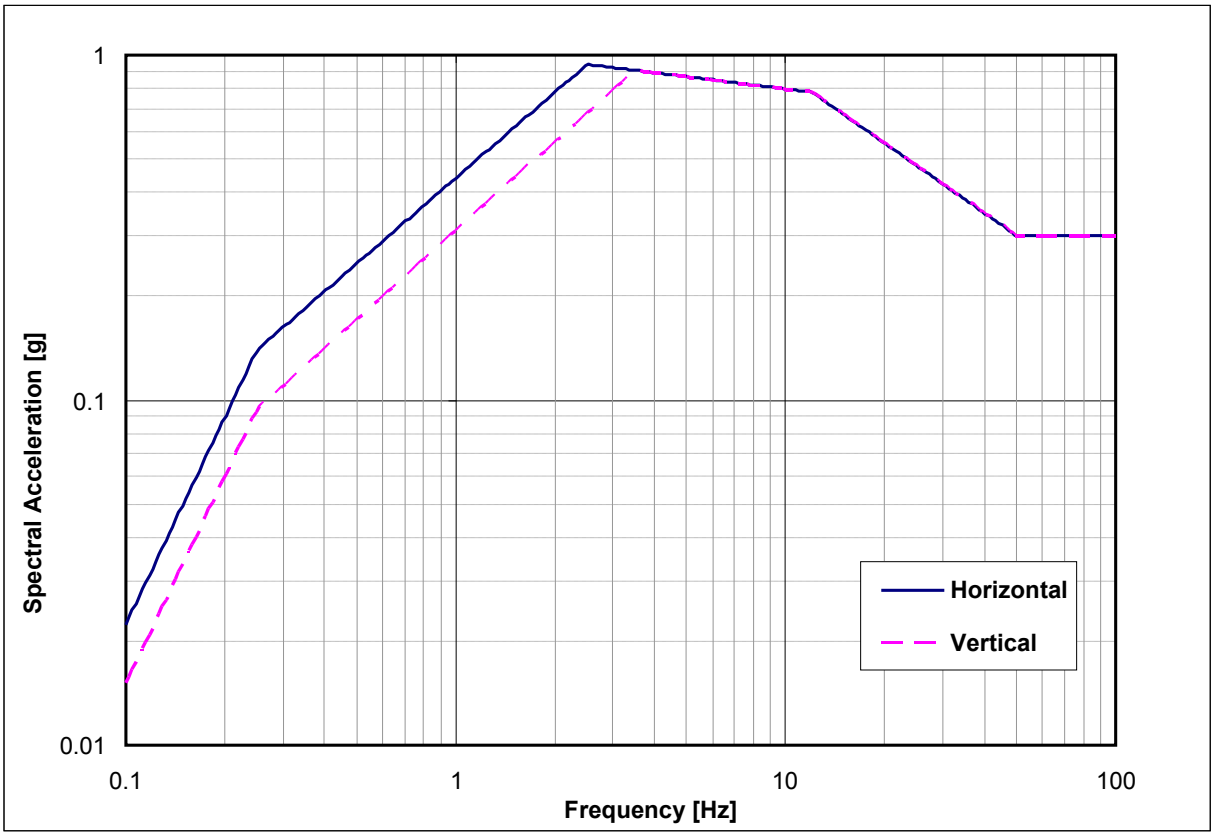

Source: Modified from Reference 4

Figure 5-1. US-APWR Certified Seismic Design Response Spectra

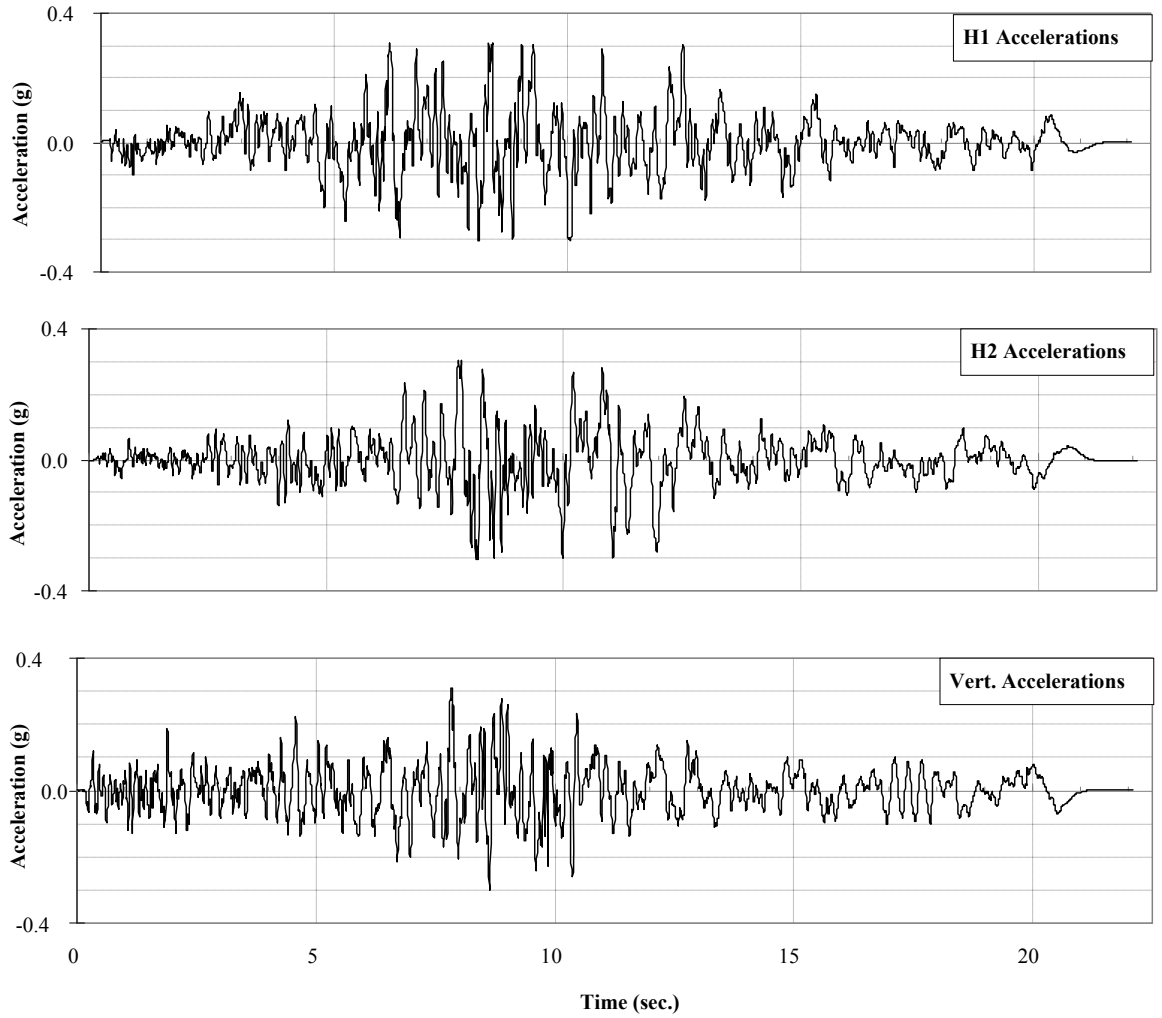

Source: Modified from Reference 4

Legend

H1: North-South (Y) Direction for Turbine Island Model

H2: East-West (X) Direction for Turbine Island Model

Vert: Vertical (Z) Direction for Turbine Island Model

Figure 5-2. US-APWR Certified Site Design Response Spectra Compatible Acceleration Time Histories

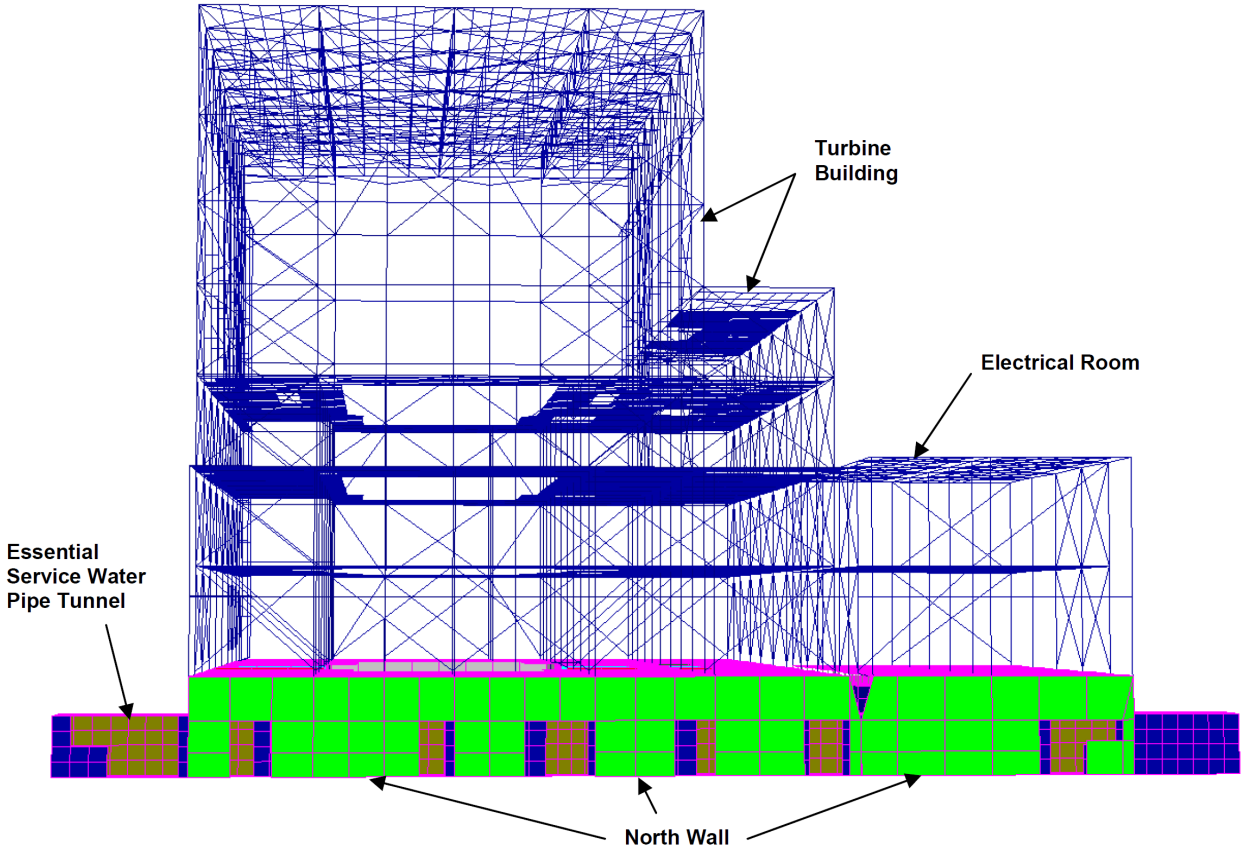

Figure 5-3. Combined Turbine Island ACS SASSI Finite Element Model - North Side, Looking South

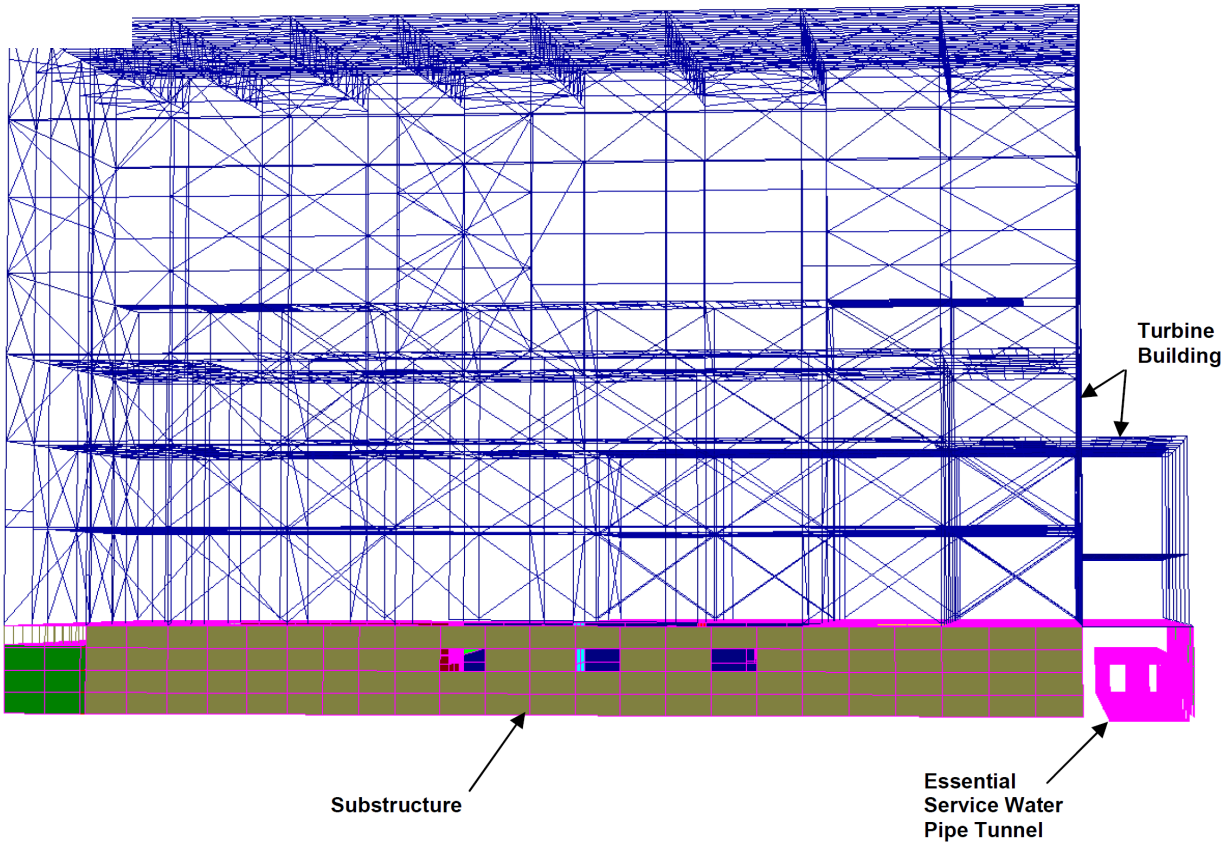

Figure 5-4. Combined Turbine Island ACS SASSI Finite Element Model - East Side, Looking West

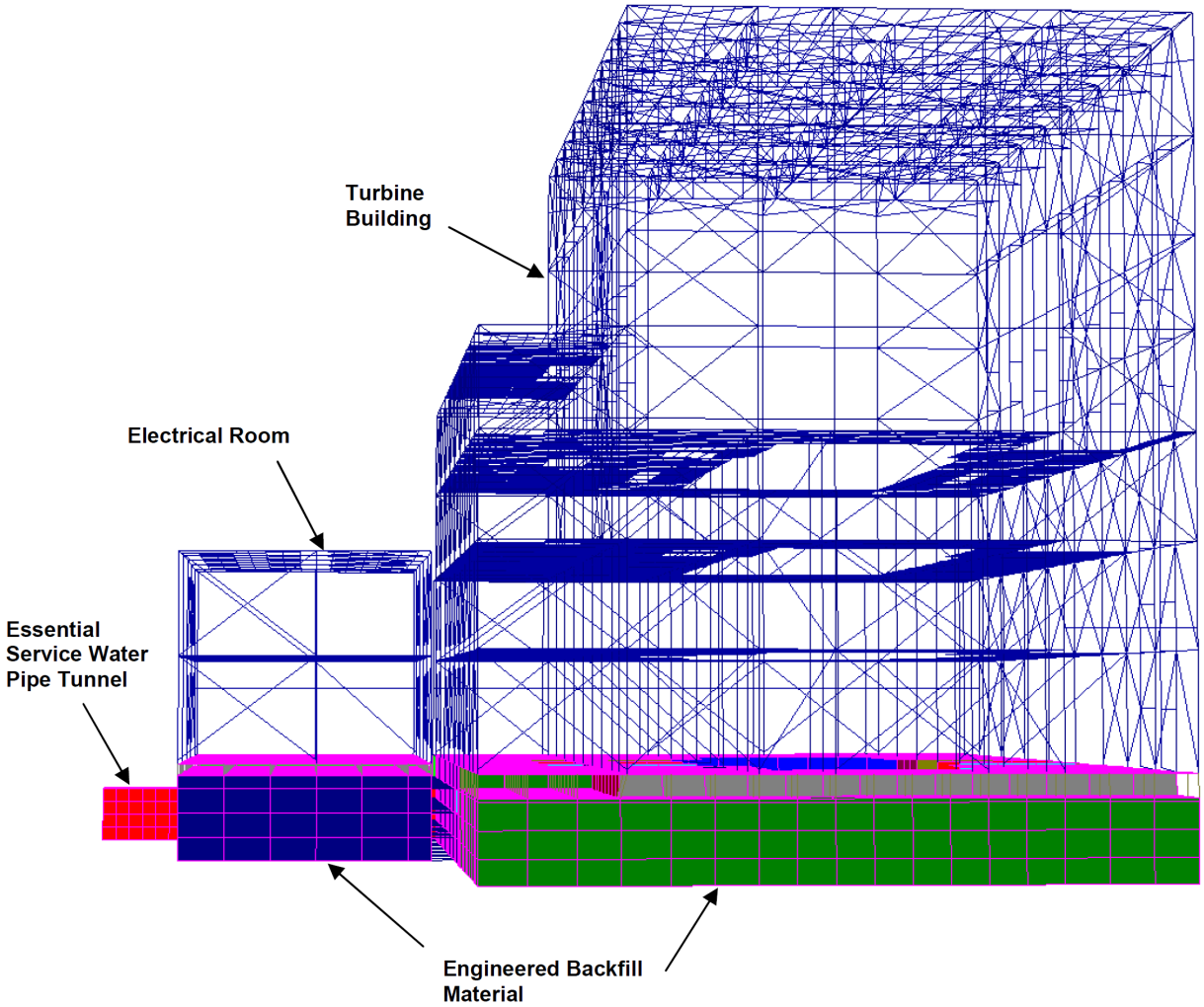

Figure 5-5. Combined Turbine Island ACS SASSI Finite Element Model - South Side, Looking North

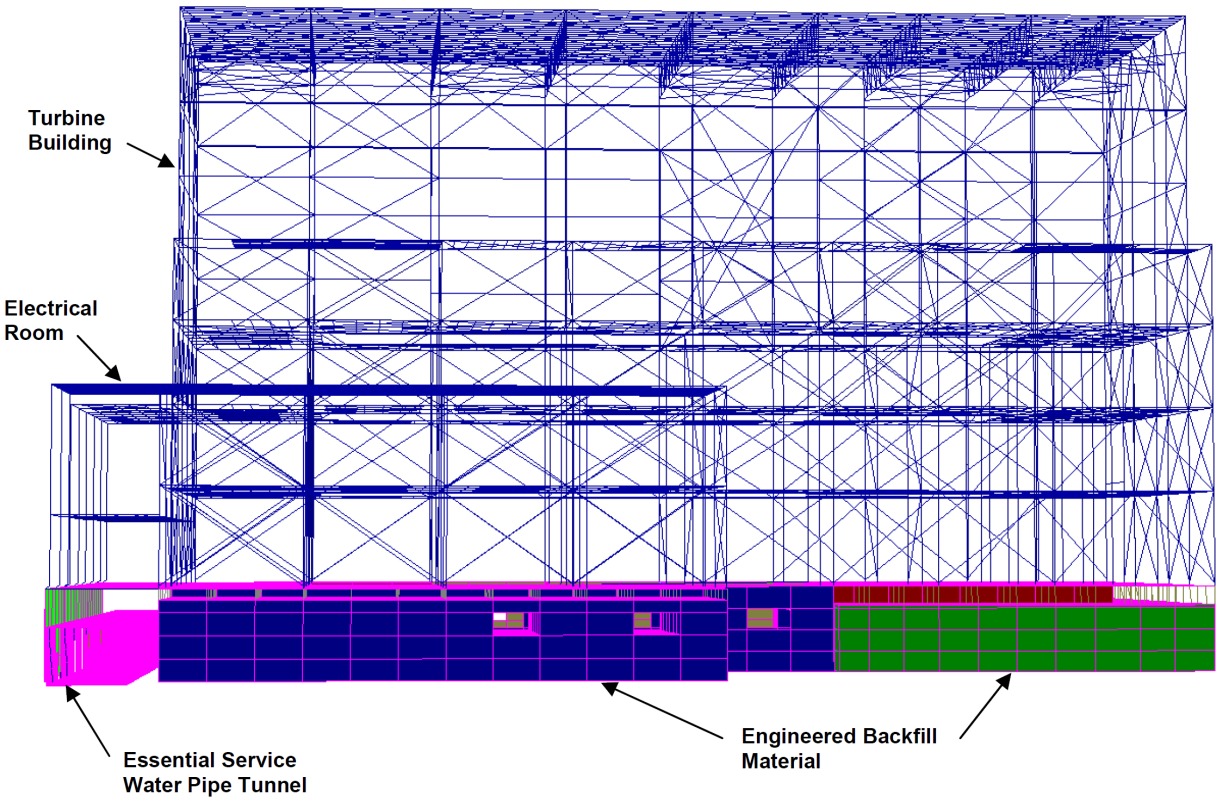

Figure 5-6. Combined Turbine Island ACS SASSI Finite Element Model - West Side, Looking East

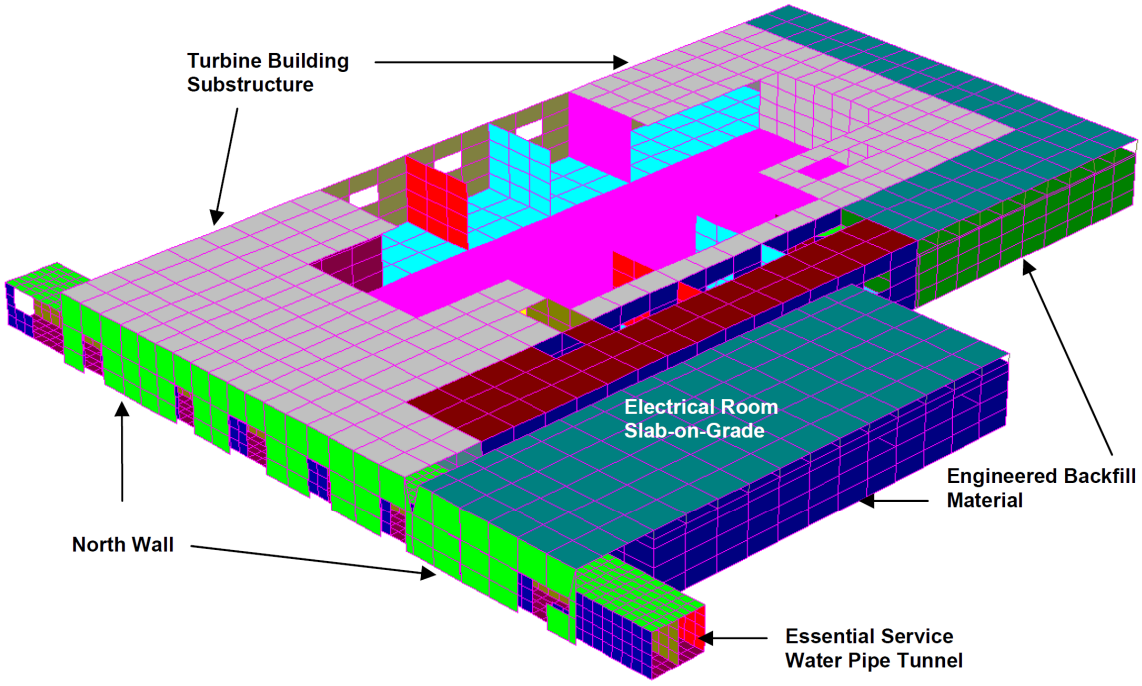

Figure 5-7. Combined Turbine Island ACS SASSI Finite Element Model - Substructures, Engineered Backfill and Essential Service Water Pipe Tunnel

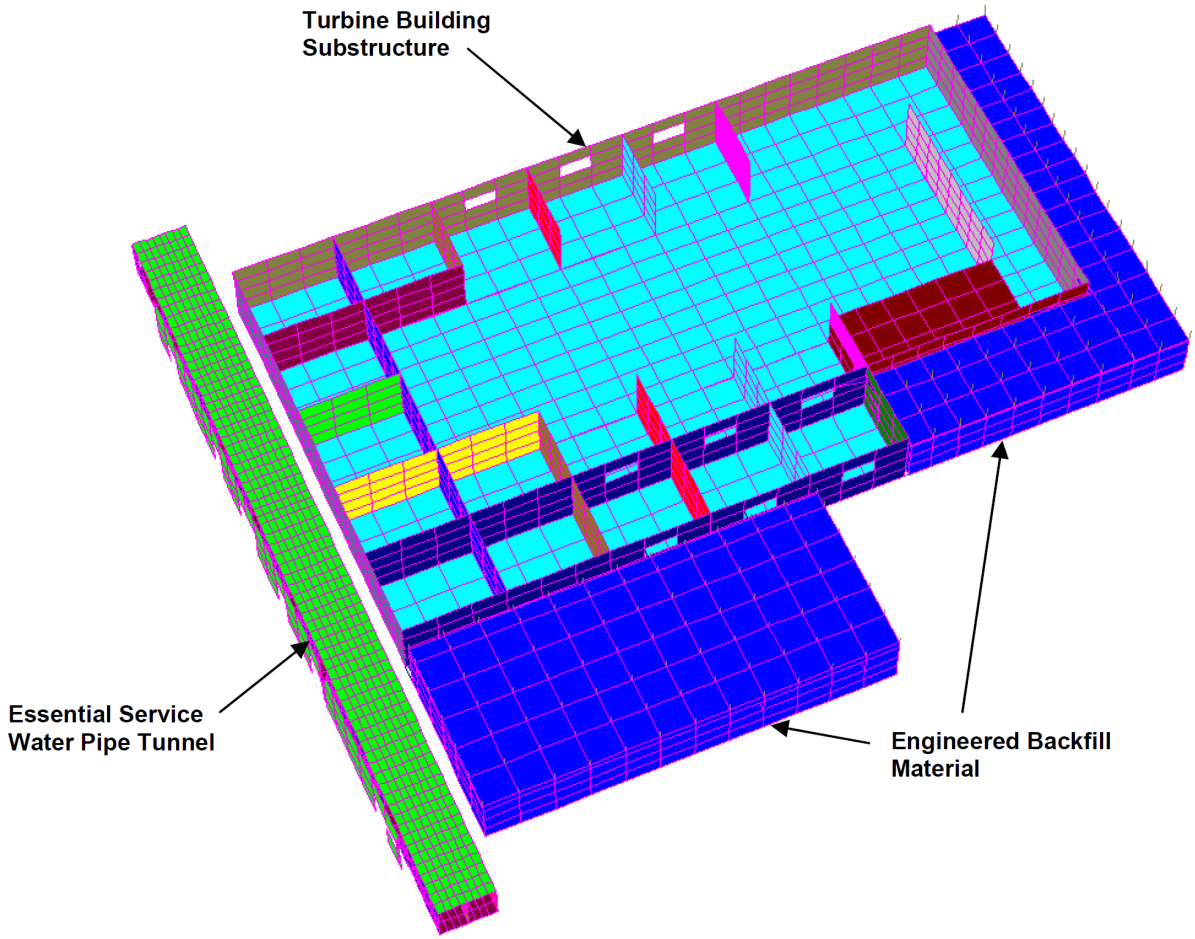

Figure 5-8. Combined Turbine Island ACS SASSI Finite Element Model – Interior of Turbine Building Substructure with First Floor Slab Removed, Engineered Backfill and Essential Service Water Pipe Tunnel

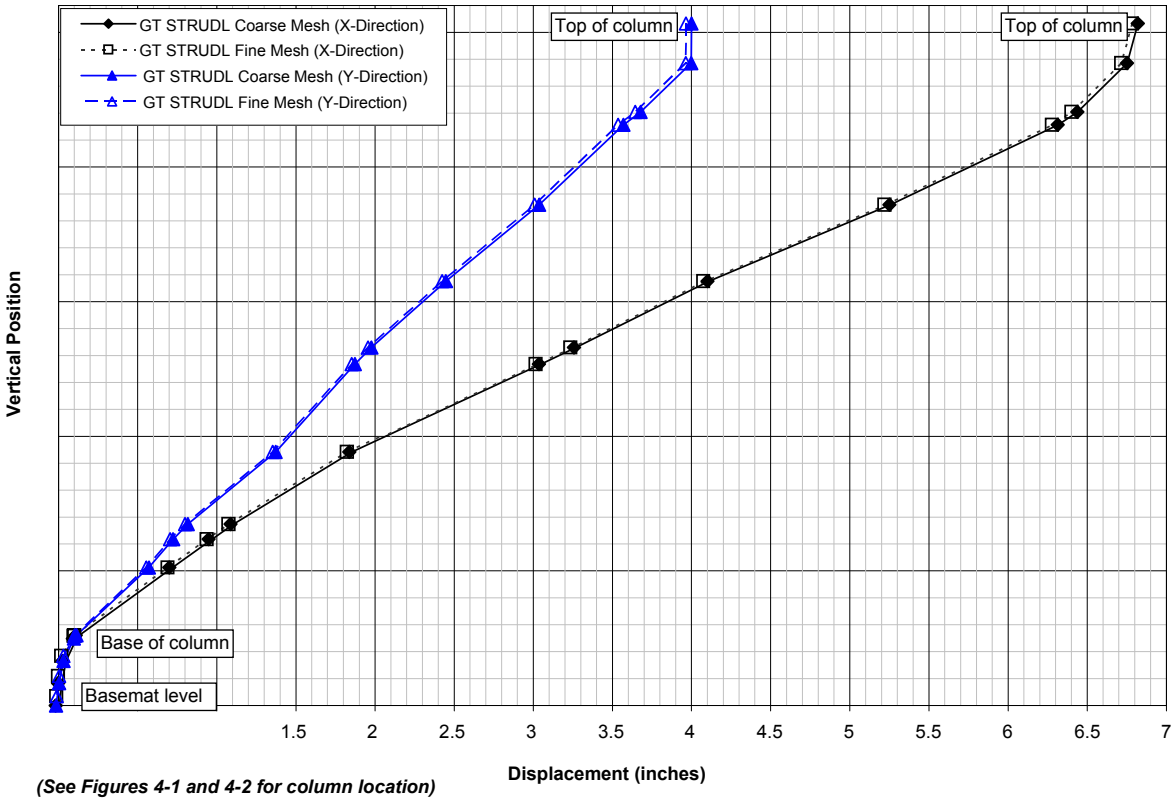

Figure 6-1. X (East-West) and Y (North-South) Directions Displacement Comparison of Fine and Coarse Mesh Models Under 1g Load Applied in X and Y Directions, Respectively Turbine Building Column BT-8T

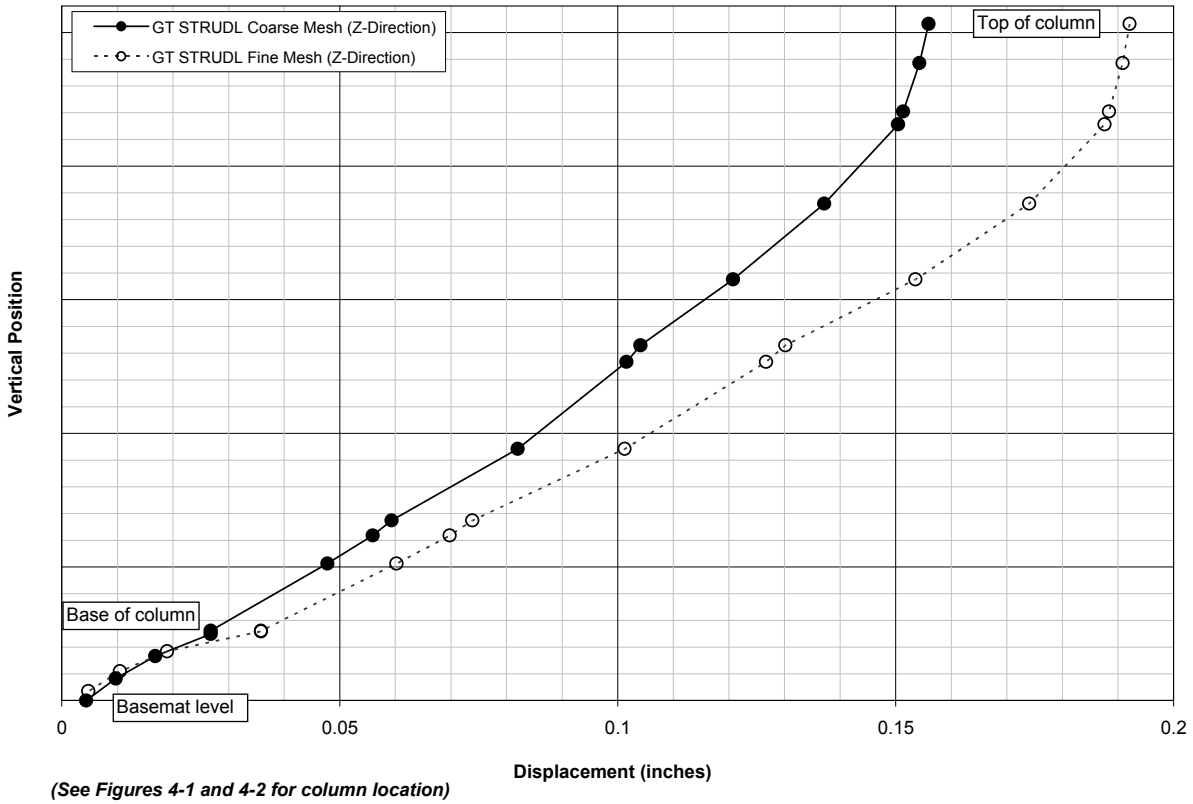

(See Figures 4-1 and 4-2 for column location)

Figure 6-2. Z (Vertical) Direction Displacement Comparison of Fine and Coarse Mesh Models Under 1g Load Applied in Z Direction Turbine Building Column BT-8T

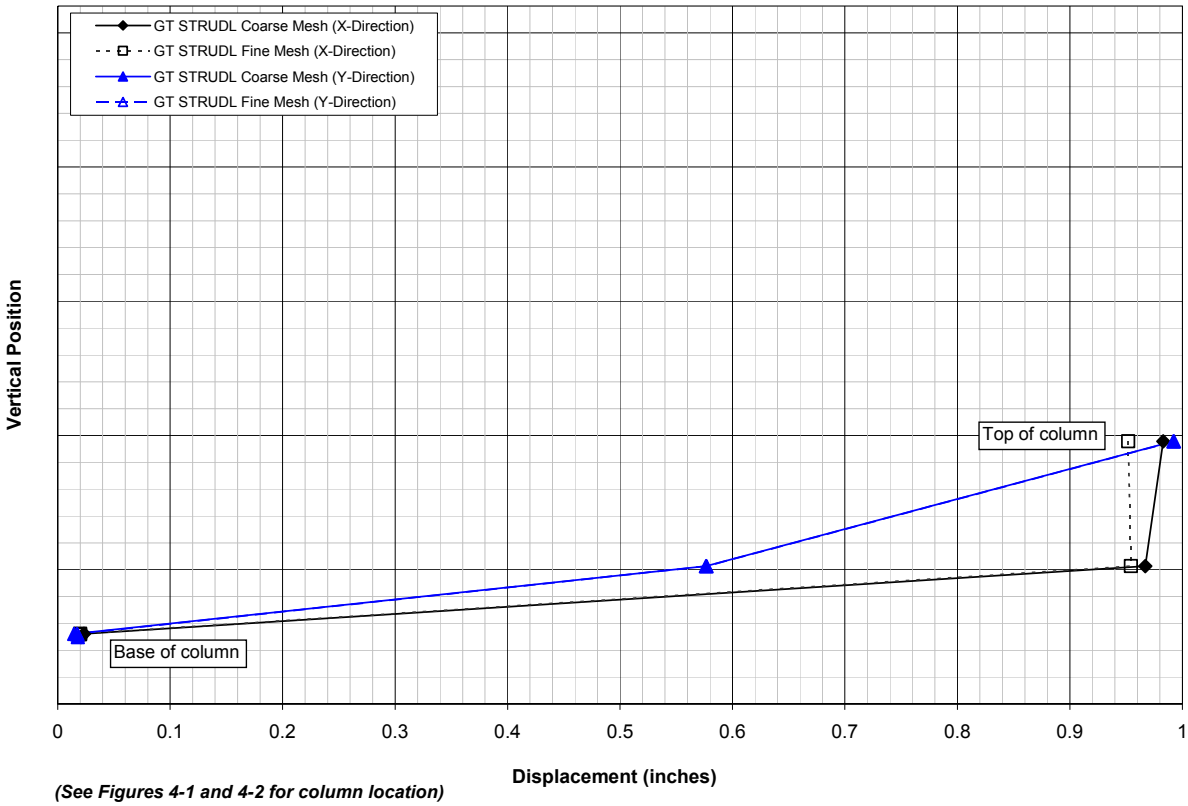

(See Figures 4-1 and 4-2 for column location)

Figure 6-3. X (East-West) and Y (North-South) Directions Displacement Comparison of Fine and Coarse Mesh Models Under 1g Load Applied in X and Y Directions, Respectively Turbine Building Column AT-3T

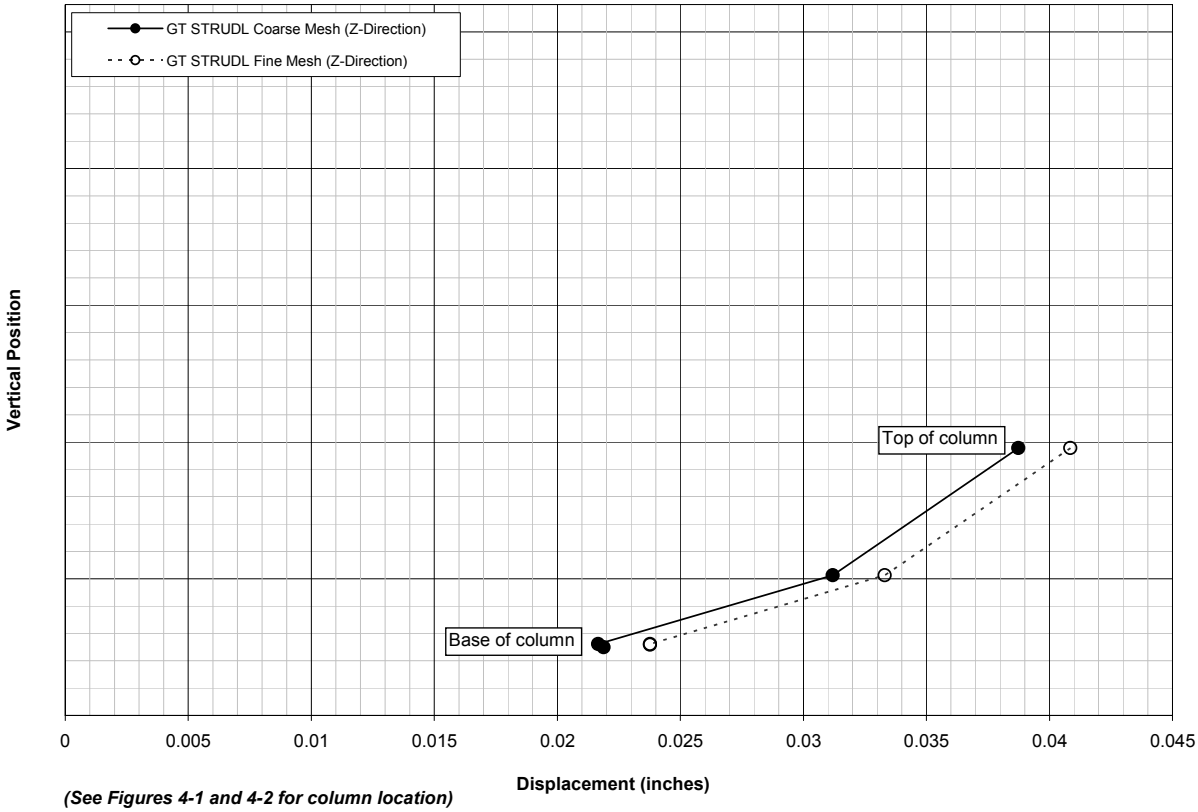

Figure 6-4. Z (Vertical) Direction Displacement Comparison of Fine and Coarse Mesh Models Under 1g Load Applied in Z Direction Turbine Building Column AT-3T

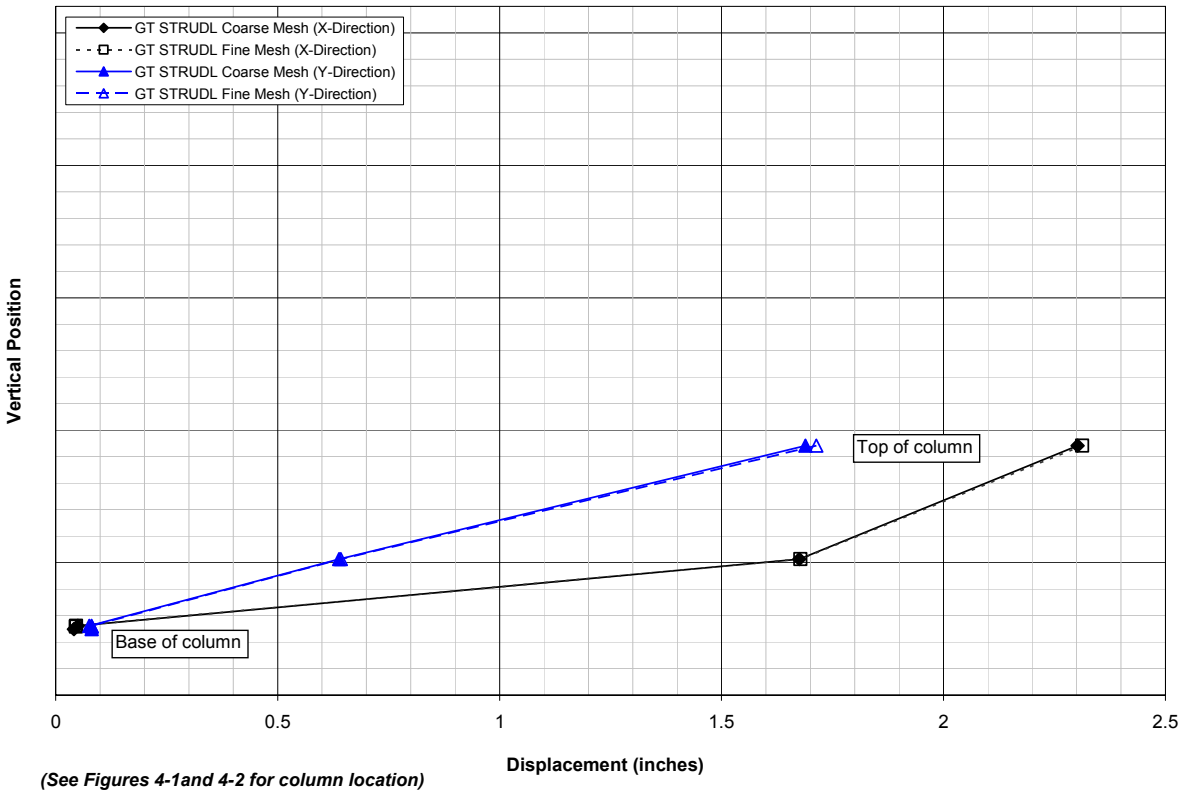

(See Figures 4-1and 4-2 for column location)

Figure 6-5. X (East-West) and Y (North-South) Directions Displacement Comparison of Fine and Coarse Mesh Models Under 1g Load Applied in X and Y Directions, Respectively Electrical Room Column AT-1T

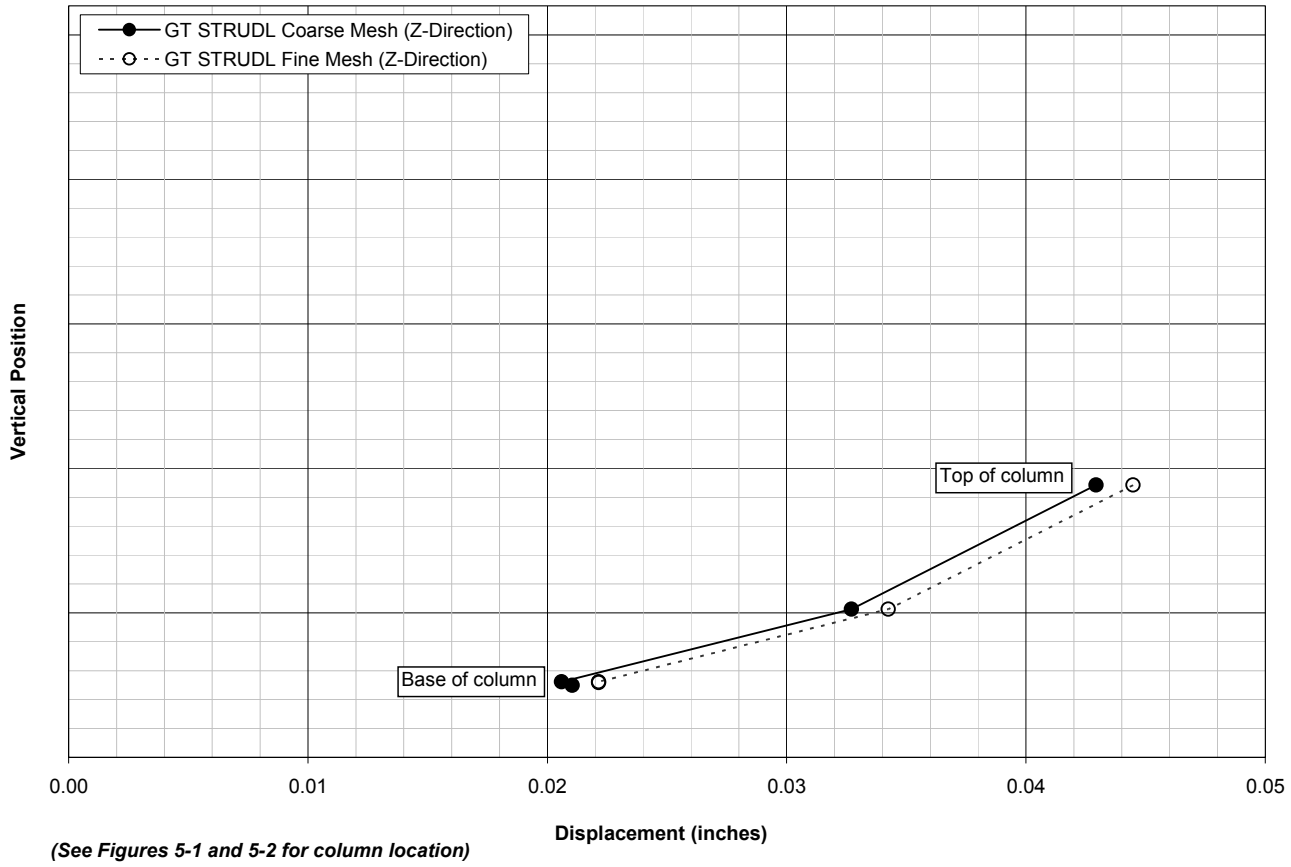

Figure 6-6. Z (Vertical) Direction Displacement Comparison of Fine and Coarse Mesh Models Under 1g Load Applied in Z Direction Electrical Room Column AT-1T

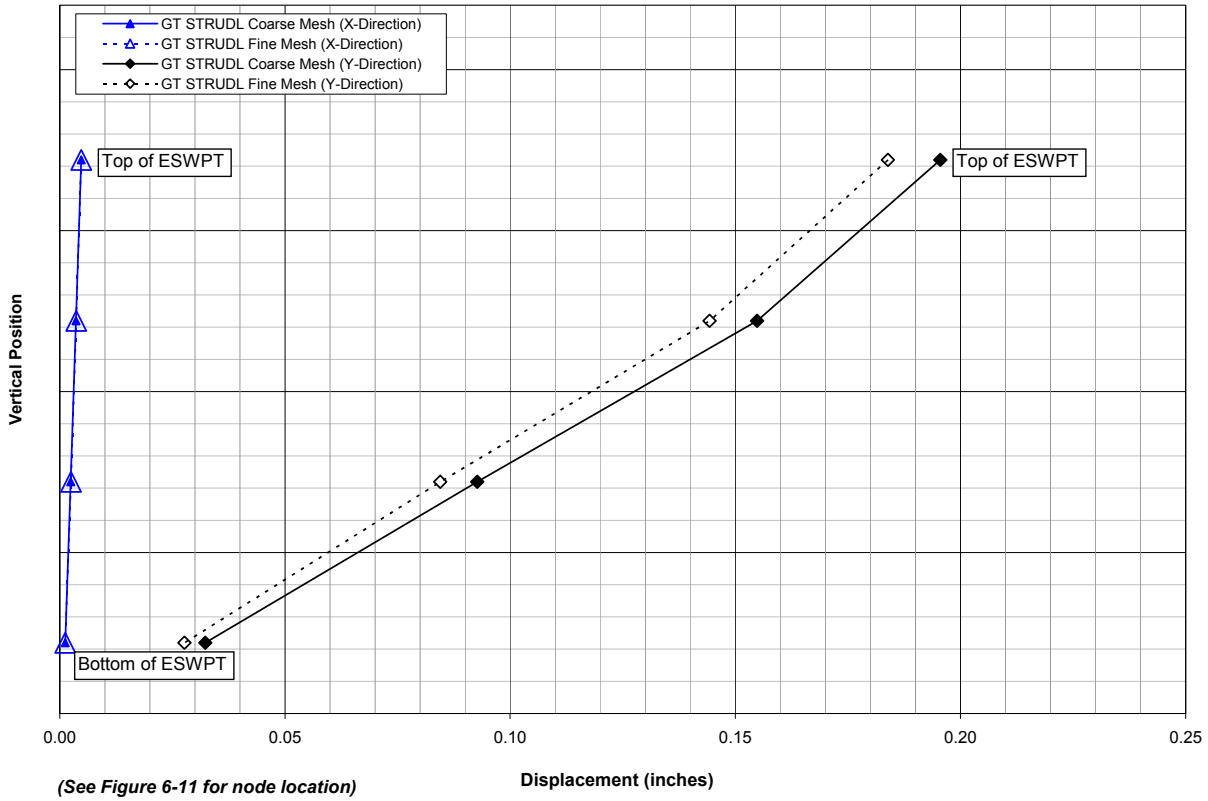

Figure 6-7. X (East-West) and Y (North-South) Directions Displacement Comparison of Fine and Coarse Mesh Models Under 1g Load Applied in X and Y Directions, Respectively Essential Service Water Pipe Tunnel ACS SASSI Node 11401

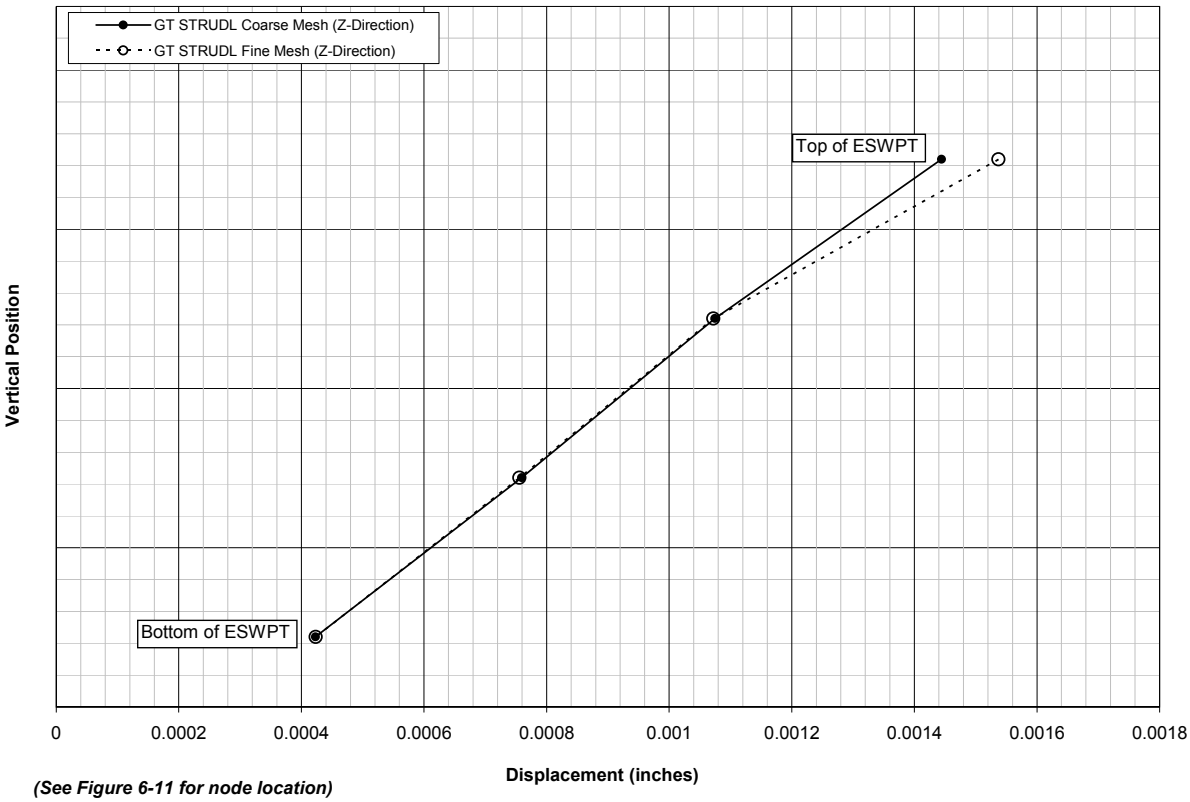

Figure 6-8. Z (Vertical) Direction Displacement Comparison of Fine and Coarse Mesh Models Under 1g Load Applied in Z Direction Essential Service Water Pipe Tunnel ACS SASSI Node 11401

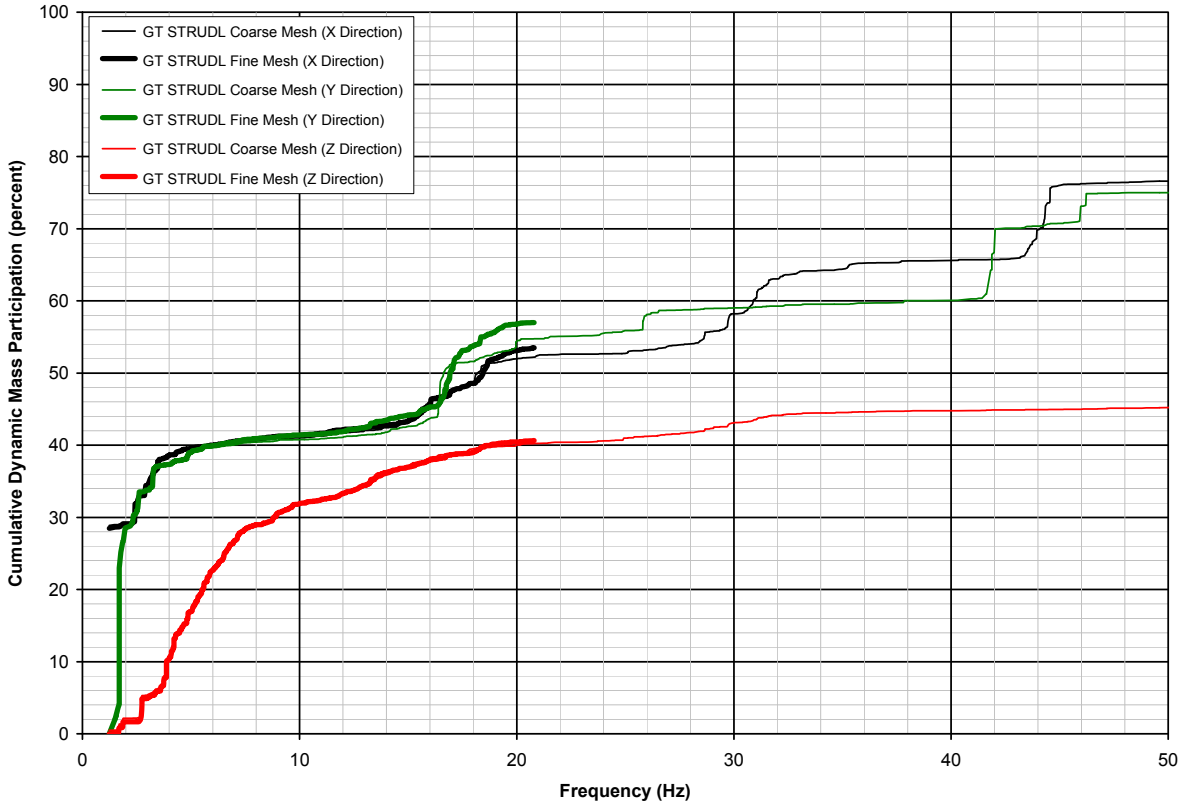

Figure 6-9. Comparison of Turbine Building and Electrical Room Mesh Dynamic Mass Participation in X (East-West), Y (North-South) and Z (Vertical) Directions

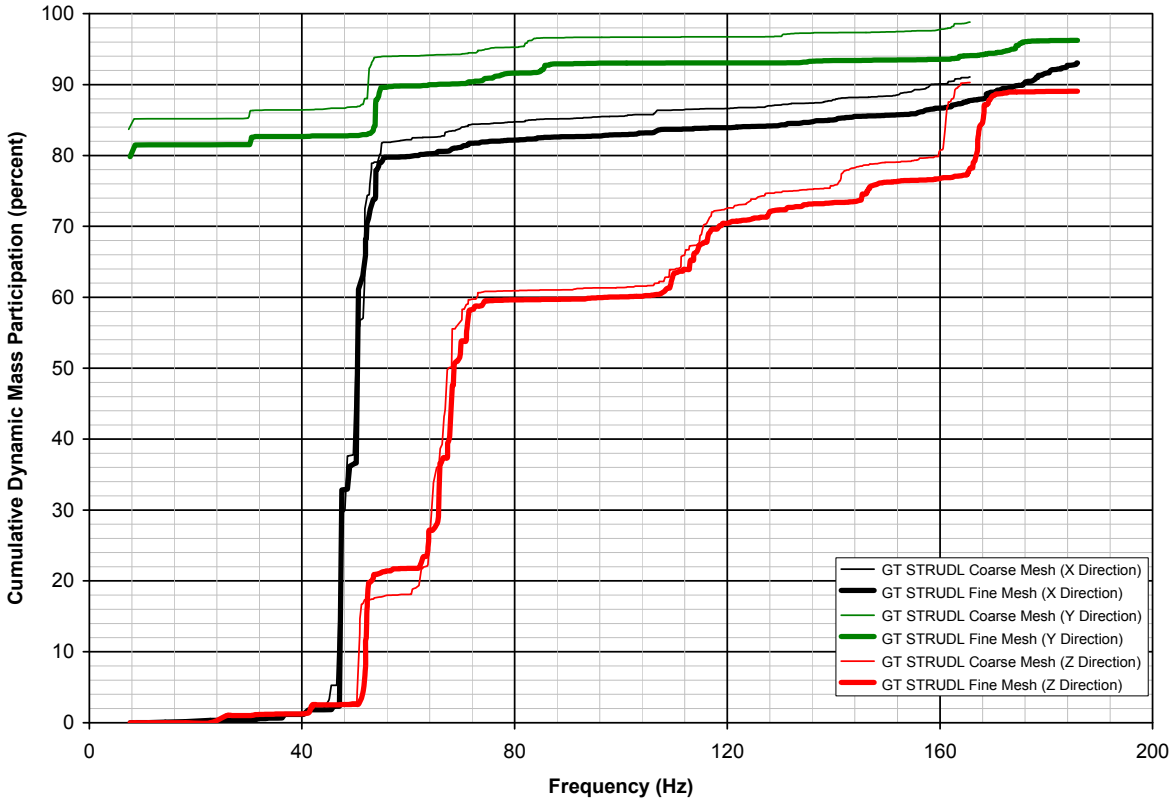

Figure 6-10. Comparison of Essential Service Water Pipe Tunnel Mesh Dynamic Mass Participation in X (East-West), Y (North-South) and Z (Vertical) Directions

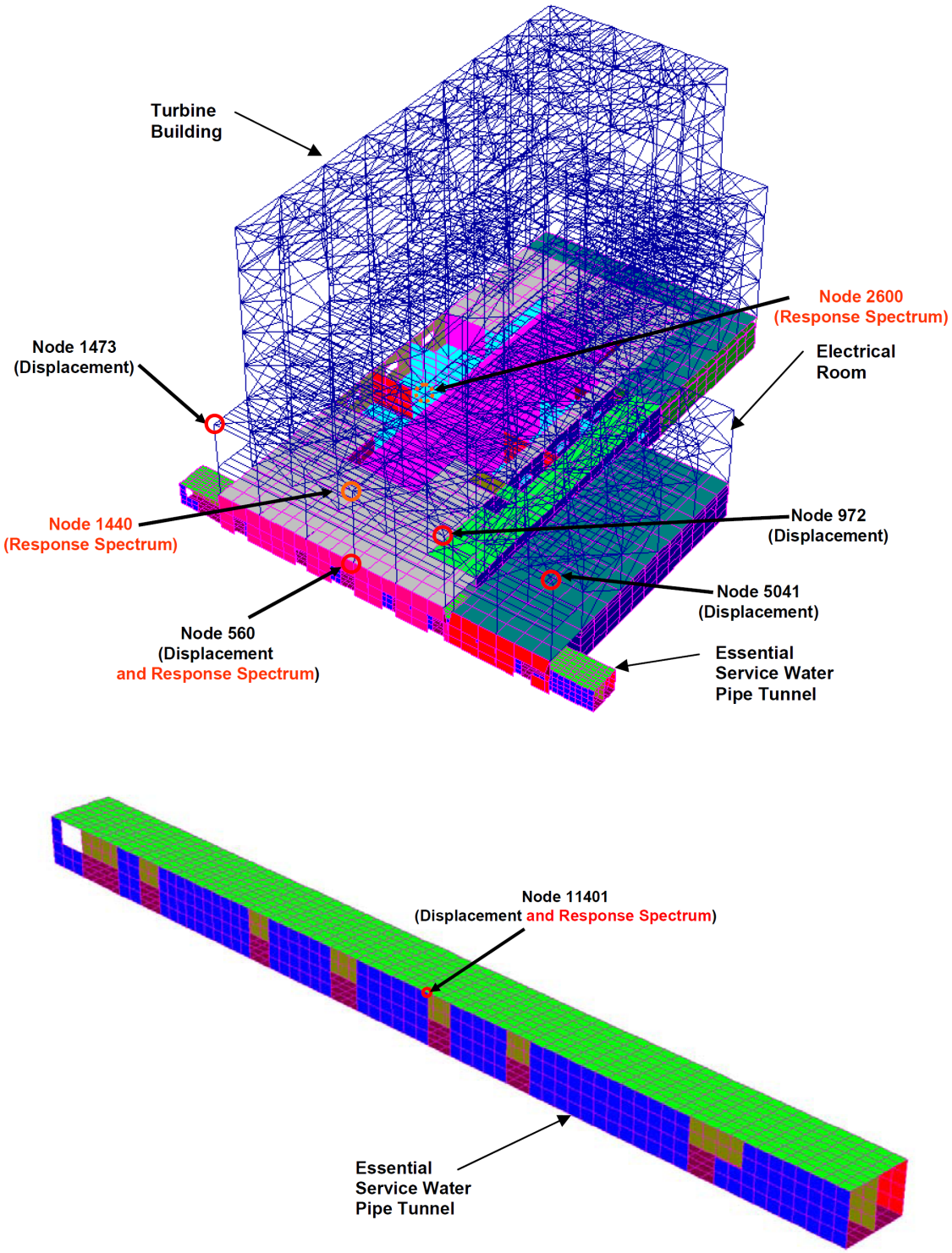

Figure 6-11. Node Locations for Fixed Base Relative Displacement Time History and Response Spectra Comparisons

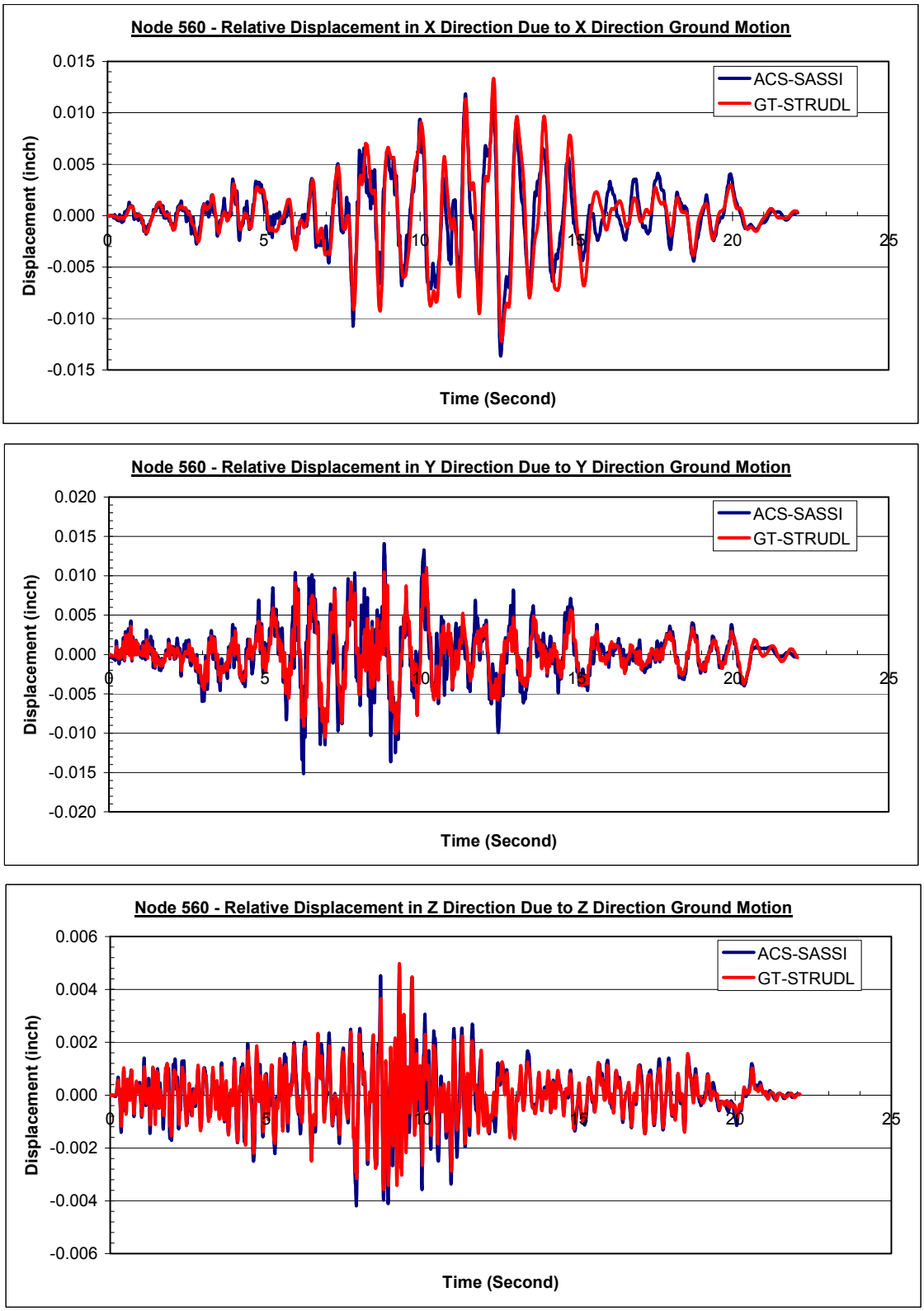

Figure 6-12. Fixed Base Relative Displacement Time History Comparison Between Fine Mesh GT STRUDL Model and ACS SASSI Model, Node 560 in X, Y, and Z Directions

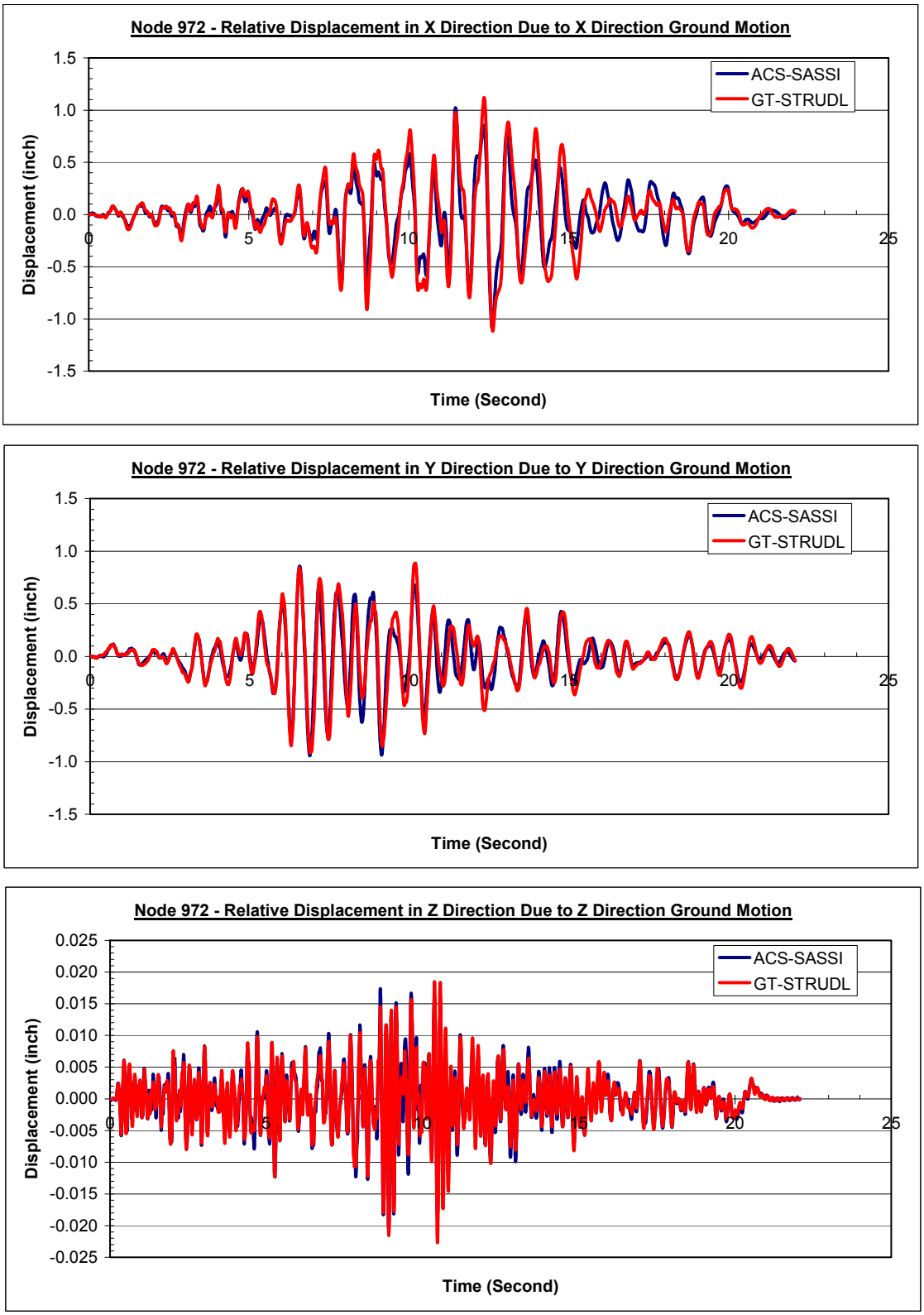

Figure 6-13. Fixed Base Relative Displacement Time History Comparison Between Fine Mesh GT STRUDL Model and ACS SASSI Model, Node 972 in X, Y, and Z Directions

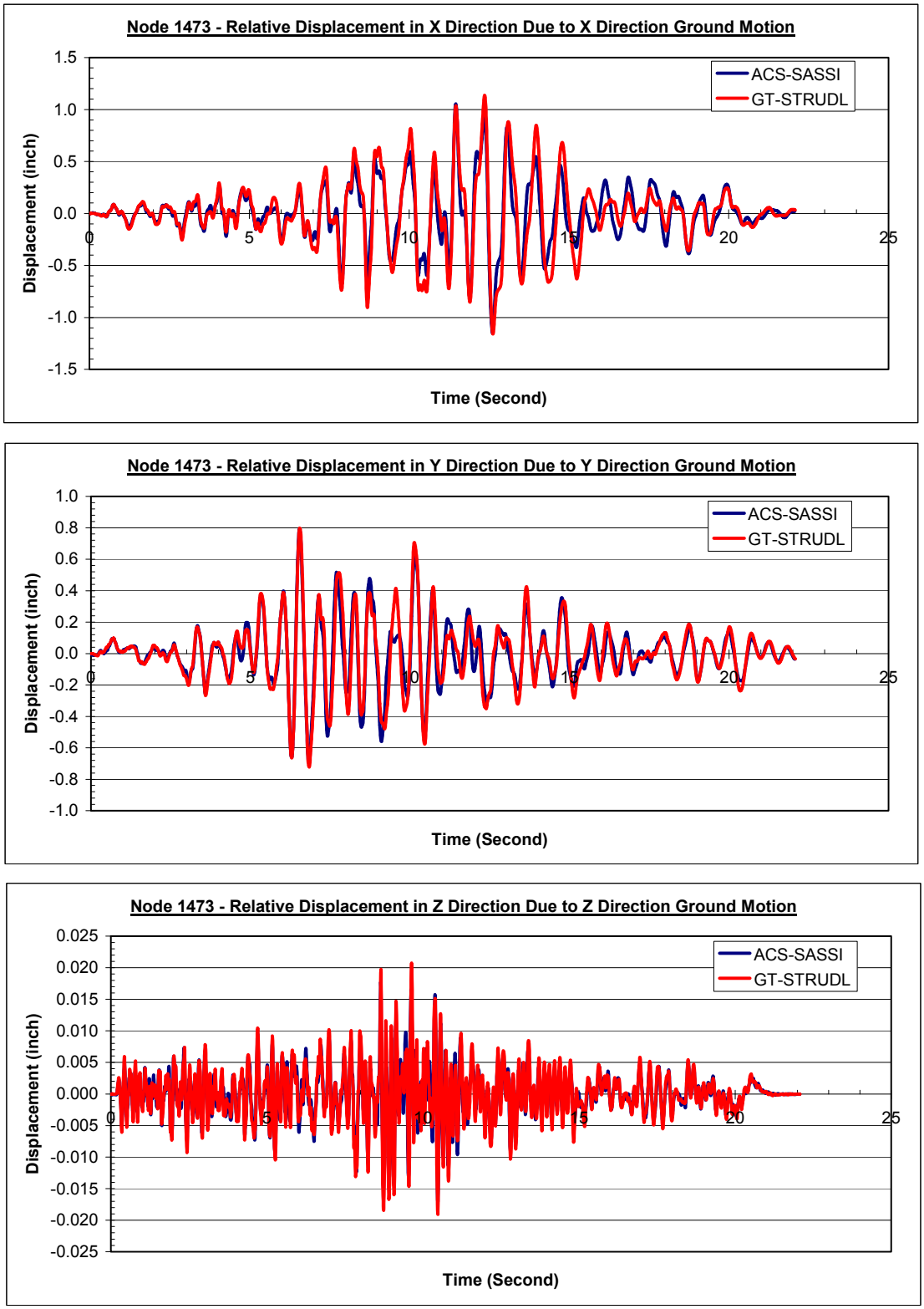

Figure 6-14. Fixed Base Relative Displacement Time History Comparison Between Fine Mesh GT STRUDL Model and ACS SASSI Model, Node 1473 in X, Y, and Z Directions

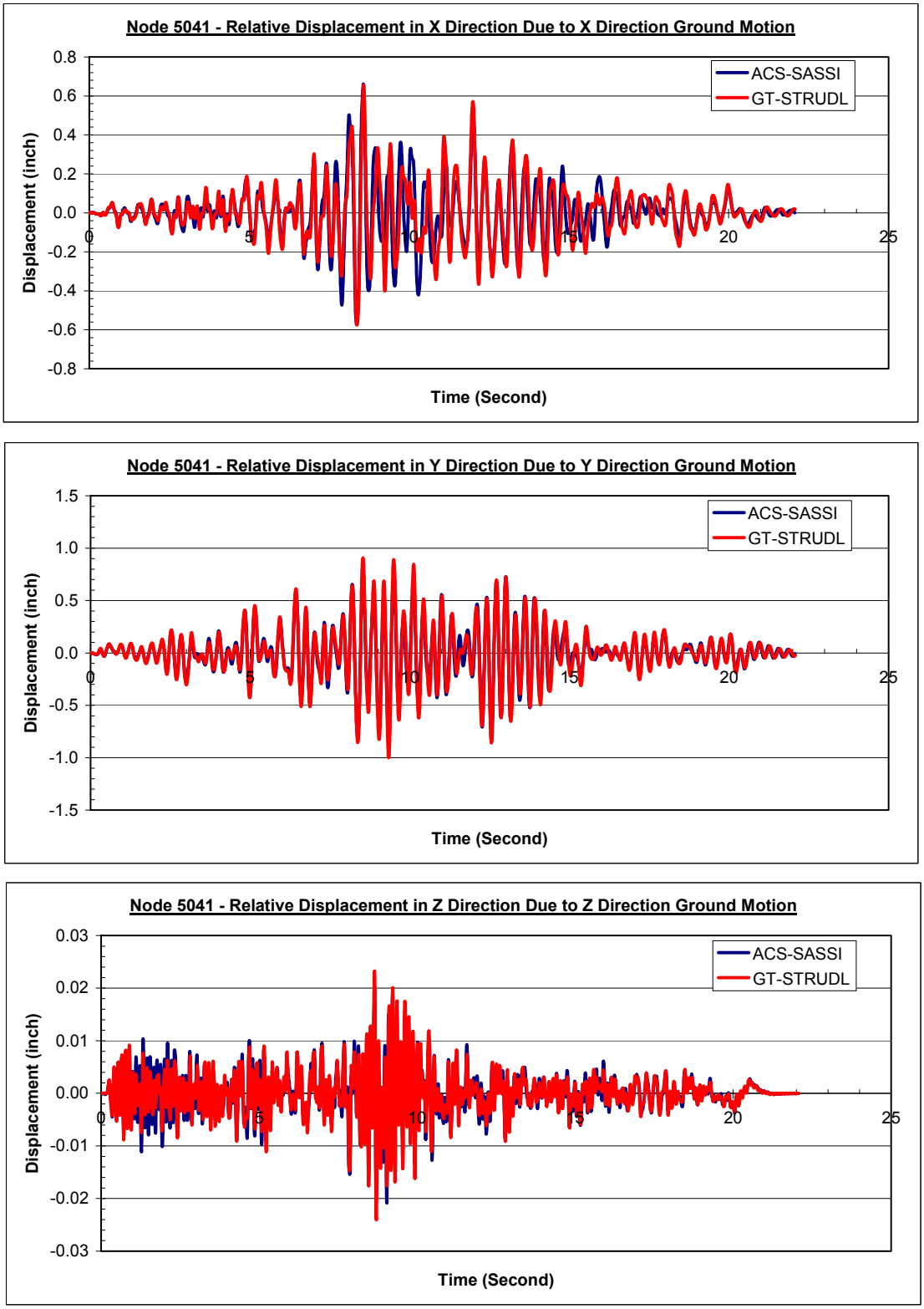

Figure 6-15. Fixed Base Relative Displacement Time History Comparison Between Fine Mesh GT STRUDL Model and ACS SASSI Model, Node 5041 in X, Y, and Z Directions

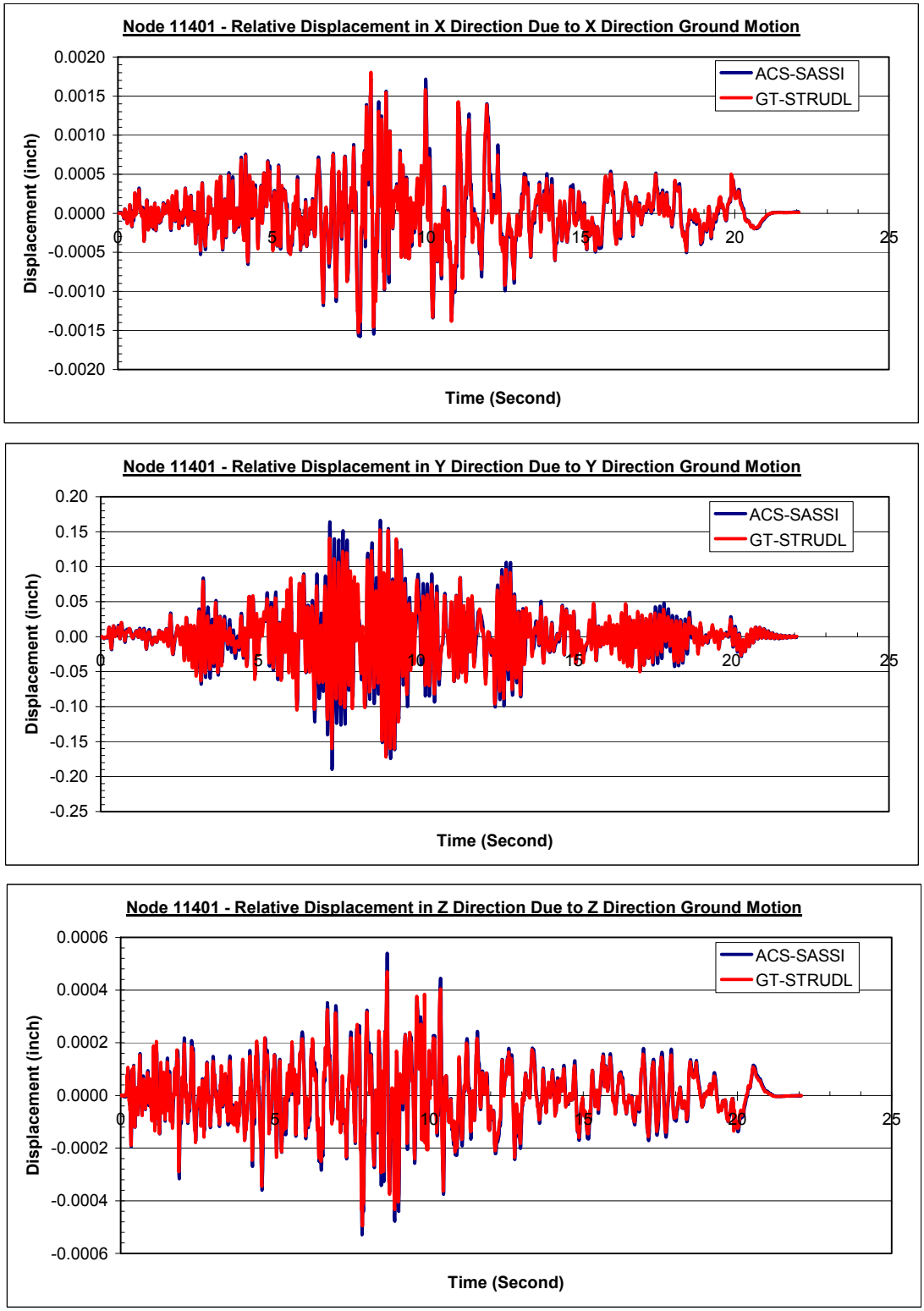

Figure 6-16. Fixed Base Relative Displacement Time History Comparison Between Fine Mesh GT STRUDL Model and ACS SASSI Model, Node 11401 in X, Y, and Z Directions

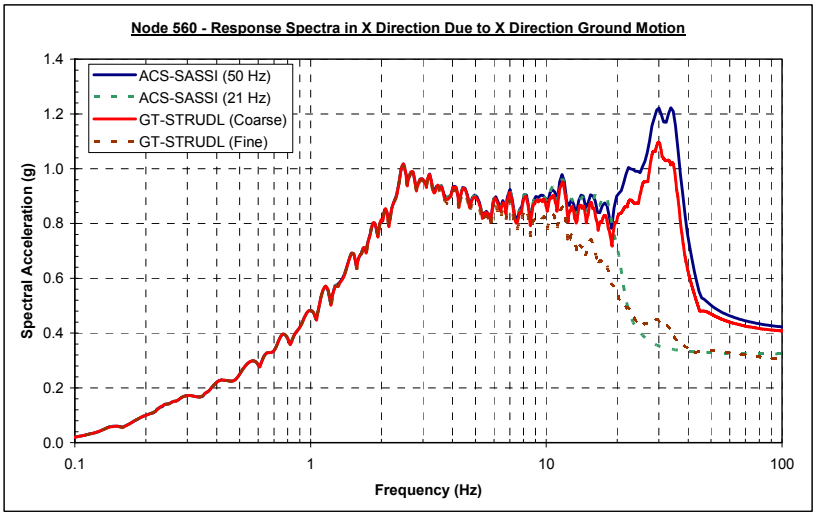

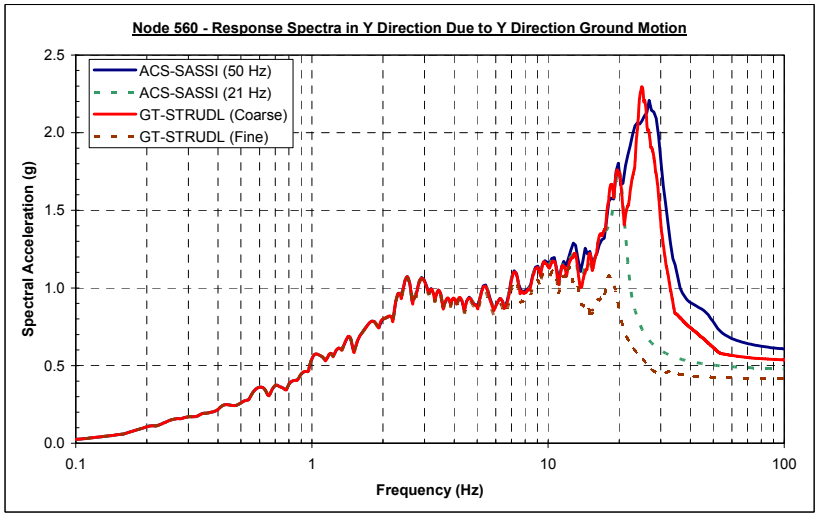

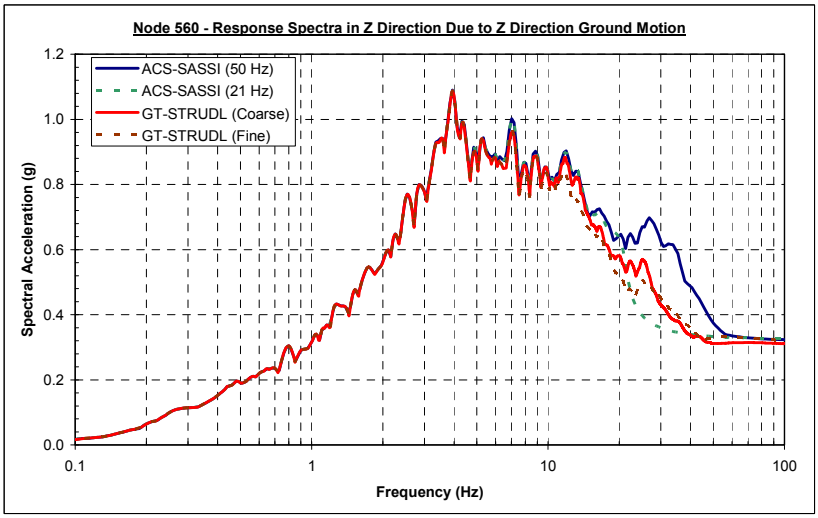

Figure 6-17. Fixed Base Response Spectra Comparison Between Fine Mesh GT STRUDL Model and ACS SASSI Model, Node 560 in X, Y, and Z Directions (5 Percent Damping)

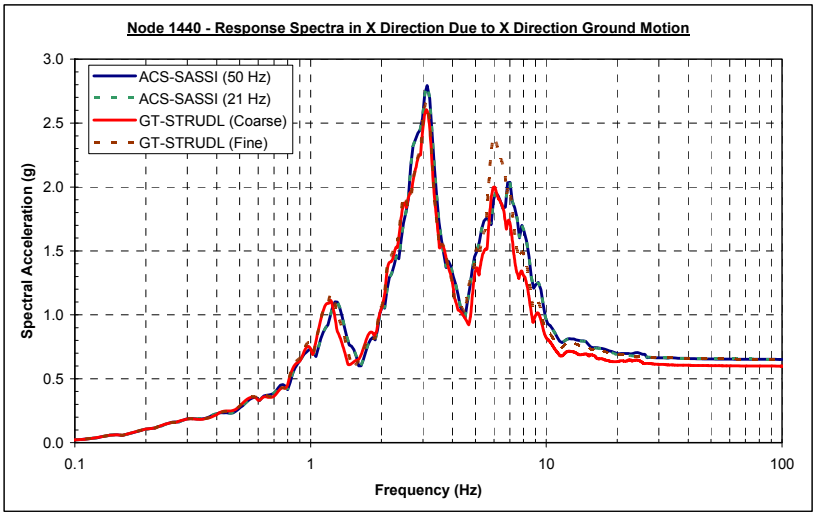

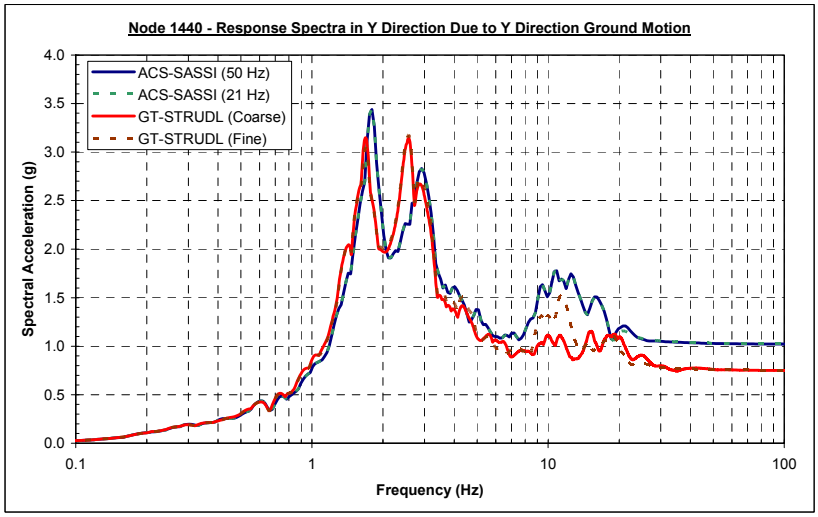

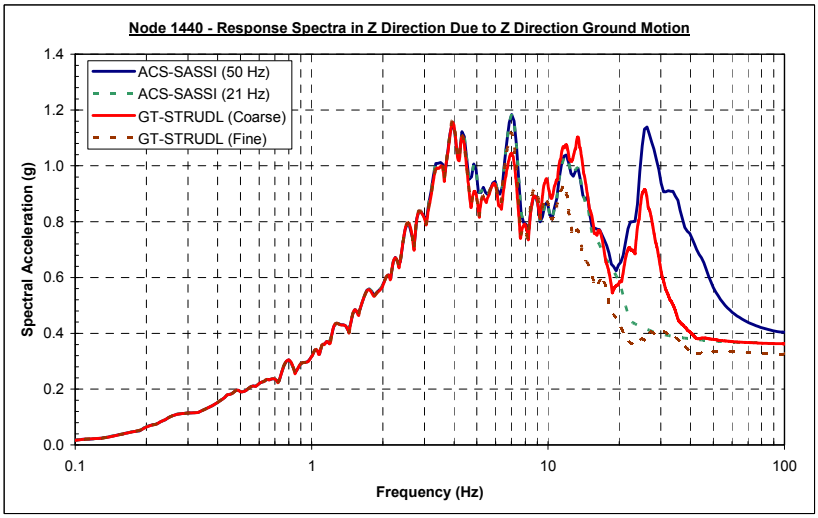

Figure 6-18. Fixed Base Response Spectra Comparison Between Fine Mesh GT STRUDL Model and ACS SASSI Model, Node 1440 in X, Y, and Z Directions (5 Percent Damping)

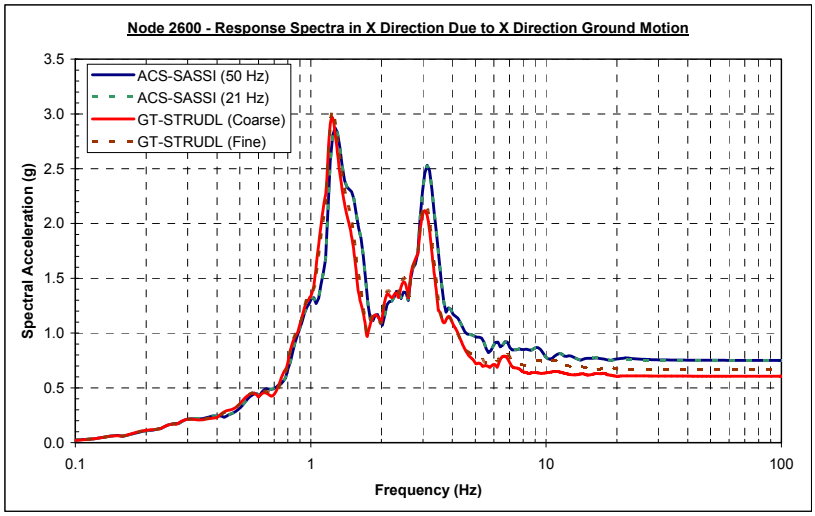

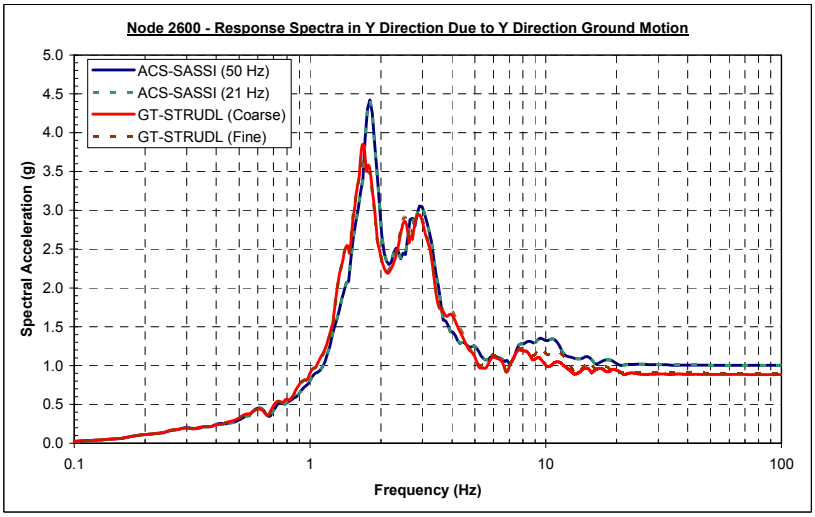

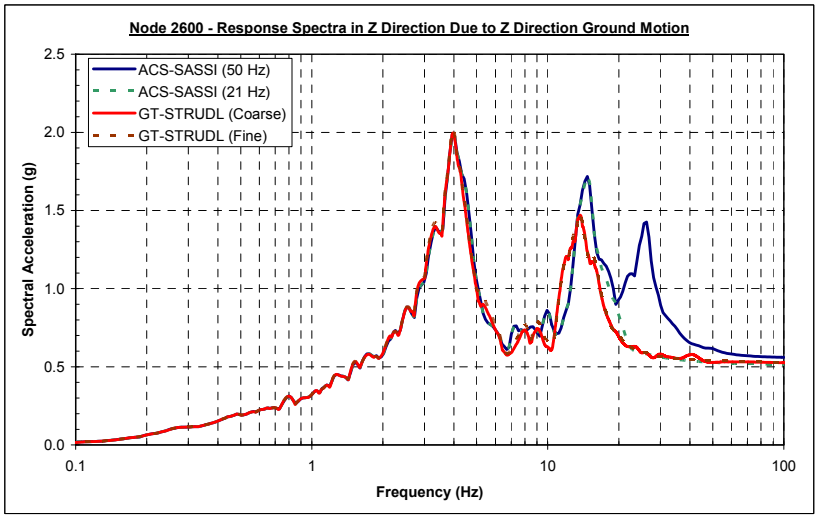

Figure 6-19. Fixed Base Response Spectra Comparison Between Fine Mesh GT STRUDL Model and ACS SASSI Model, Node 2600 in X, Y, and Z Directions (5 Percent Damping)

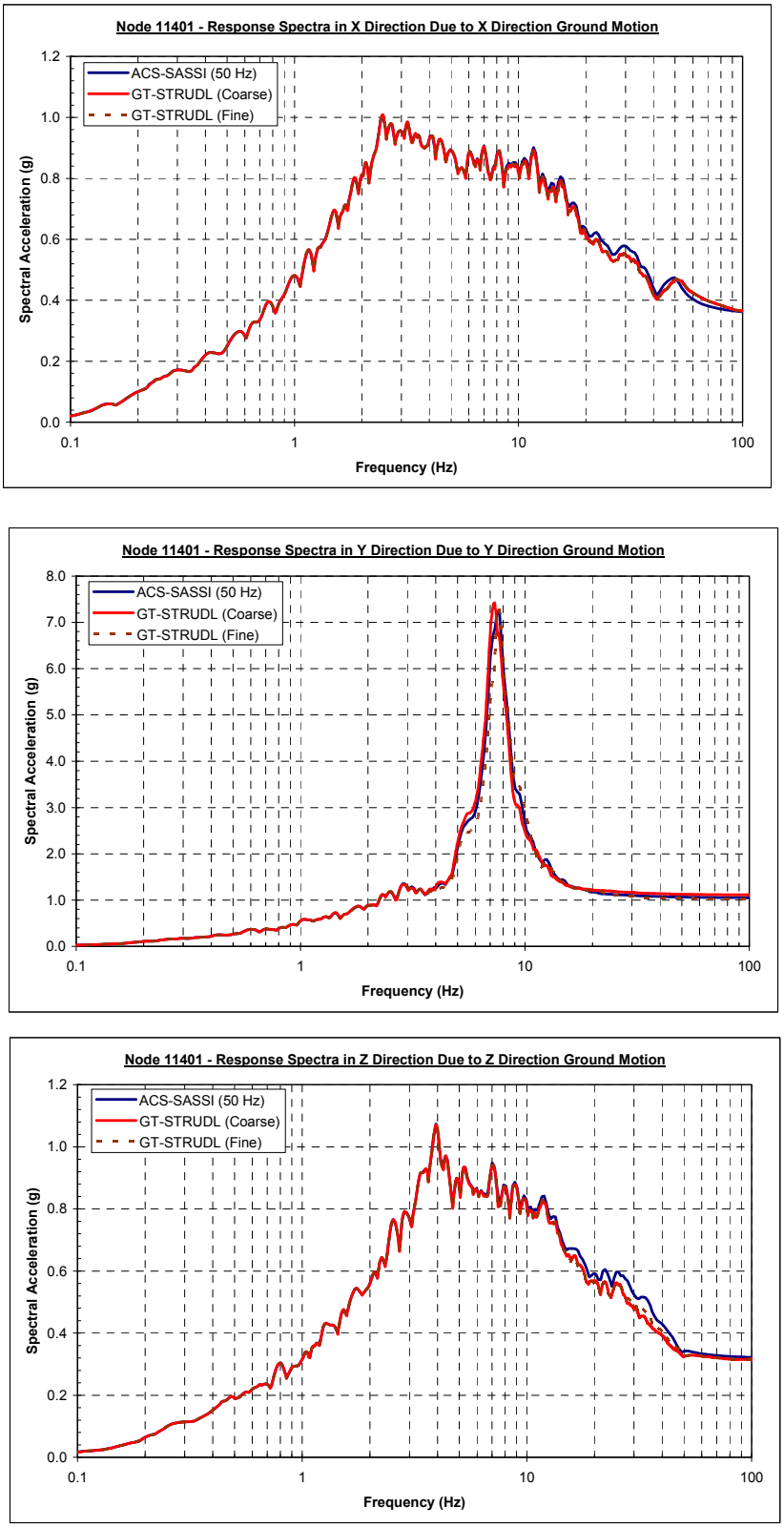

Figure 6-20. Fixed Base Response Spectra Comparison Between Fine Mesh GT STRUDL Model and ACS SASSI Model, Node 11401 in X, Y, and Z Directions (5 Percent Damping)

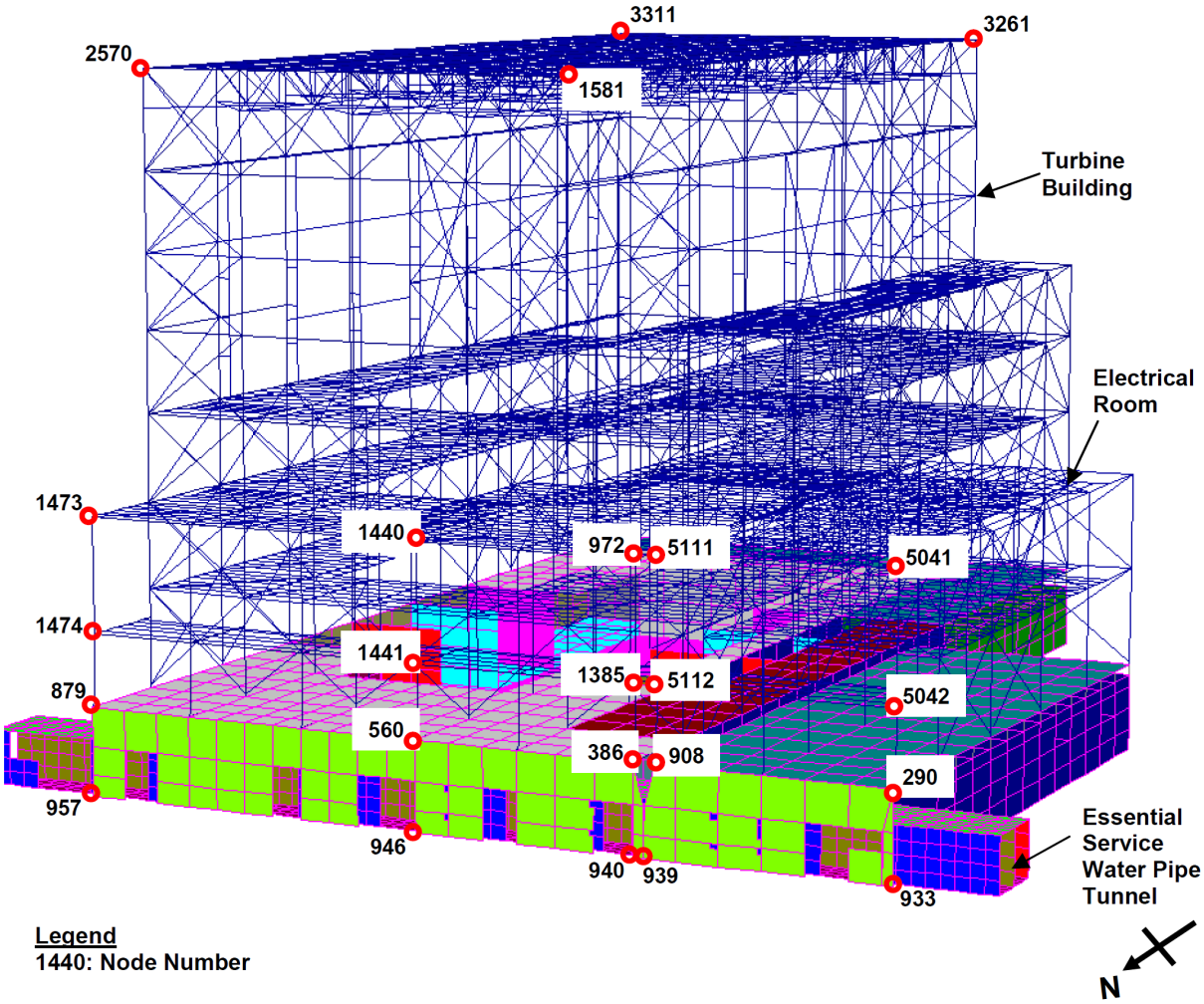

Figure 7-1. Selected Node Locations in Turbine Island for Computing Relative Displacements

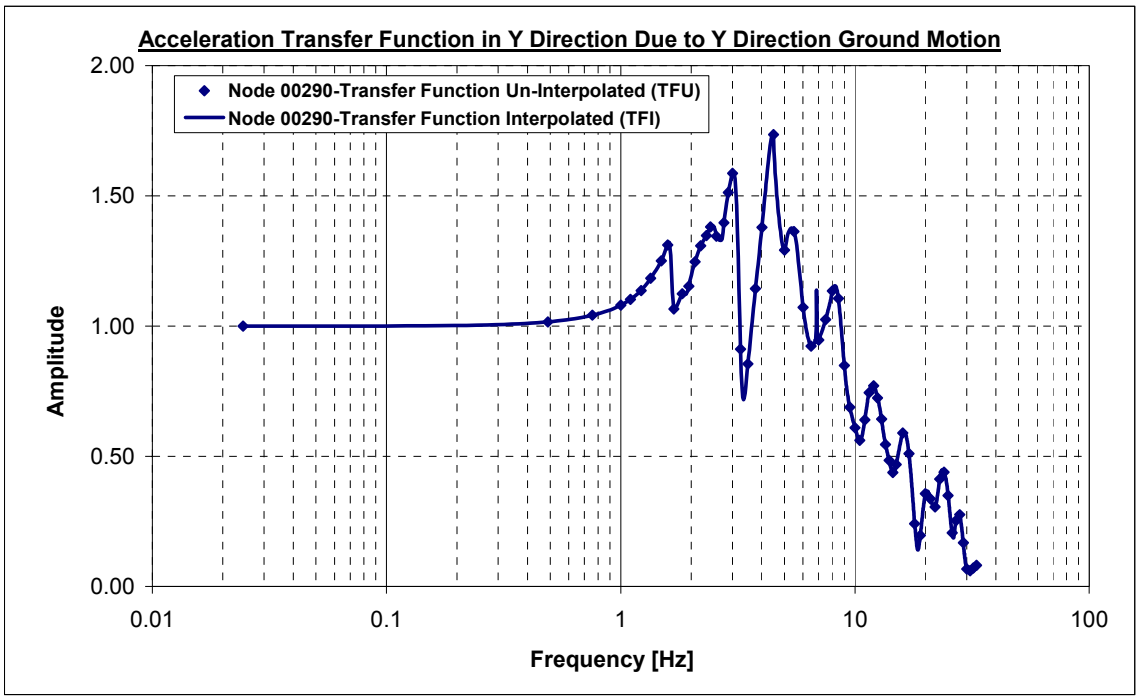

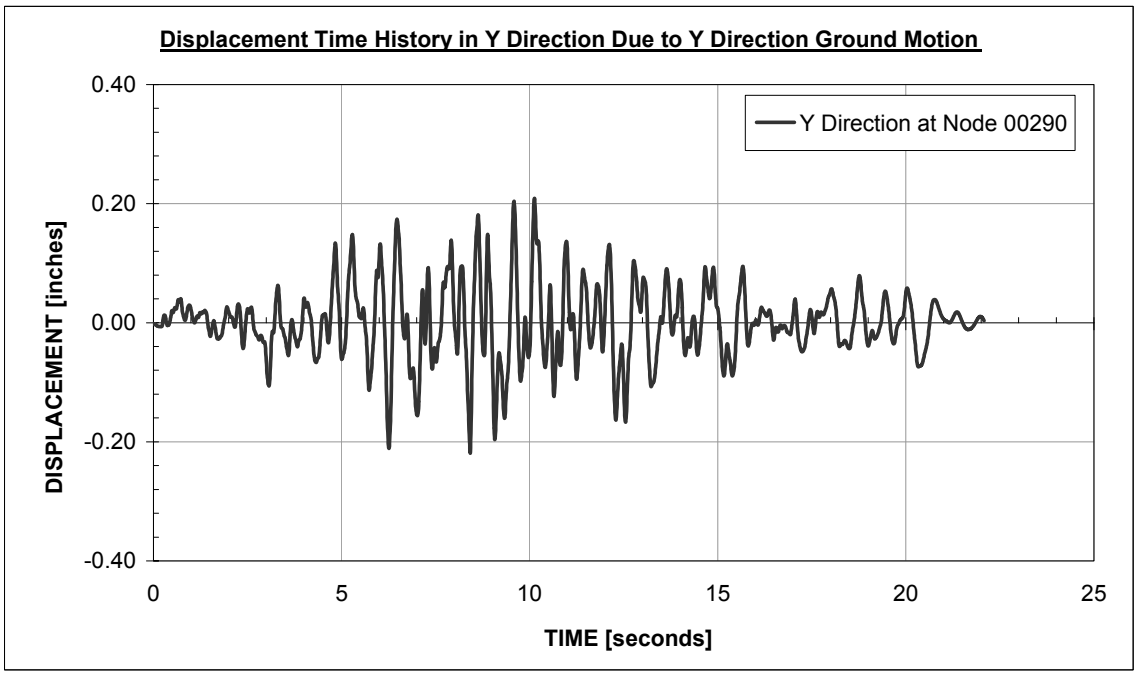

Figure 7-2. Acceleration Transfer Function and Relative Displacement with Respect to Free-Field Input Motion at Node 290 - Y Direction (North-South) for Profile 270-200

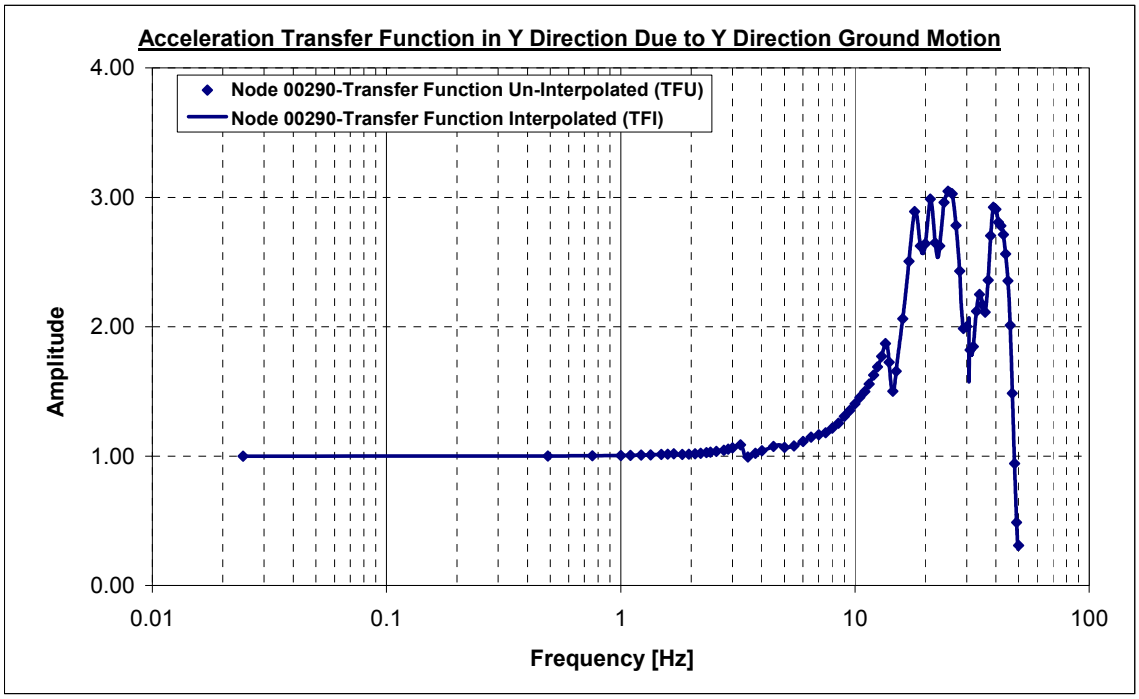

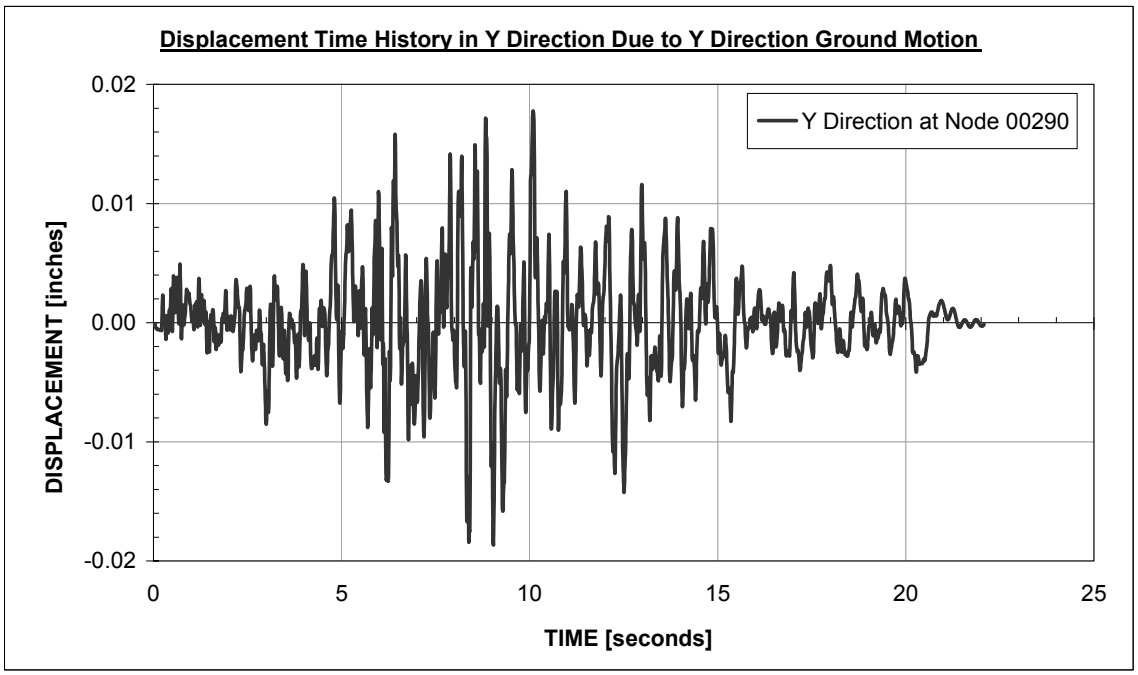

Figure 7-3. Acceleration Transfer Function and Relative Displacement with Respect to Free-Field Input Motion at Node 290 - Y Direction (North-South) for Profile 2032-100

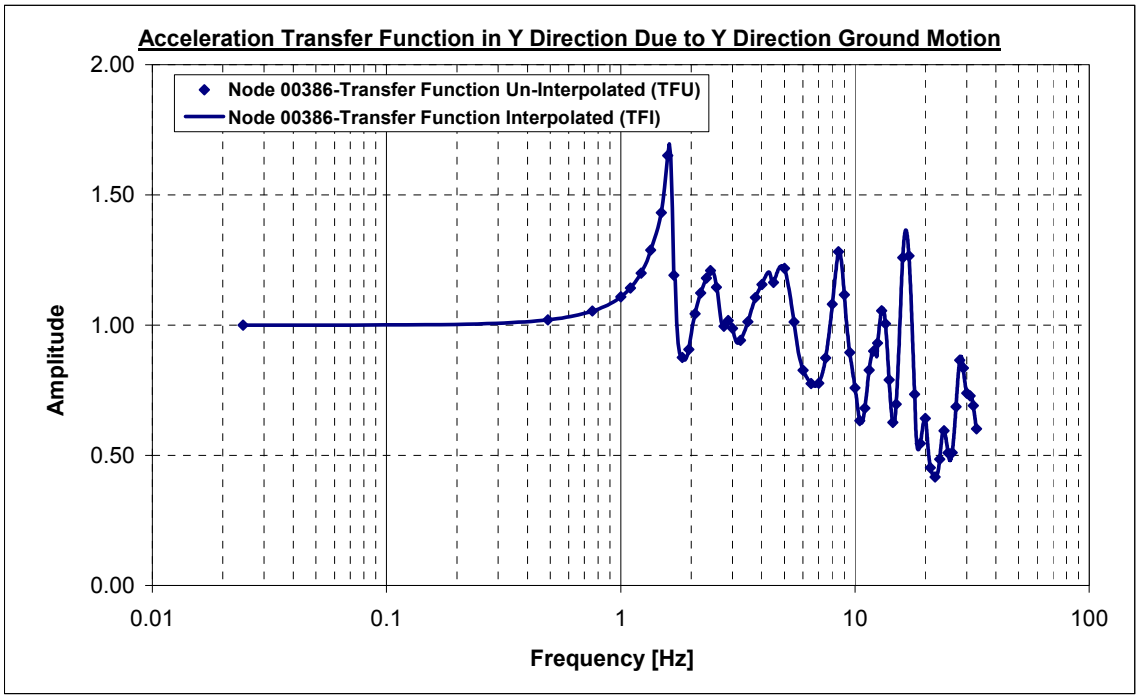

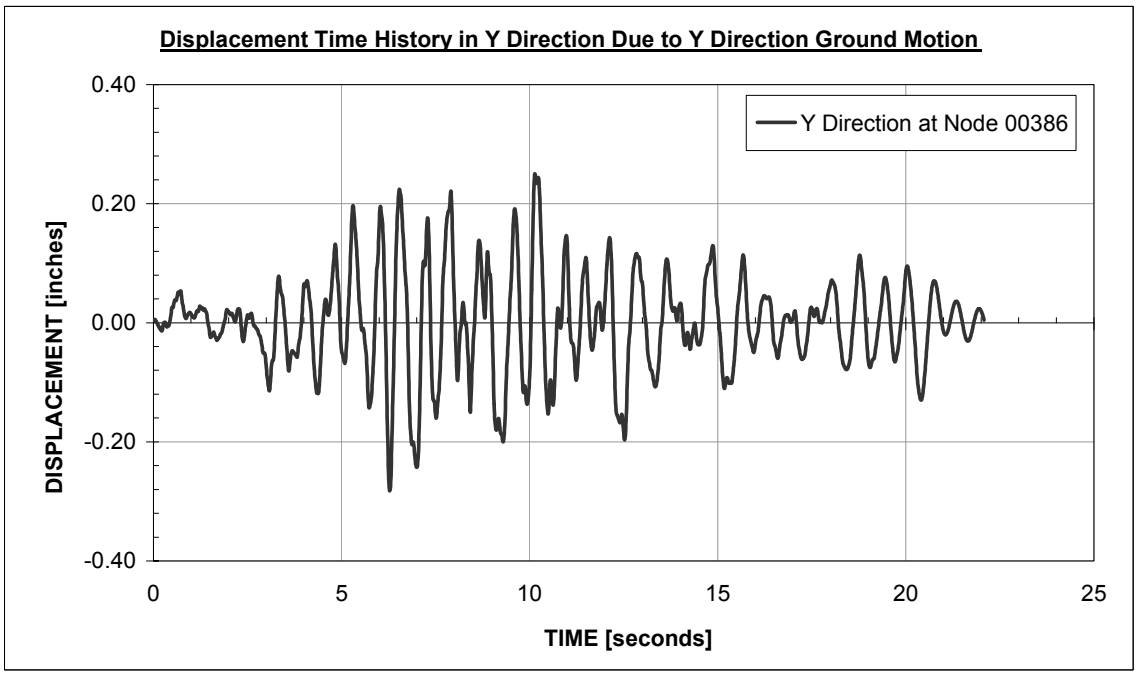

Figure 7-4. Acceleration Transfer Function and Relative Displacement with Respect to Free-Field Input Motion at Node 386 - Y Direction (North-South) for Profile 270-200

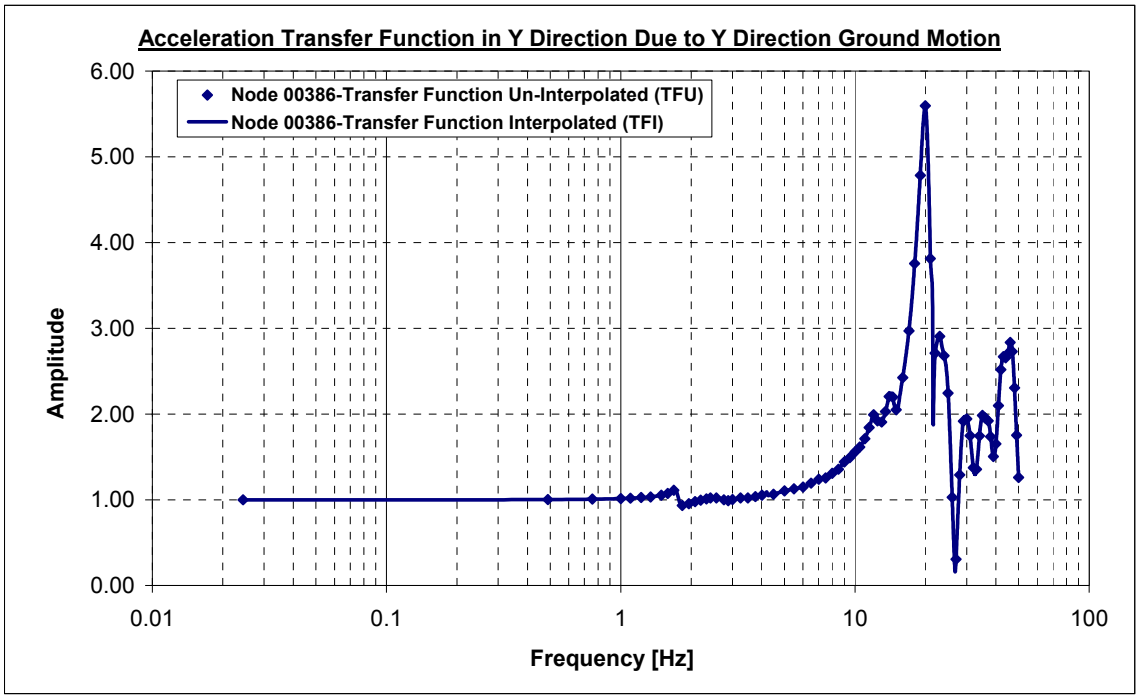

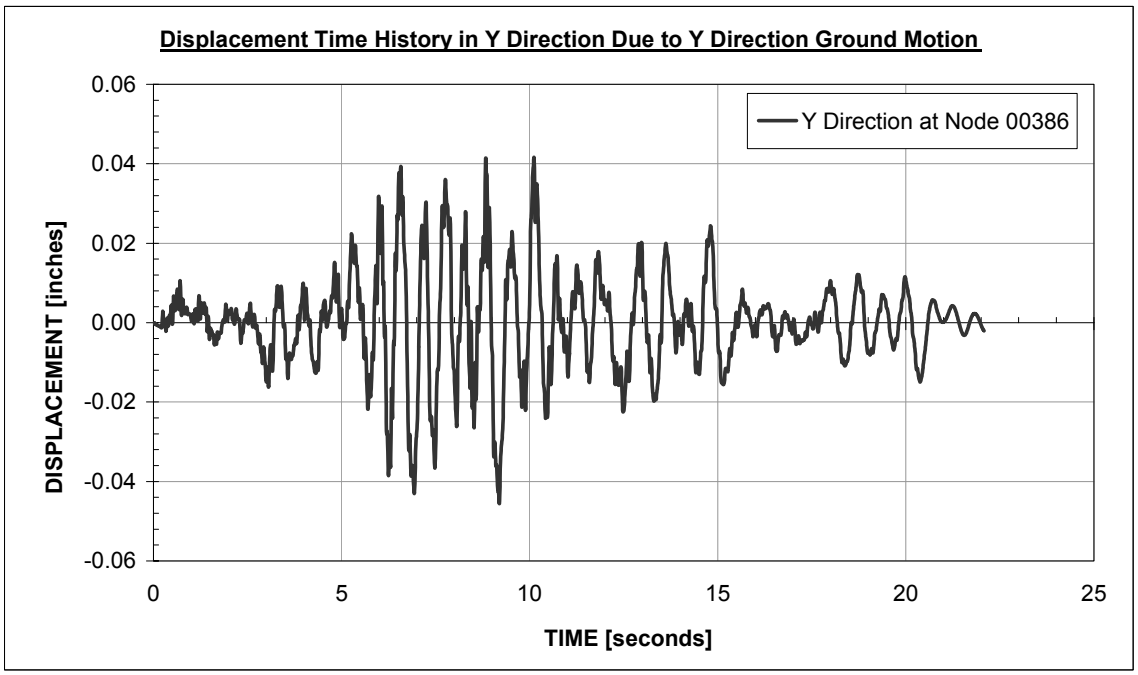

Figure 7-5. Acceleration Transfer Function and Relative Displacement with Respect to Free-Field Input Motion at Node 386 - Y Direction (North-South) for Profile 2032-100

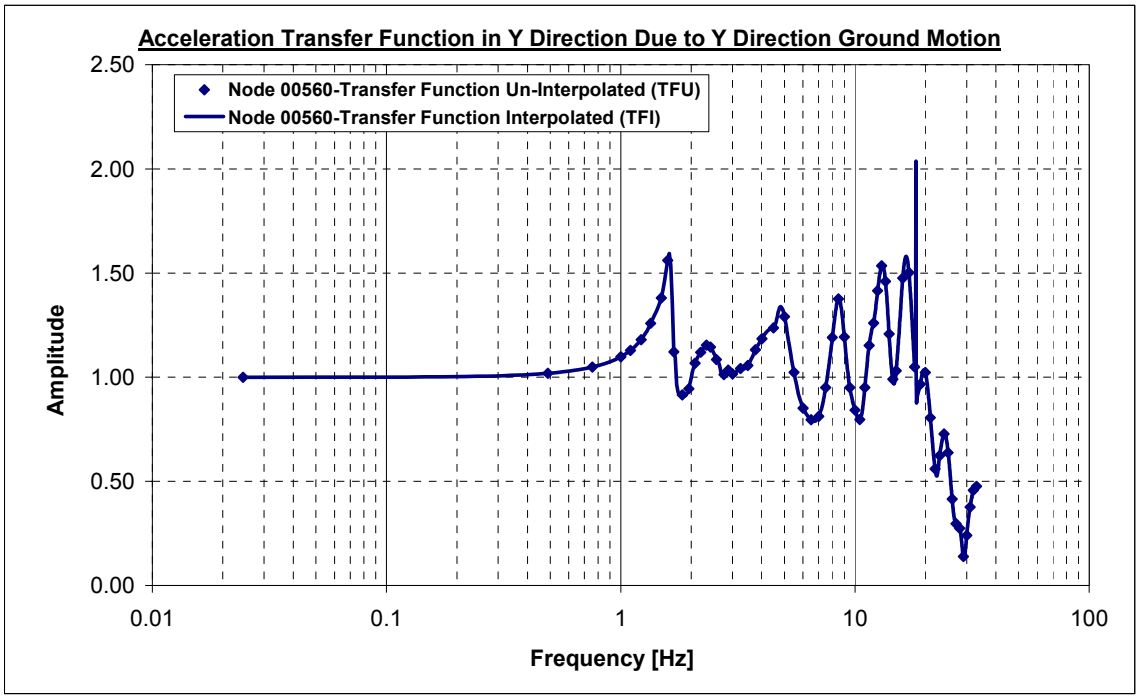

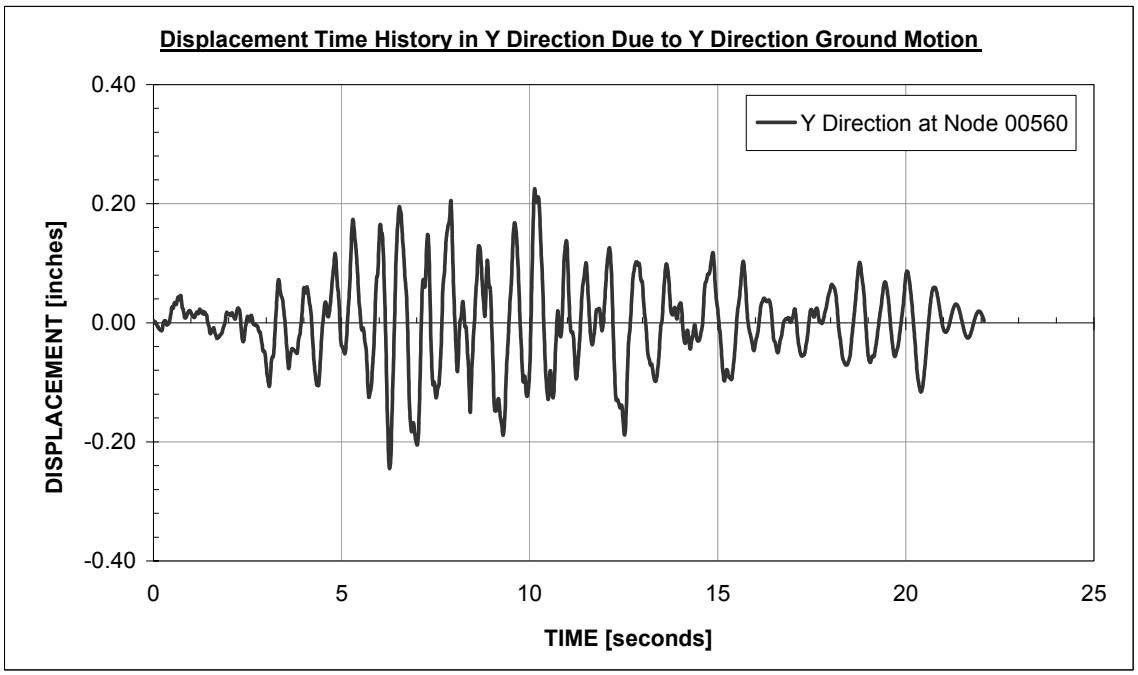

Figure 7-6. Acceleration Transfer Function and Relative Displacement with Respect to Free-Field Input Motion at Node 560 - Y Direction (North-South) for Profile 270-200

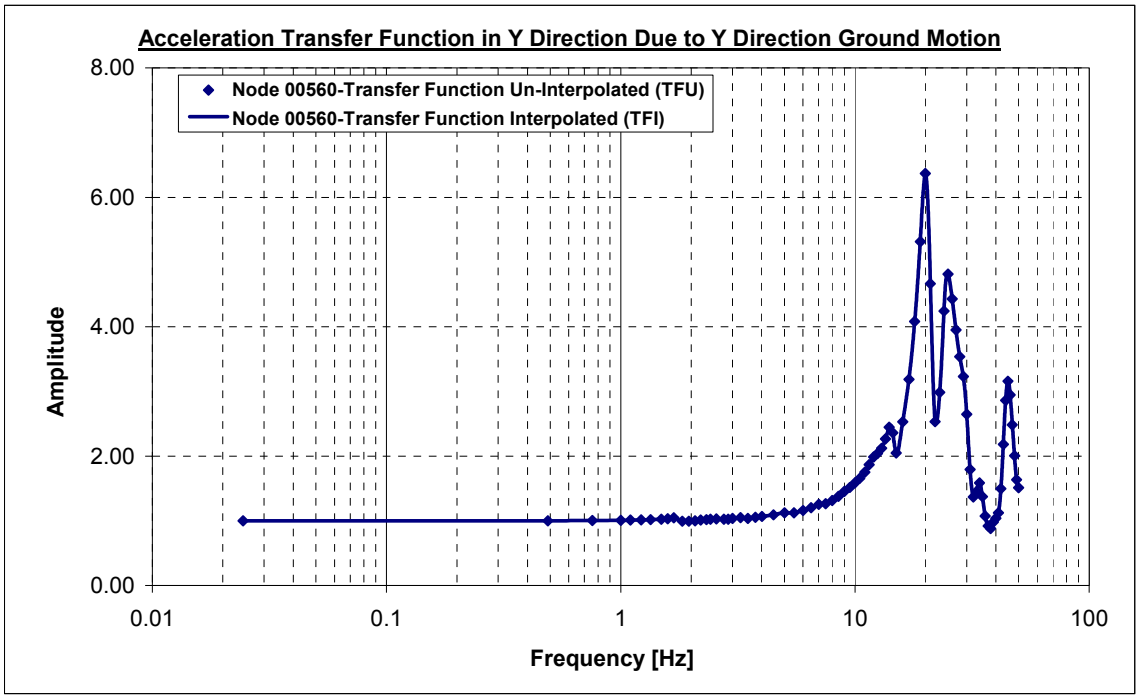

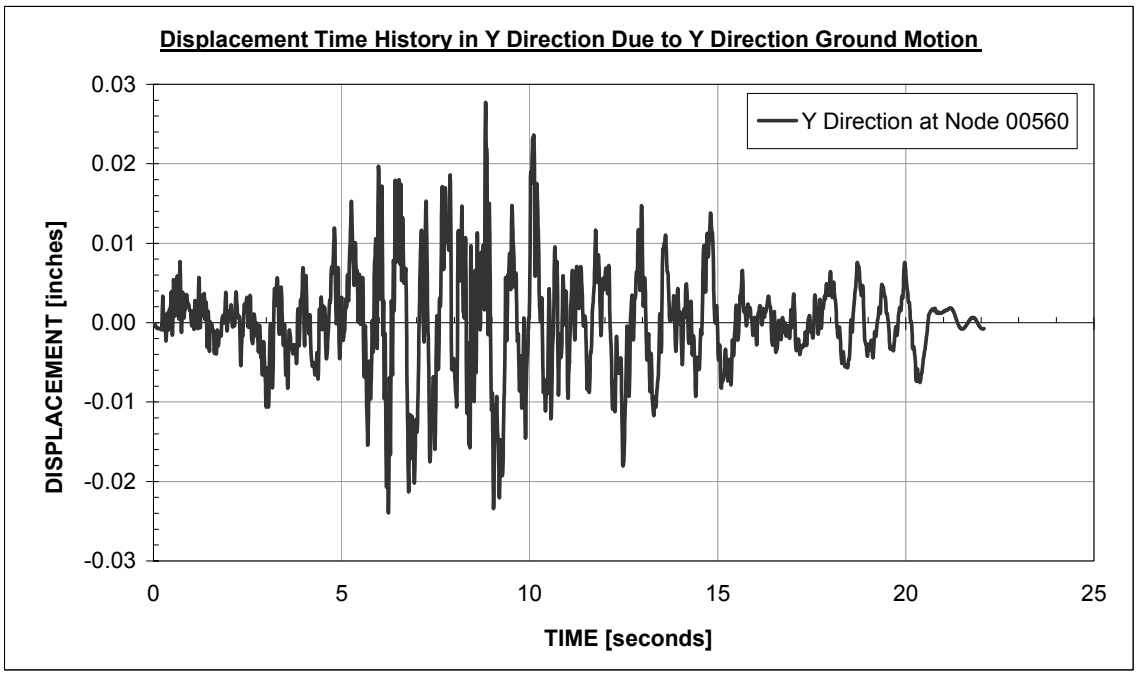

Figure 7-7. Acceleration Transfer Function and Relative Displacement with Respect to Free-Field Input Motion at Node 560 - Y Direction (North-South) for Profile 2032-100

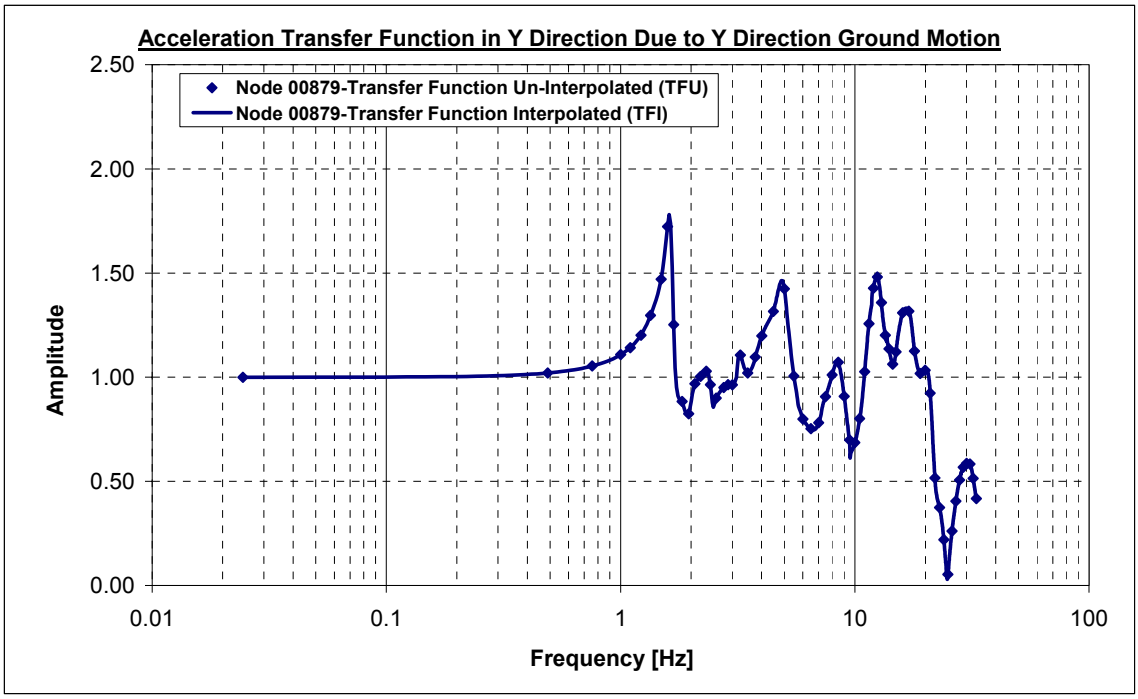

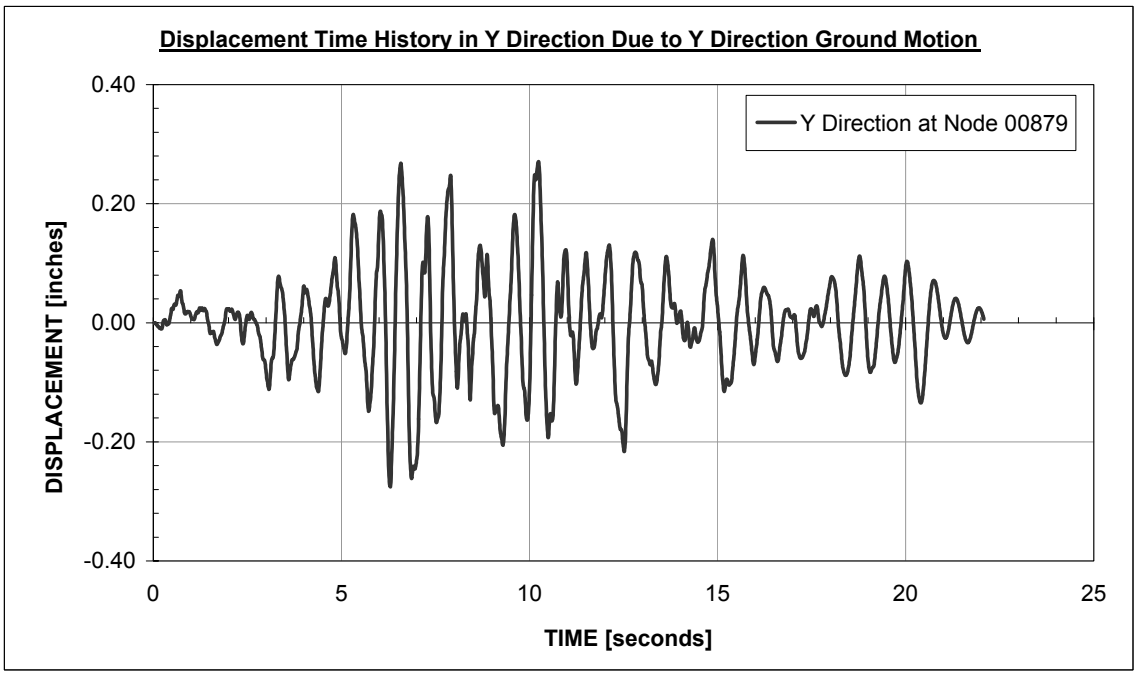

Figure 7-8. Acceleration Transfer Function and Relative Displacement with Respect to Free-Field Input Motion at Node 879 - Y Direction (North-South) for Profile 270-200

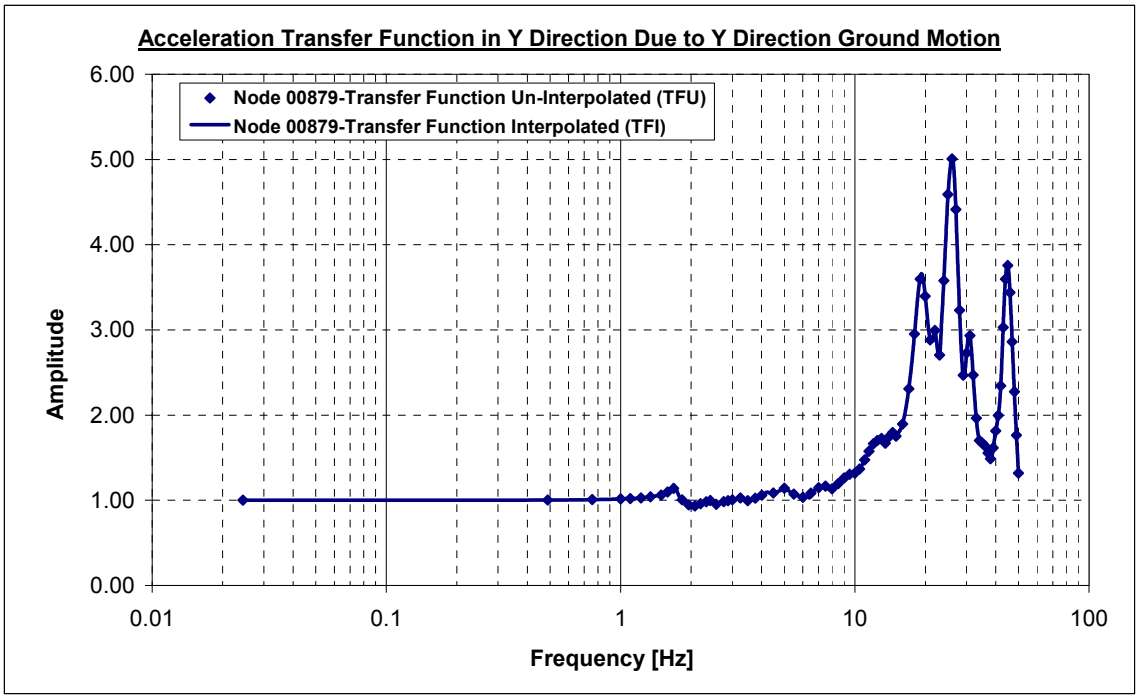

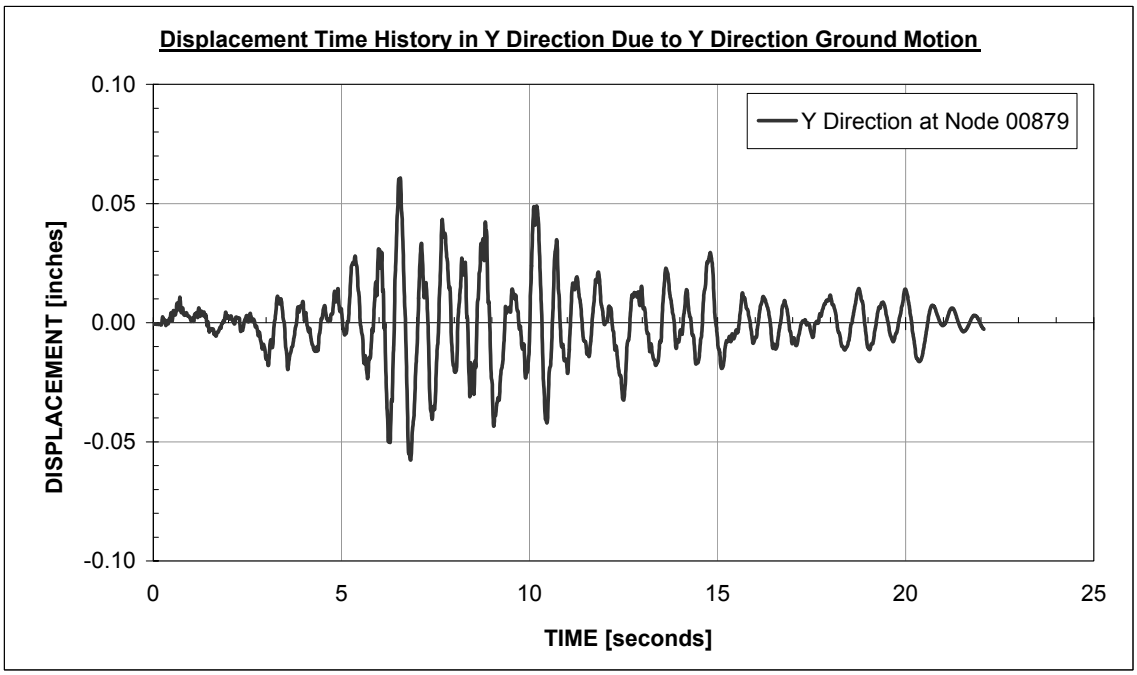

Figure 7-9. Acceleration Transfer Function and Relative Displacement with Respect to Free-Field Input Motion at Node 879 - Y Direction (North-South) for Profile 2032-100

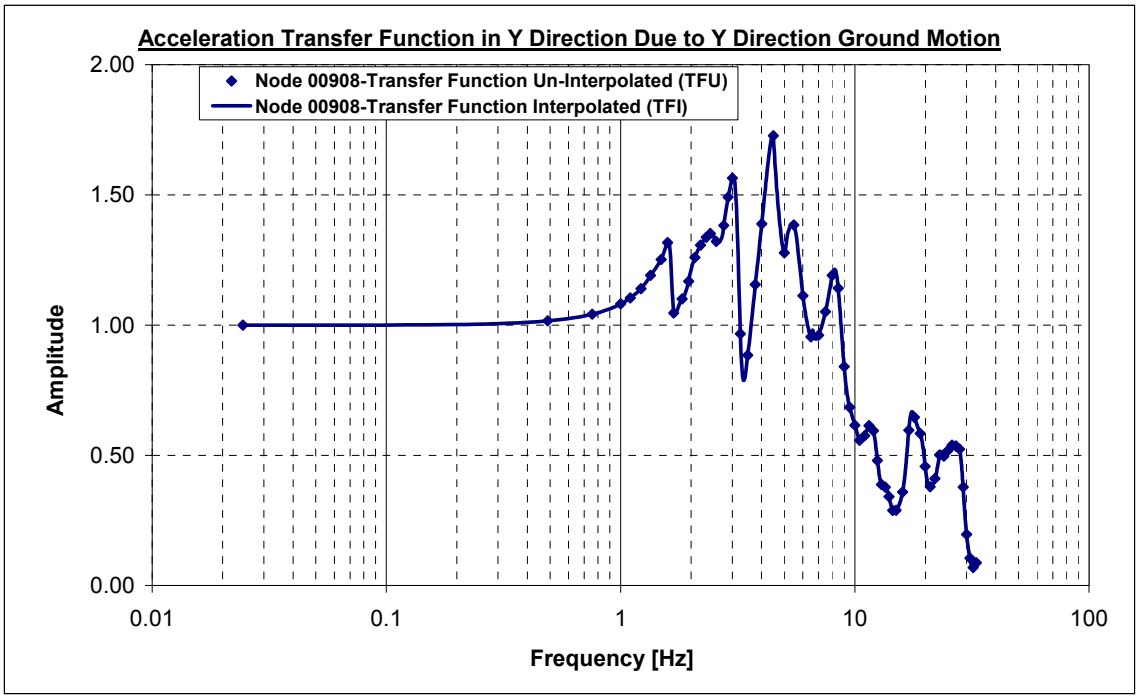

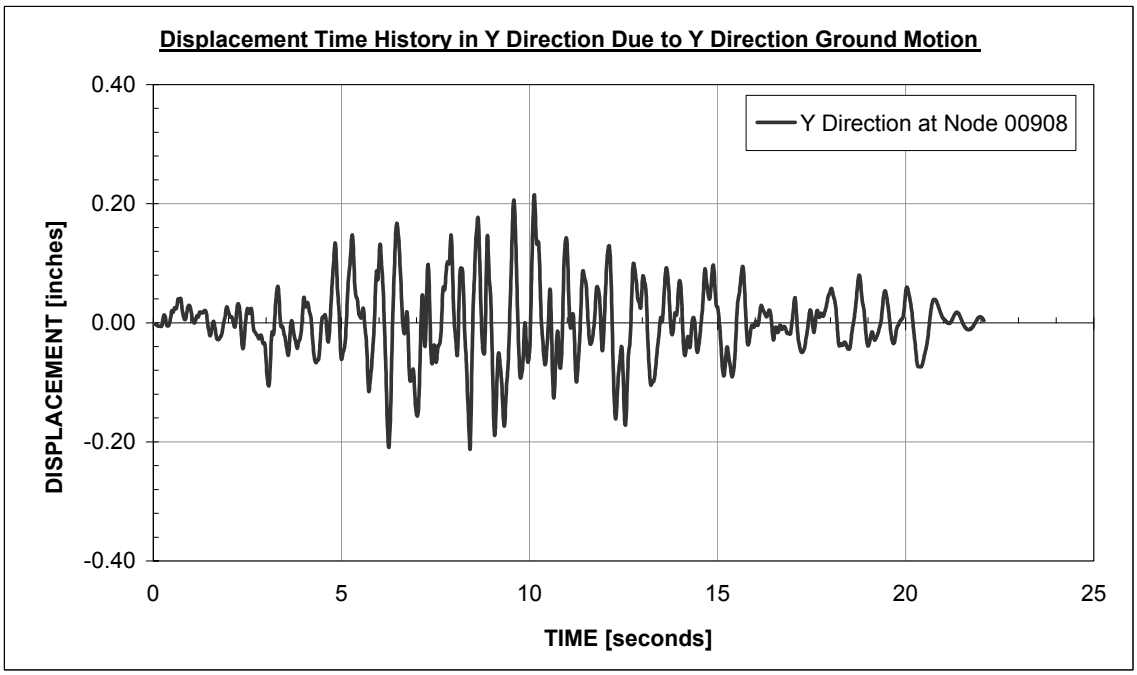

Figure 7-10. Acceleration Transfer Function and Relative Displacement with Respect to Free-Field Input Motion at Node 908 - Y Direction (North-South) for Profile 270-200

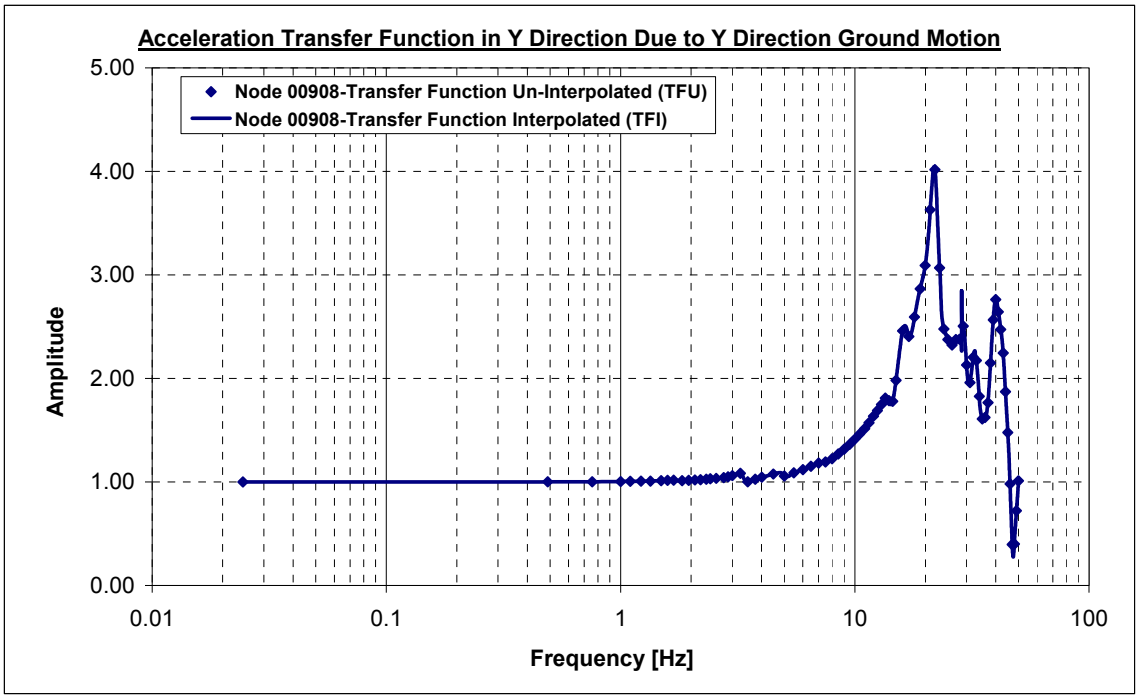

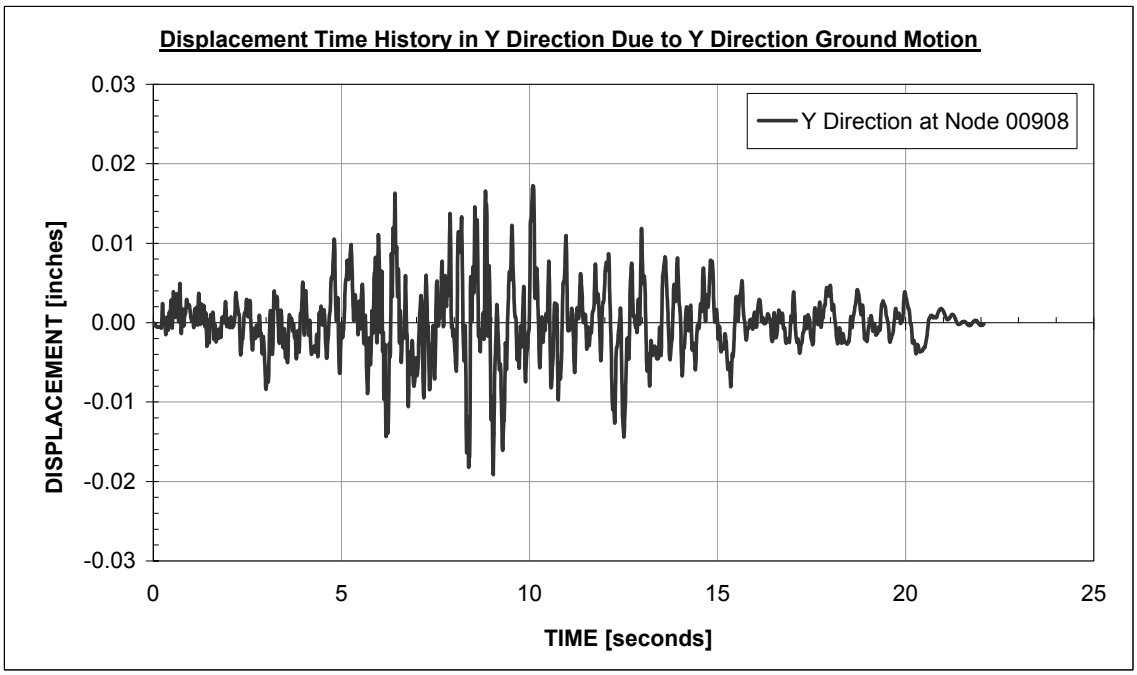

Figure 7-11. Acceleration Transfer Function and Relative Displacement with Respect to Free-Field Input Motion at Node 908 - Y Direction (North-South) for Profile 2032-100

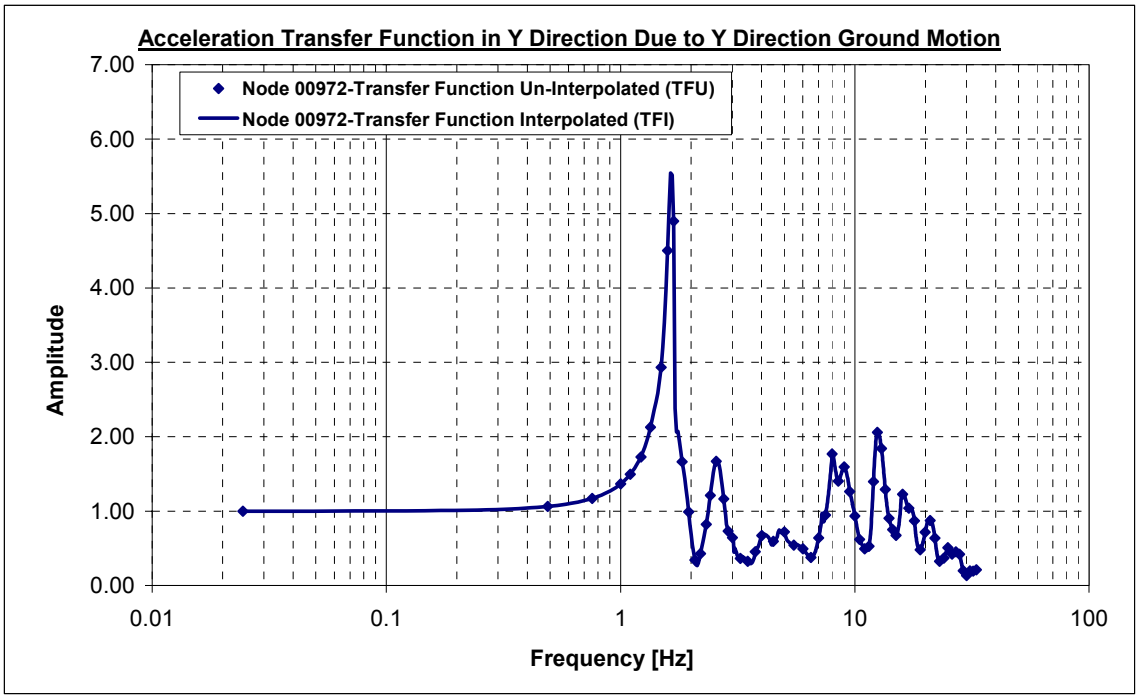

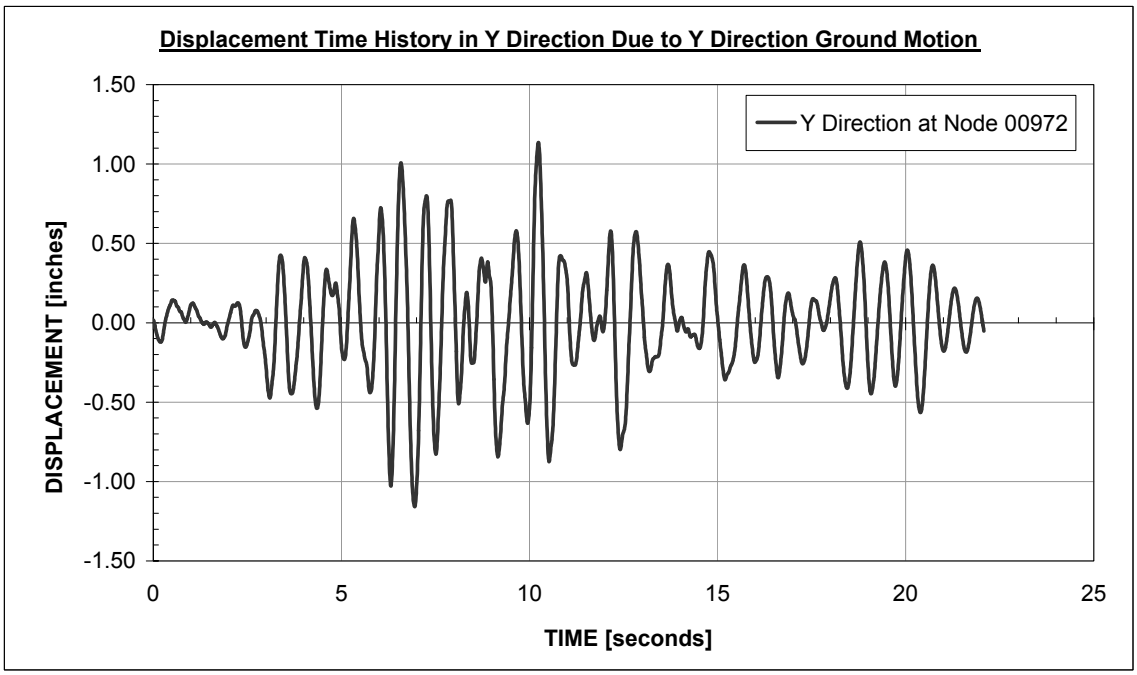

Figure 7-12. Acceleration Transfer Function and Relative Displacement with Respect to Free-Field Input Motion at Node 972 - Y Direction (North-South) for Profile 270-200

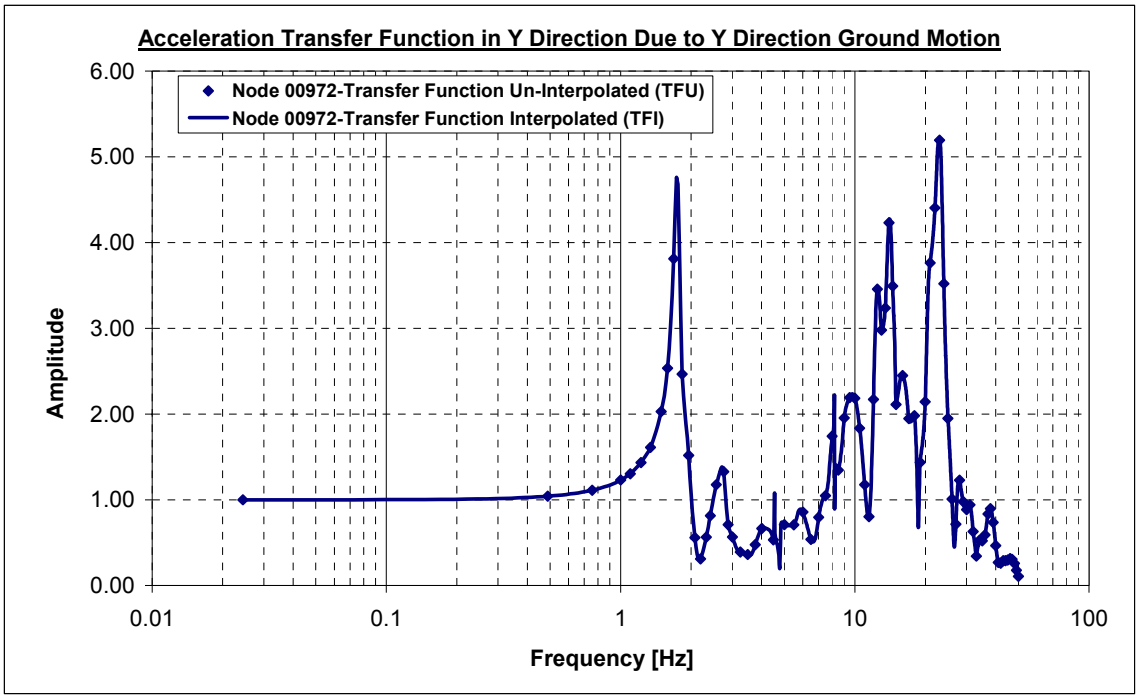

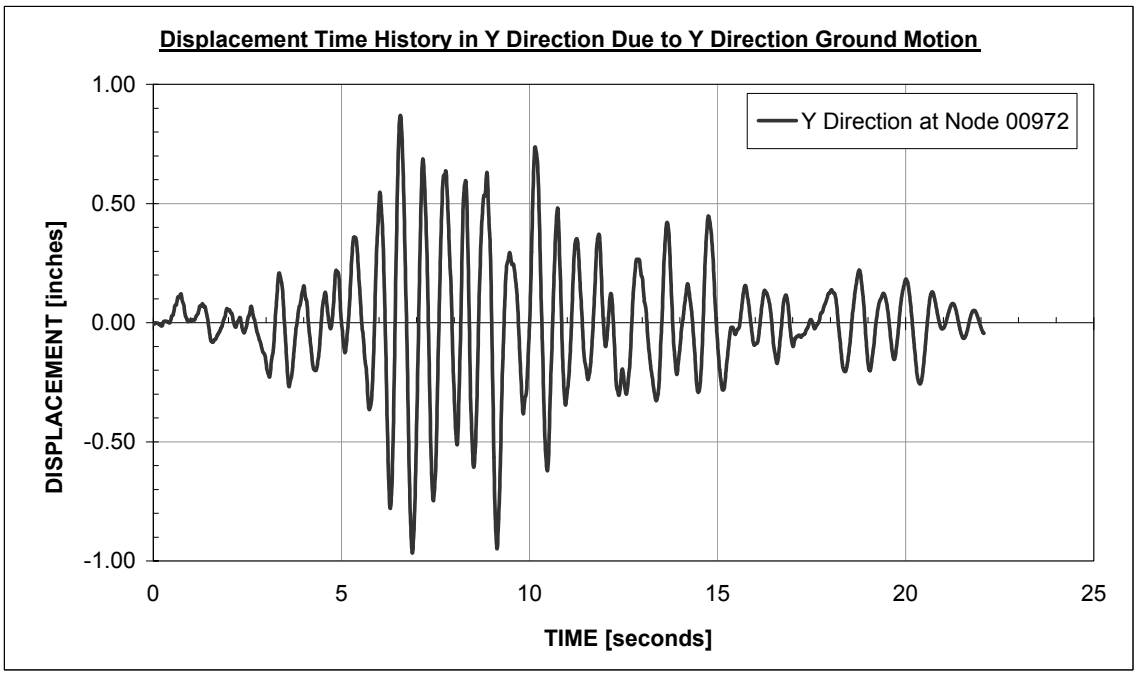

Figure 7-13. Acceleration Transfer Function and Relative Displacement with Respect to Free-Field Input Motion at Node 972 - Y Direction (North-South) for Profile 2032-100

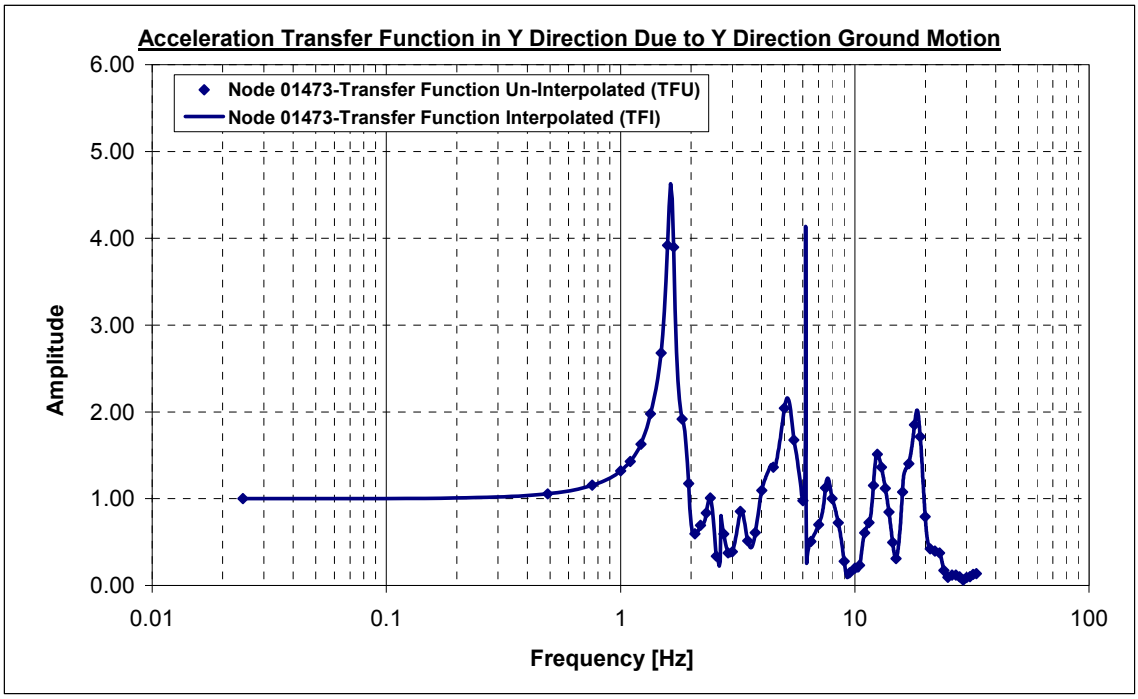

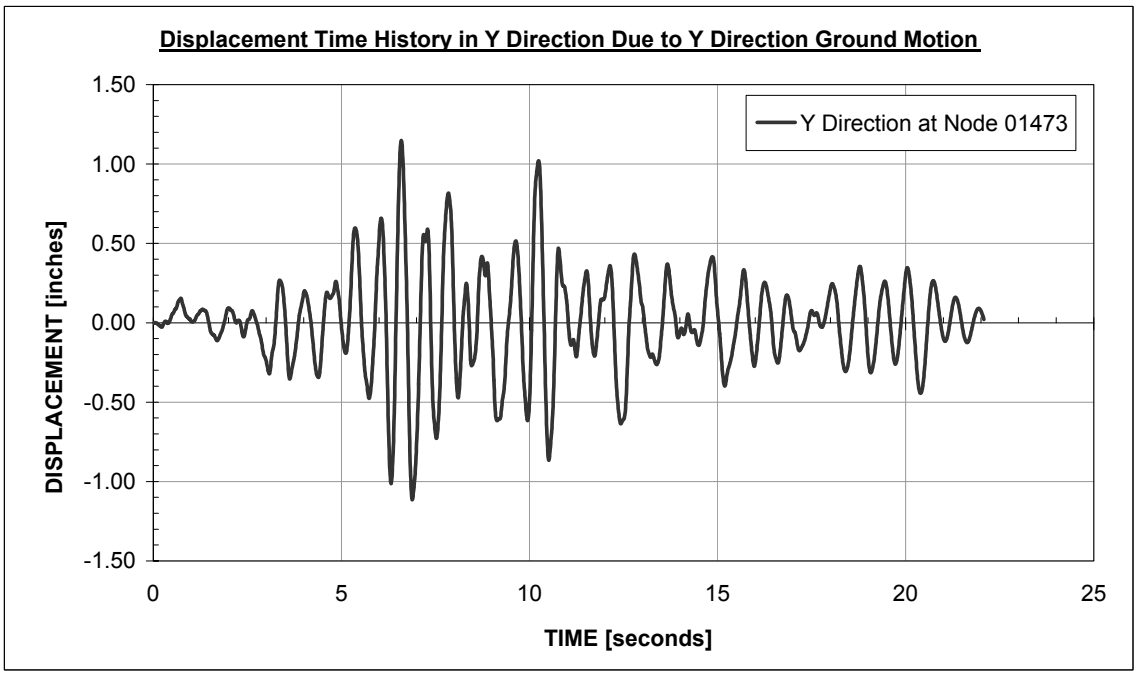

Figure 7-14. Acceleration Transfer Function and Relative Displacement with Respect to Free-Field Input Motion at Node 1473 - Y Direction (North-South) for Profile 270-200

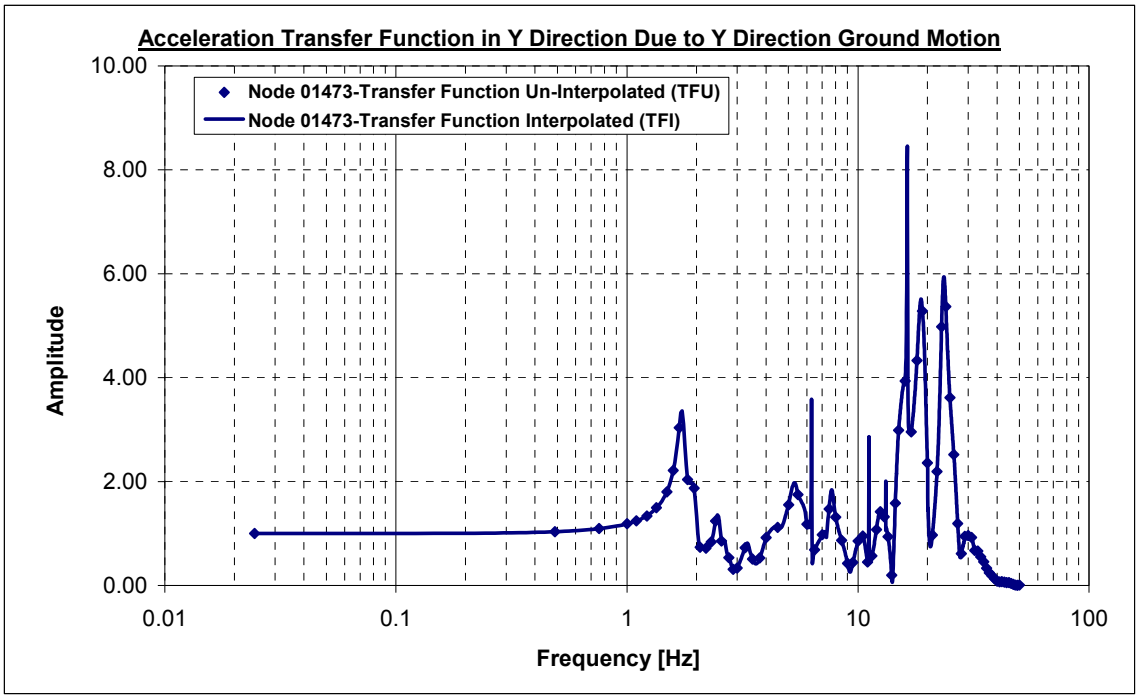

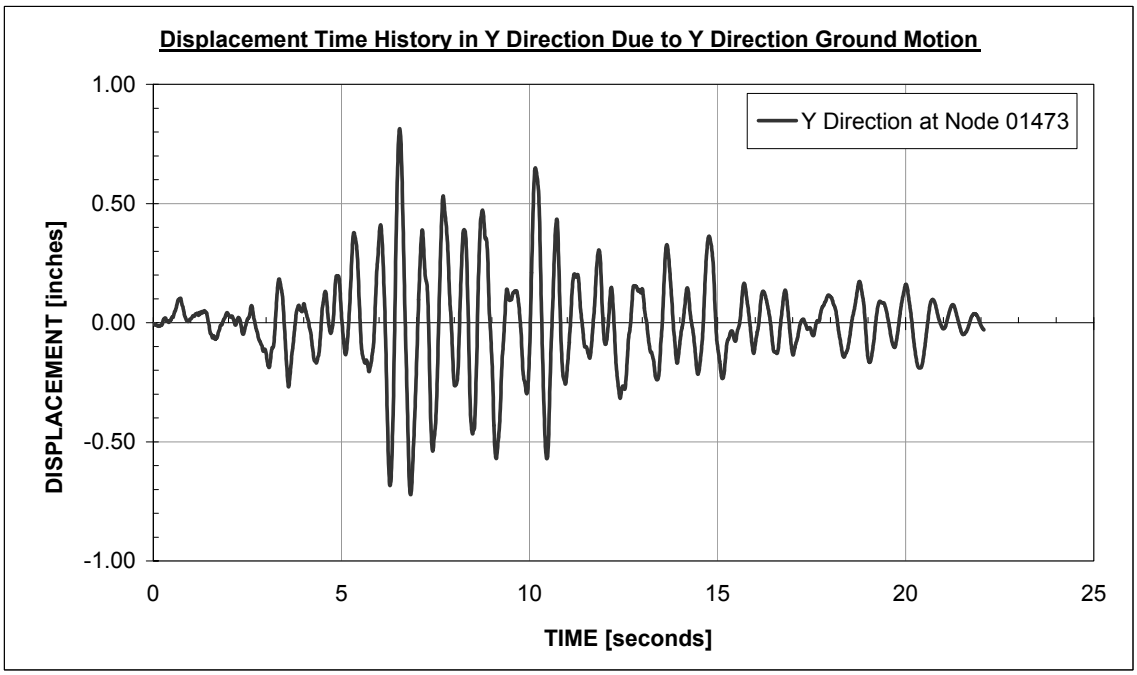

Figure 7-15. Acceleration Transfer Function and Relative Displacement with Respect to Free-Field Input Motion at Node 1473 - Y Direction (North-South) for Profile 2032-100

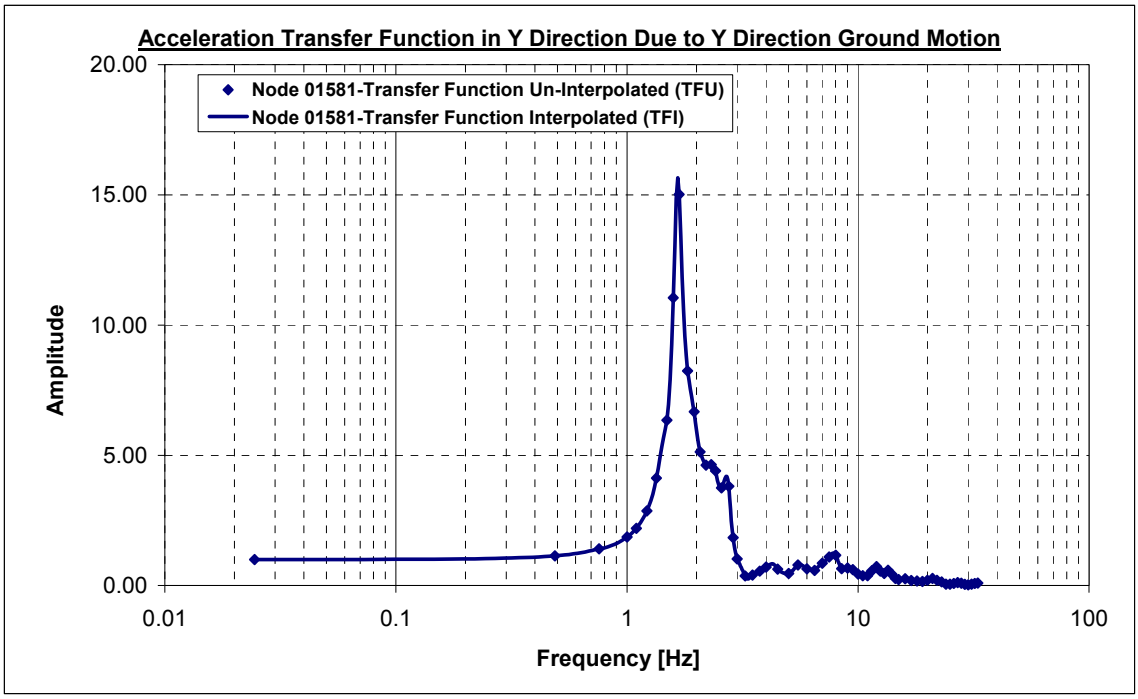

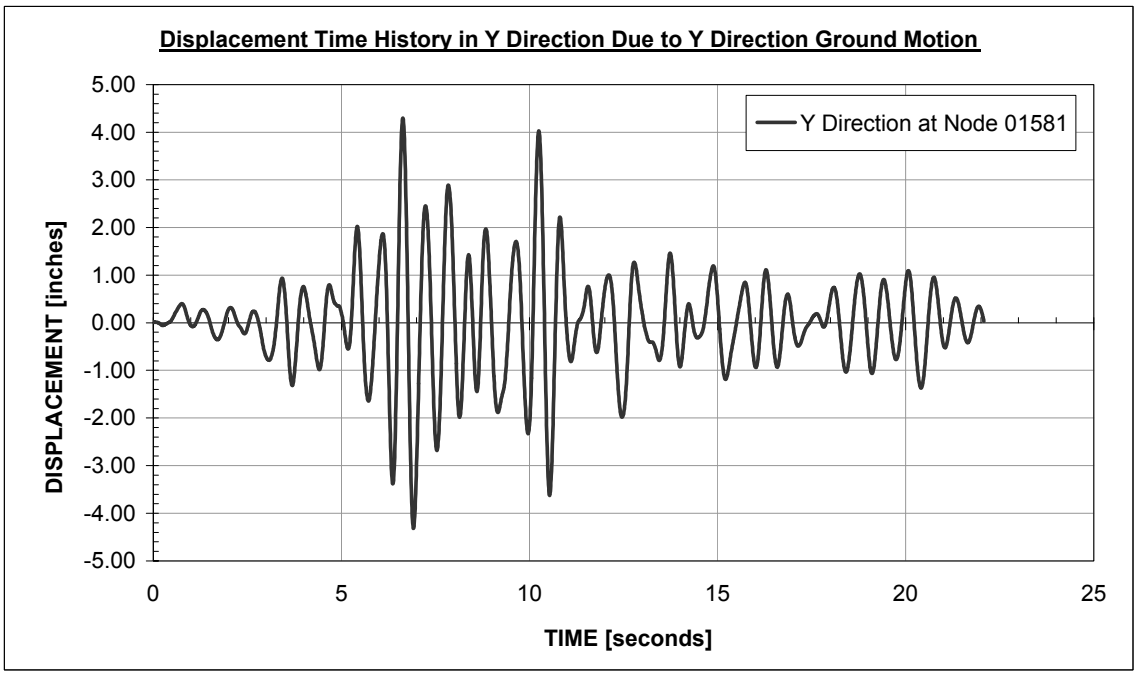

Figure 7-16. Acceleration Transfer Function and Relative Displacement with Respect to Free-Field Input Motion at Node 1581 - Y Direction (North-South) for Profile 270-200

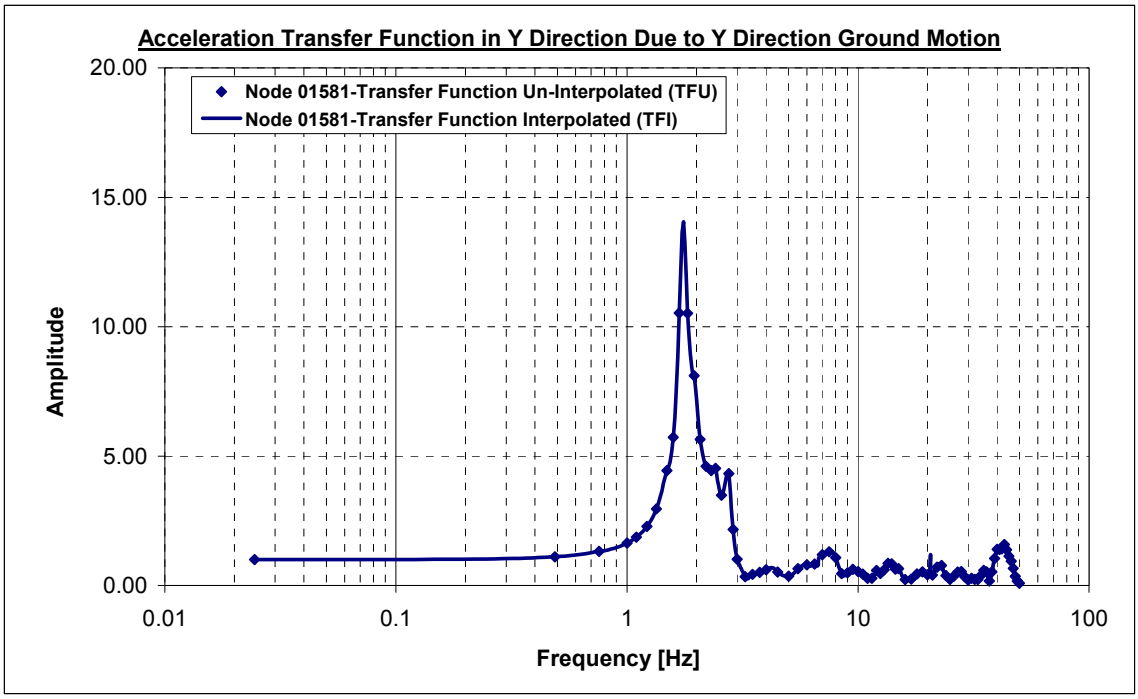

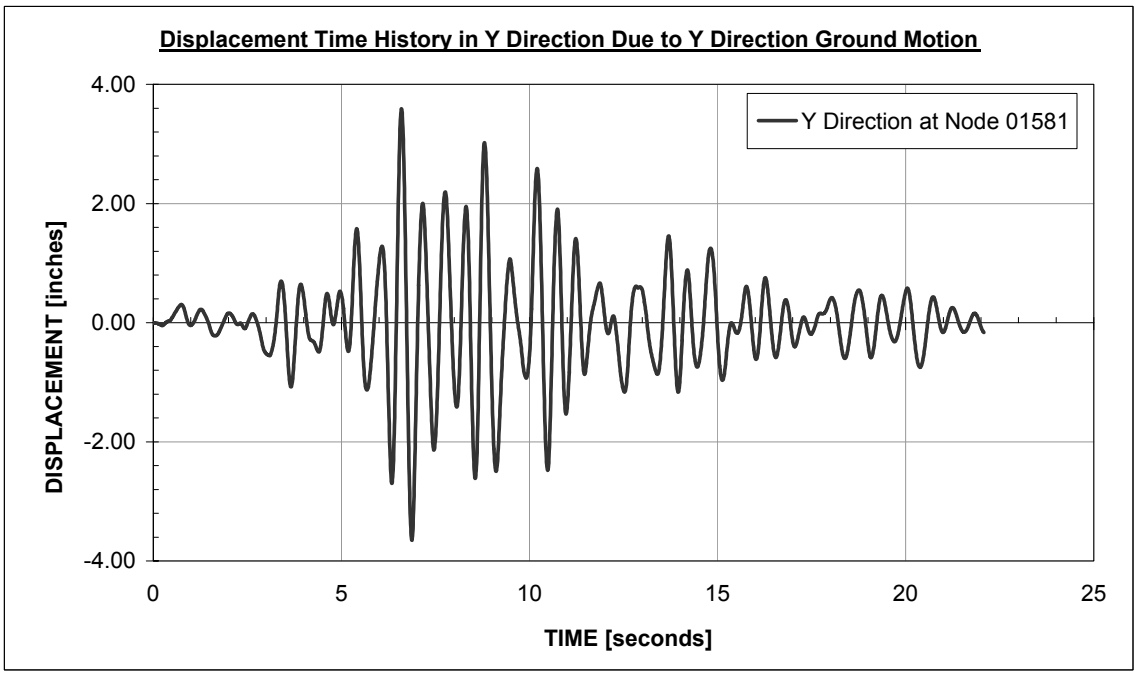

Figure 7-17. Acceleration Transfer Function and Relative Displacement with Respect to Free-Field Input Motion at Node 1581 - Y Direction (North-South) for Profile 2032-100

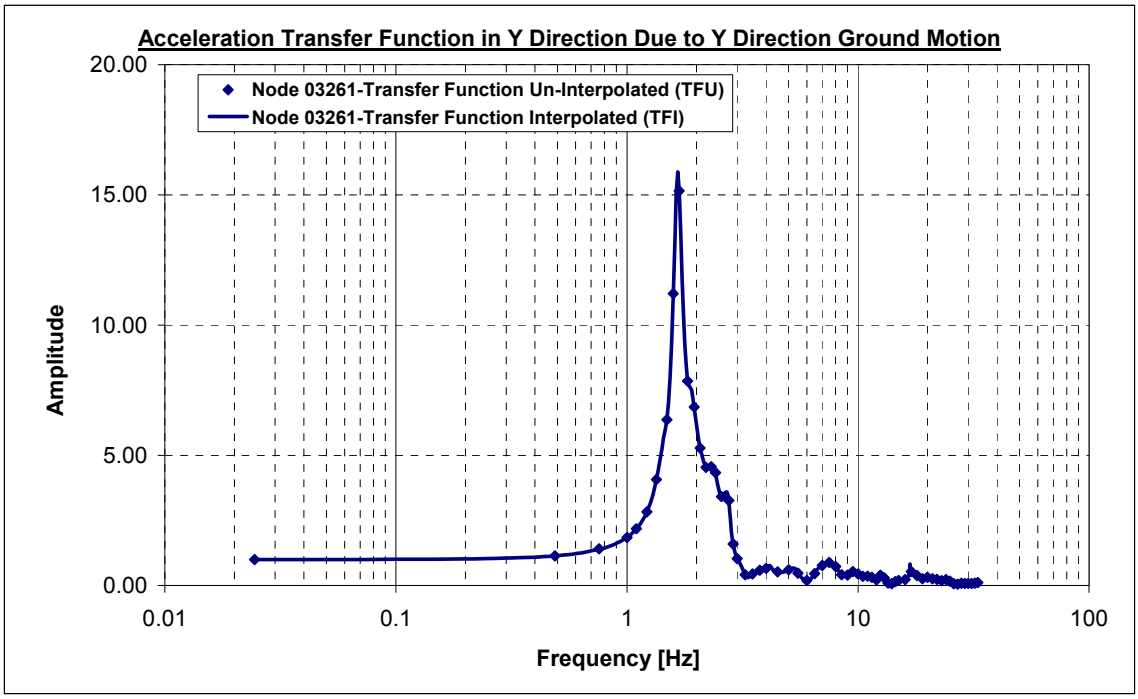

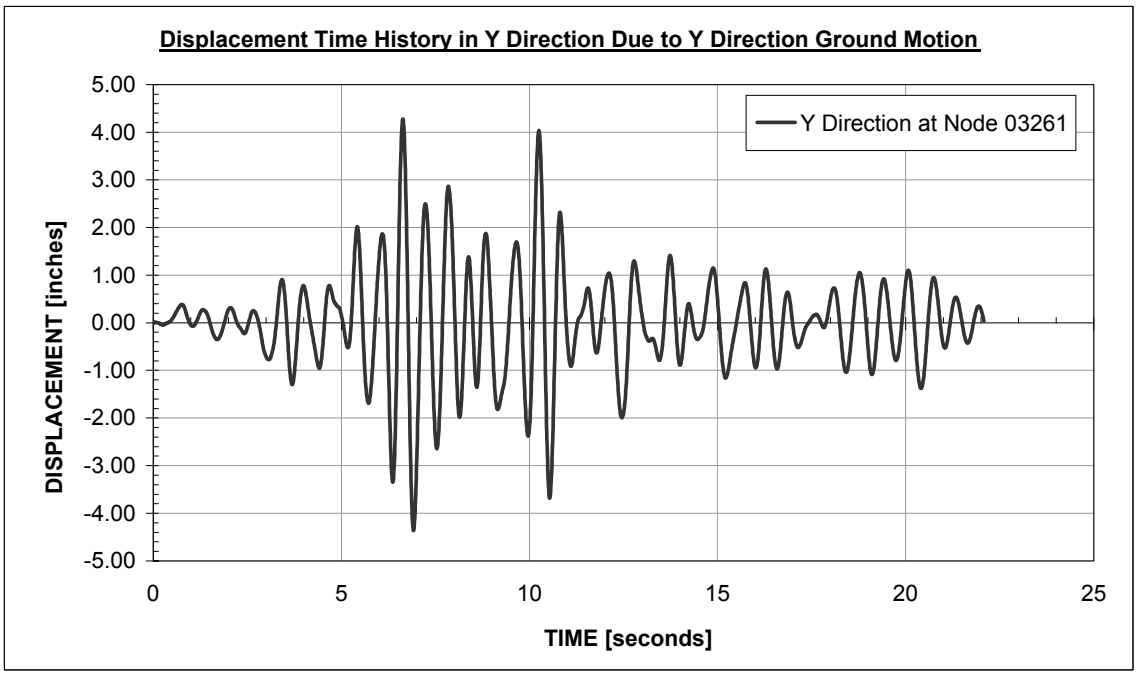

Figure 7-18. Acceleration Transfer Function and Relative Displacement with Respect to Free-Field Input Motion at Node 3261 - Y Direction (North-South) for Profile 270-200

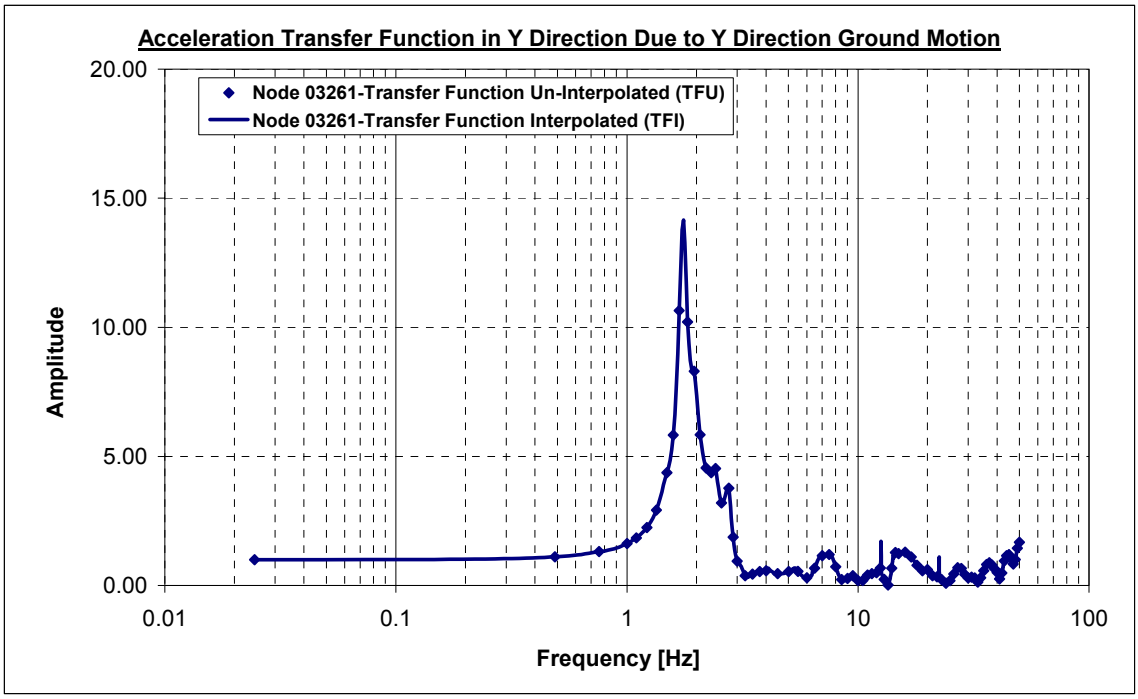

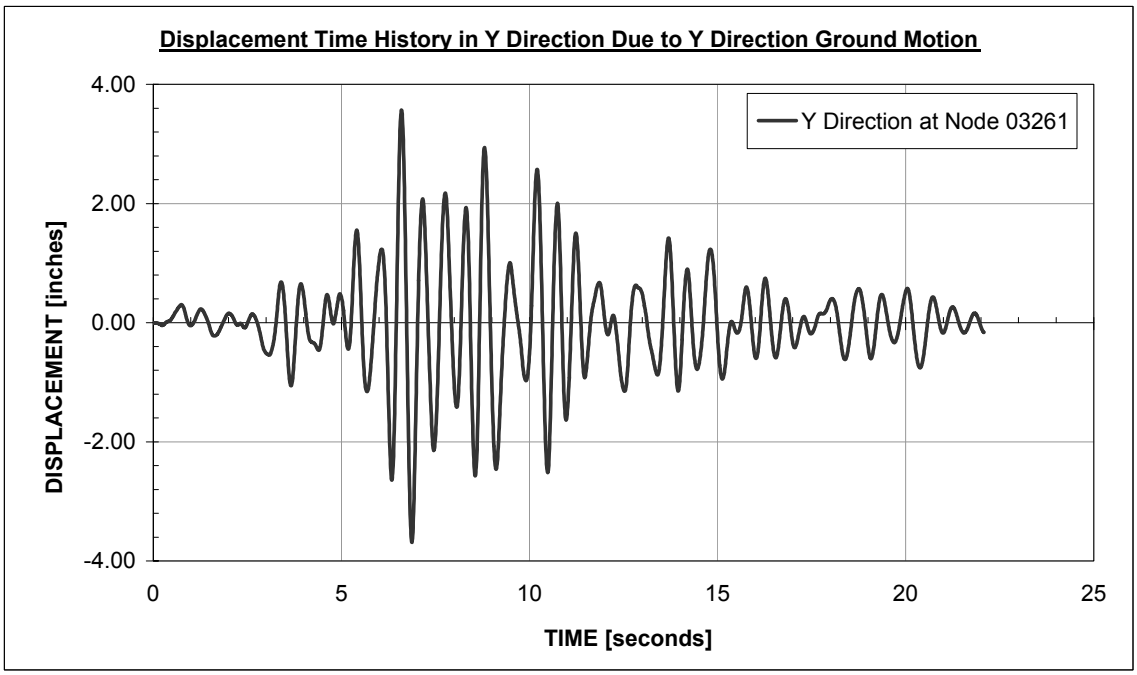

Figure 7-19. Acceleration Transfer Function and Relative Displacement with Respect to Free-Field Input Motion at Node 3261 - Y Direction (North-South) for Profile 2032-100

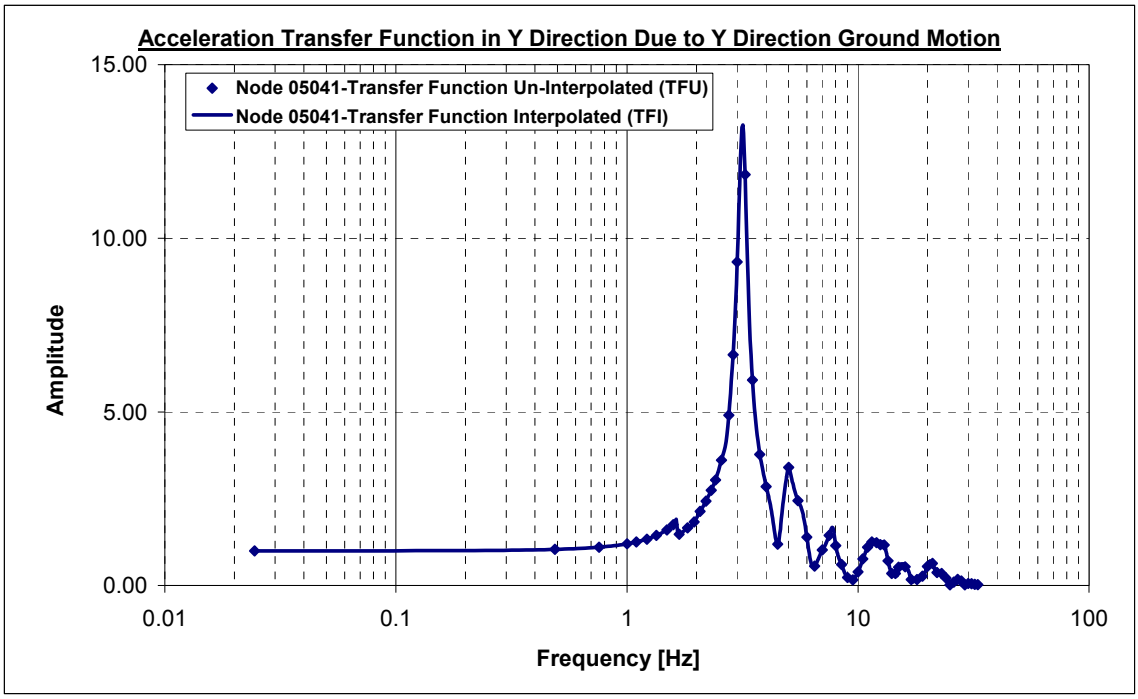

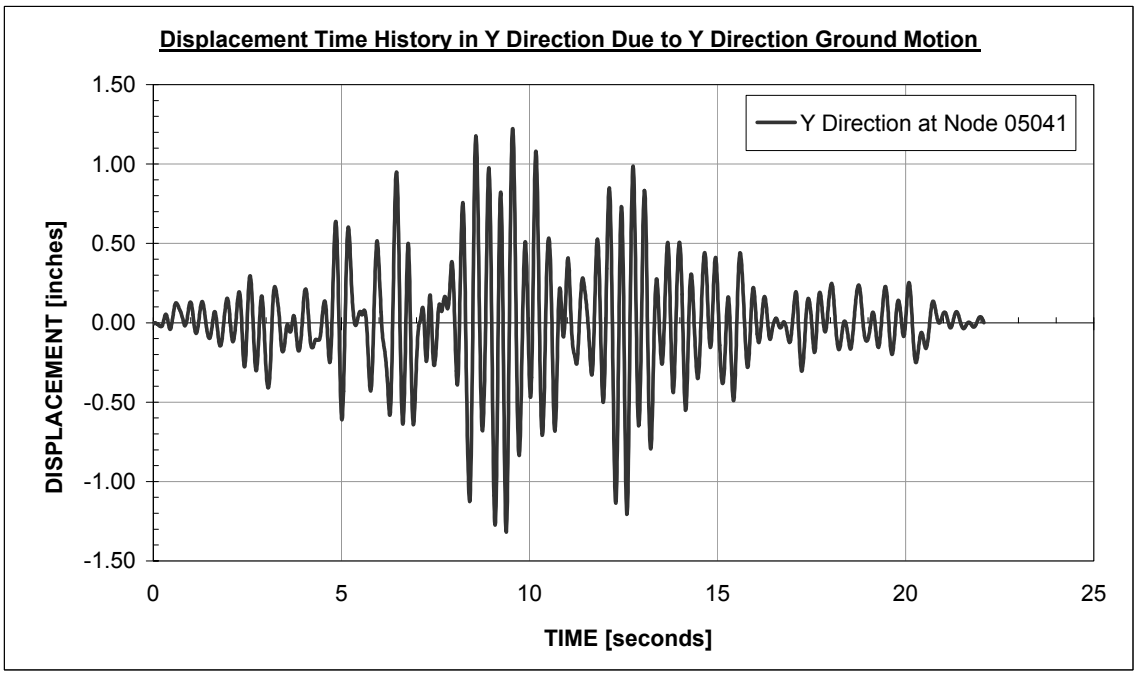

Figure 7-20. Acceleration Transfer Function and Relative Displacement with Respect to Free-Field Input Motion at Node 5041 - Y Direction (North-South) for Profile 270-200

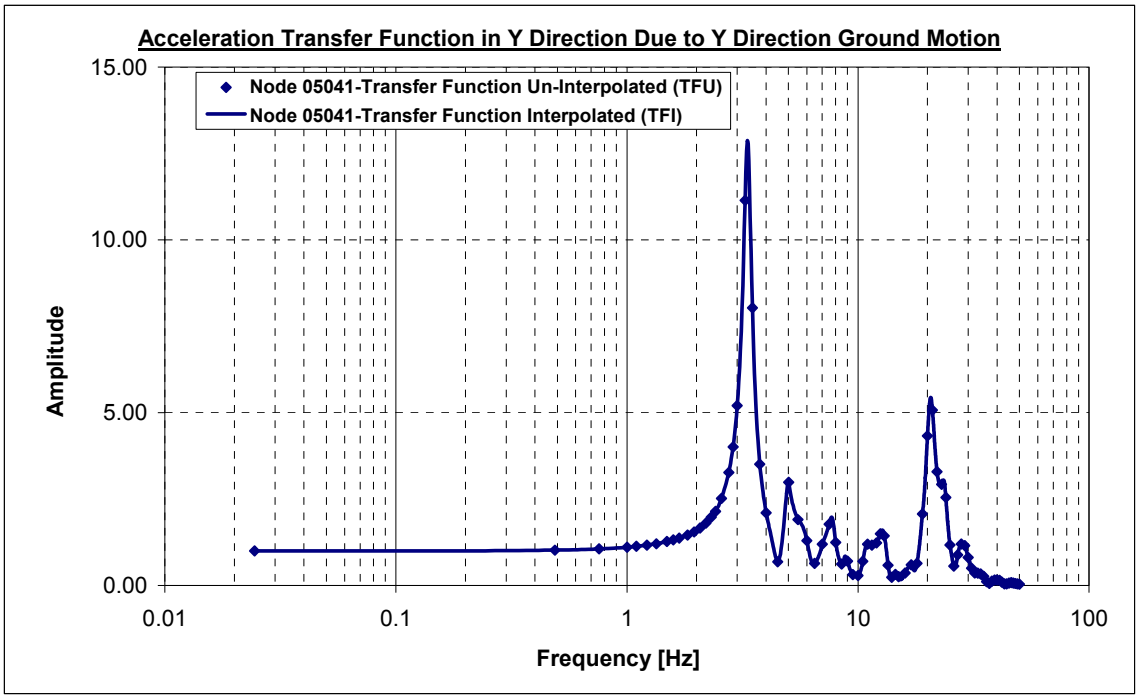

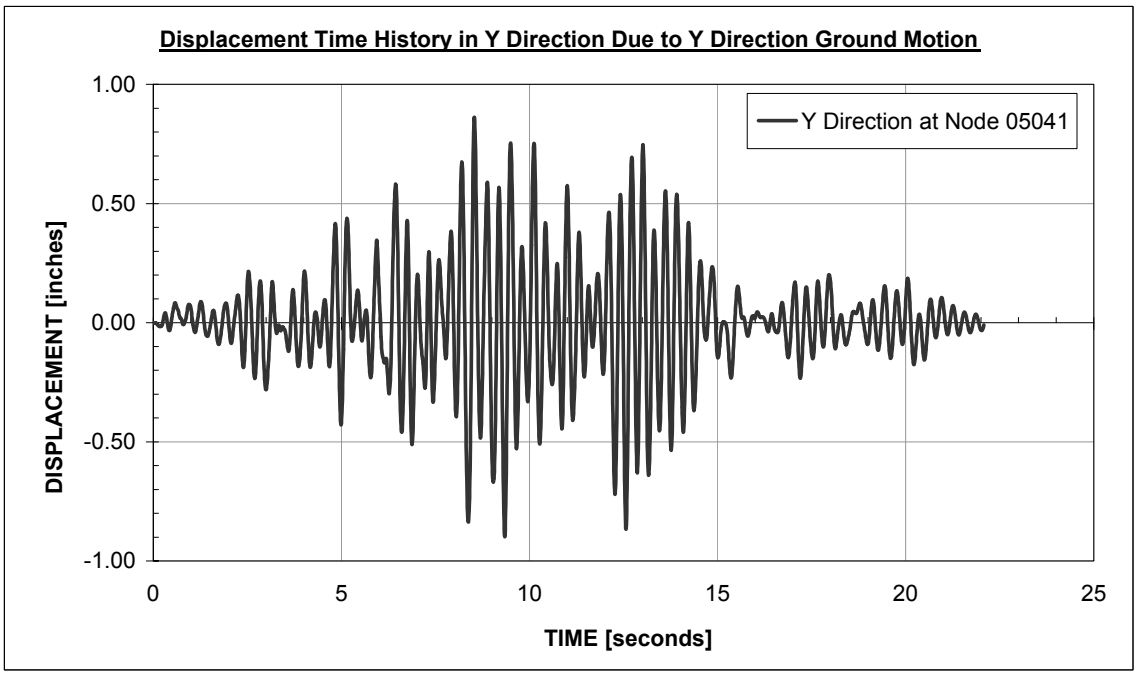

Figure 7-21. Acceleration Transfer Function and Relative Displacement with Respect to Free-Field Input Motion at Node 5041 - Y Direction (North-South) for Profile 2032-100Reference 13

Reference 13: Comparison T/B height in the analysis with DCD

The Design Control Document (DCD), Revision 2, indicates that the roof elevation for the Turbine Building is at elevation 165'-4". T/B height will increase 169'-10" in DCD next revision to change ceiling structure to truss frame from I-shape girder.
For this analysis and to account for various Plant Operators which may have other maintenance requirements, the Turbine Building roof elevation in this report was increased to elevation 193'-1". This increase in height permits the Plant Operator to remove various pieces of equipment without the need to remove additional sections of the turbine and the turbine piping. By not having to remove the additional turbine piping, the maintenance that is being done in the turbine area can be done more safely and without the possibility of damaging additional pieces of equipment and piping. It is felt that the increase in height of the Turbine Building roof will also create an upper bound condition on the Turbine Building SSI and GT STRUDL analyses. By using the same sections properties for steel members in the lower roof design as was used in the high roof analysis, it is anticipated that deflections and member stresses in the lower roof will be less than or equal to those of the high roof design. Because the lower roof design generates smaller seismic forces. In addition, the lower roof configuration itself contributes to less seismic responses (less deflections and member stresses).

	T/B for Analysis	DCD Next Revision (Rev.3)	DCD Rev.2
Building Height	193'-1"	169'-10"	165'-4"
Outline of TB	Figure-1	Figure-2	Figure-3
Ceiling Structure	Truss frame	Truss frame	I-shape girder
Crane Hook Height	Increase of crane hook height for maintenance (Option)	Base	Base

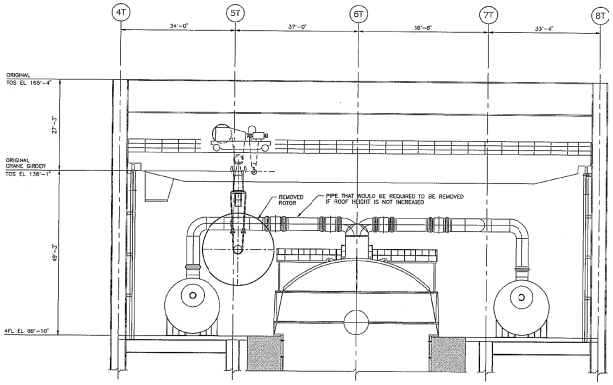

Figure-3 DCD Rev.2

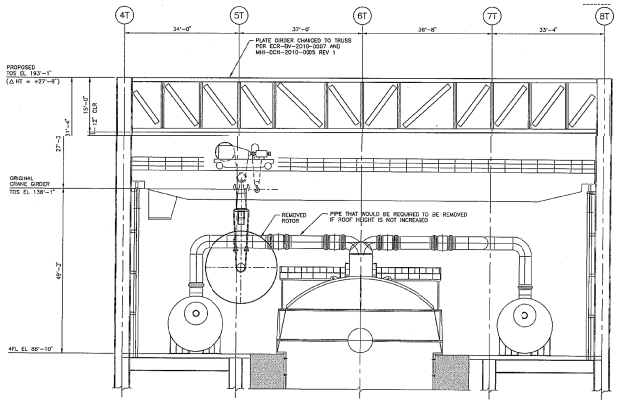

Figure-2 DCD Next Revision (Rev.3)

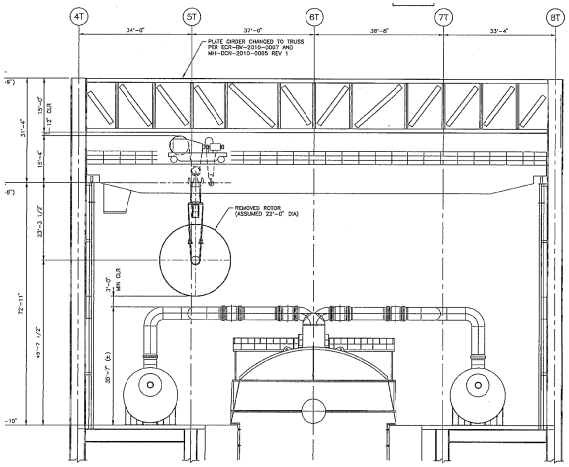

Figure-1 T/B for Analysis